COMPARATIVE ELECTROCHEMISTRY, ELECTRONIC ABSORPTION SPECTROSCOPY AND SPECTROELECTROCHEMISTRY OF THE MONOMETALLIC RUTHENIUM POLYPYRIDYL COMPLEXES

$[Ru(bpy)(dpb)_2](PF_6)_2$

$[Ru(bpy)_2(dpb)](PF_6)_2$

$[Ru(bpy)_2(dpq)](PF_6)_2$

$[Ru(bpy)(dpq)_2](PF_6)_2$

by

Alan Duchovnay

Thesis submitted to the Faculty of the
Virginia Polytechnic Institute and State University
in partial fulfillment of the requirements for the degree of

MASTER OF SCIENCE

in

Chemistry

Karen J. Brewer, Chair
Joseph S. Merola
Brian E. Hanson

13 April 2011
Blacksburg, Virginia

Keywords: Spectroelectro Chemistry, Ruthenium

COMPARATIVE ELECTROCHEMISTRY, ELECTRONIC ABSORPTION SPECTROSCOPY AND SPECTROELECTROCHEMISTRY OF THE MONOMETALLIC RUTHENIUM POLYPYRIDYL COMPLEXES

$[Ru(bpy)(dpb)_2](PF_6)_2$

$[Ru(bpy)_2(dpb)](PF_6)_2$

$[Ru(bpy)_2(dpq)](PF_6)_2$

$[Ru(bpy)(dpq)_2](PF_6)_2$

Alan Duchovnay

ABSTRACT

The novel compound $[Ru(bpy)(dpb)_2(PF_6)_2$ was synthesized, in a manner similar to the literature synthesis of $[Ru(bpy)(dpq)_2(PF_6)_2$. For the sake of completeness, the related analogs, $[Ru(bpy)_2(dpb)](PF_6)_2$, $[Ru(bpy)_2(dpq)](PF_6)_2$ and $[Ru(bpy)(dpq)_2](PF_6)_2$ were also synthesized. Alumina adsorption chromatography was used for purification purposes. Liquid secondary ion mass spectroscopy was used to confirm identity of compounds. The new compound contained 1% electroactive impurity as determined by OSWV. Spectroelectrochemical studies were conducted with both a bulk H-cell and a ~0.2 mm pathlength, optically transparent thin layer electrode (OTTLE) cell. High reversibility (ca 99%) is possible with dilute solutions (ca 10^{-4} M) and the OTTLE cell as compared to ca 50% with the H-cell. Spectroelectrochemical data supported the following electronic transitions for the new compound $[Ru(bpy)(dpb)_2](PF_6)_2$: (1) the Ru ($d\pi$) $\rightarrow$dpb MLCT at 552 nm, (2) a d$\rightarrow$ d at 242 nm, a bpy $\pi \rightarrow \pi^*$ at 285 nm. (3) The location of the Ru ($d\pi$) $\rightarrow$bpy MLCT peak is obscured by shoulders from 390-420 nm. (4)

The strong peak at 316 nm may be dpb $\pi \rightarrow \pi_2^*$, the location of the lower energy intraligand dpb $\pi \rightarrow \pi_1^*$ is uncertain. Upon oxidation of the metal center, no LMCT was observed within the UV-VIS range. This is in direct contrast to the results of Gordon et al. This author hypothesizes that their LMCT found in the visible region was actually the result of incomplete electrochemical conversion and that a LMCT should be seen in the NIR. The spectroelectrochemical properties of $[Ru(bpy)(dpq)_2](PF_6)_2$ were also presented for the first time. These results indicated that the 256 nm transition was d $\rightarrow$ d and not bpy $\pi \rightarrow \pi_2^*$ as suggested by Rillema et al.

DEDICATION

To my many mentors and my faithful dog, Blacker.

ACKNOWLEDGMENTS

I would like to express my gratitude to my advisor, Dr. Karen Brewer. I would also like to thank Kim Harrick and Ann Campbell for their help in obtaining mass spectroscopy data.

TABLE OF CONTENTS

LIST OF ABBREVIATIONS

Bpy	2,2’-Bipyridine
BL	Bridging Ligand
CT	Charge Transfer
dpb	2,3-Bis(2-pyridyl)benzoquinaxoline
dpp	2,3-Bis(2-pyridyl)pyrazine
dpq	2,3-Bis(2-pyridyl)quinoxaline
ES	Excited State
GS	Ground State
HOMO	Highest-Occupied Molecular Orbital
IL	Intraligand
LF	Ligand Field
LSIMS	Liquid Secondary Ion Mass Spectroscopy
LMCT	Ligand to Metal Charge Transfer
LUMO	Lowest Unoccupied Molecular Orbital
MLCT	Metal to Ligand Charge Transfer
MO	Molecular Orbital
NHE	Normal Hydrogen Electrode
TBAH	Tetrabutylammonium hexafluorophospate
UV	Ultraviolet
Vis	Visible

LIST OF TABLES

LIST OF FIGURES

CHAPTER ONE: INTRODUCTION

The aim of this research was to probe the redox and spectroscopic properties of ruthenium(II) complexes of the polyazine bridging ligand 2,3-bis(2-pyridyl)benzoquinoxaline and the structurally related 2,3-bis(2-pyridyl)quinoxaline analogs.

A brief overview of the history and chemistry of ruthenium is relevant to understanding the chemistry of ruthenium polypyridyl compounds. Ruthenium was first found in 1826, by G. W. Osann, from platinum residues found in Ruthenia, a district of Russia. It was isolated and characterized by K. K. Klaus in 1844. It occurs naturally in the mineral laurite $(Ru,Os)S_2$ and in the alloy osmiridium (Os, Ru and Ir).[1] Being inert to acids including aqua regia, the alloy is dissolved in an alkaline oxidizing mixture of KOH and KNO_3, to form the salt K_2RuO_4. The osmate cation is then oxidized to OsO_4 by acidification and removed by distillation. The remaining ruthenium complex is converted to RuO_4 by NaOH addition and isolated by distillation.[2] The addition of concentrated HCl to the $RuO_4(aq)$ yields the water-soluble compound $RuCl_3 \bullet 3H_2O$.[3] The actual composition includes both the monomeric Ru(III) form and polynuclear ruthenium (IV) oxy and hydroxy chloro species .[4] Metallic ruthenium is produced from RuO_4 by reduction with H_2.[5]

Ruthenium exhibits a large range of oxidation states, from 0 (Ru metallic and $Ru(CO)_5$ to +8 (RuO_4) and subsequently a large number of ruthenium complexes have been synthesized. Ruthenium's coordination chemistry as a second row, Group VIII, transition metal is greatly influenced by the stability of the low spin d^6 configuration. Ru(II) forms stable octahedral complexes that are substitutionally inert with many π-acid ligands such as the chelating ligand 2,2'-bipyridine (bpy).

Intense interest in the ruthenium polypyridyl complexes started with the discovery of the dramatic luminescence of $[Ru(bpy)_3]Cl_2$ in 1959.[6] It is therefore appropriate to review the Ultraviolet-Visible spectroscopy, electrochemistry, and spectroelectrochemistry of this compound.

The Ultraviolet-Visible electronic absorption spectrum of $[Ru(bpy)_3](PF_6)_2$ in acetonitrile is shown in Figure 1.1. The lowest energy peak at 450 nm is a Ru(II) ($d\pi$) $\rightarrow$ bpy (π^*) charge transfer (bpy ^{1}MLCT). At low temperature (77K), in an ethanol- methanol glass there is a shoulder at 550 nm which is thought to be a ^{3}MLCT.[7] The molar absorptivity for this spin forbidden transition is 600 cm^{-1} M^{-1} (vs 1.45 x 10^4 cm^{-1} M^{-1} for the ^{1}MLCT at 452 nm).[7] It is also possible to have ^{1}MLCT's terminating on higher energy π^* orbital. Balzani *et al.*[8] assign a higher energy MLCT at 240 nm whereas Kalyanasundaram[7] describes two higher energy MLCTs at 238 nm and 250 nm. Intraligand transitions also occur. The peak at 288 nm is assigned to a bpy $\pi \rightarrow \pi_1^*$ transition. Higher energy peaks at 185 nm and 205 nm are attributed to bpy $\pi \rightarrow \pi_3^*$ and bpy $\pi \rightarrow \pi_2^*$ transitions.[9]

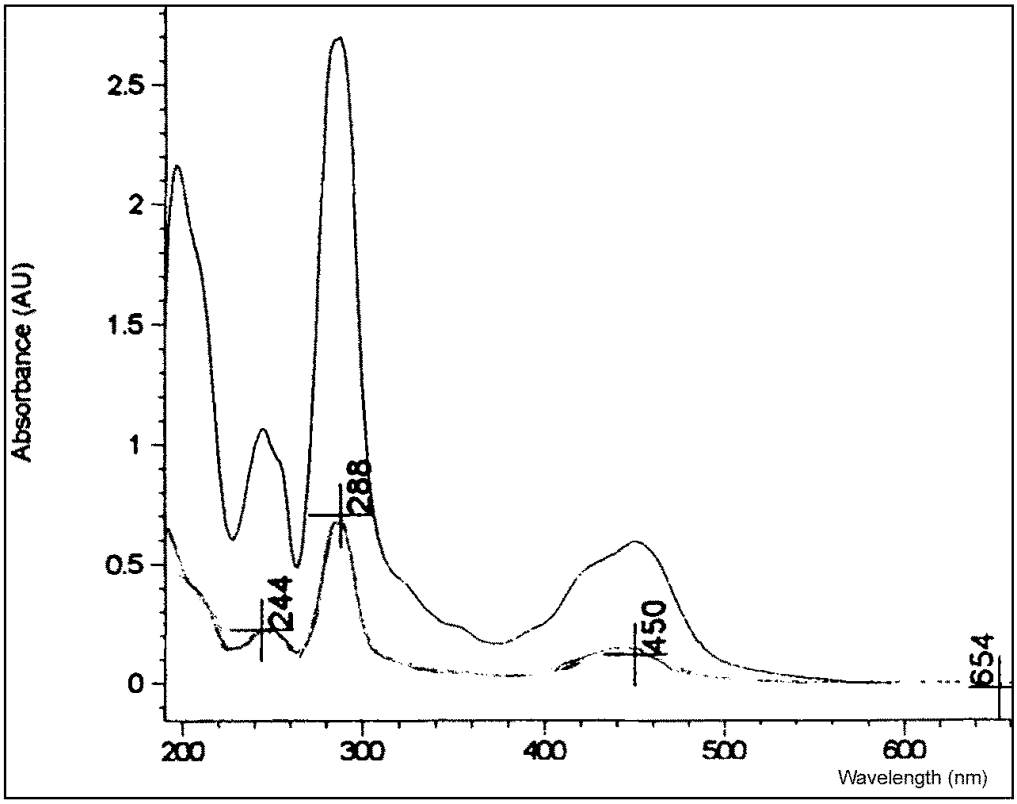

Figure 1.1 Electronic absorption spectra of $[Ru(bpy)_3](PF_6)_2$ in acetonitrile (where bpy = 2,2' bipyridine).

Although the metal centered $d\pi \rightarrow d\sigma^*$ is a Laporte forbidden transition (gerade to gerade), Balzani *et al.*,[8] Lytle and Hercules [10] and Harriman [11] assign the small shoulders at 23 nm, 345 nm and 250 nm and peak at 238 nm to metal centered transitions. Note that Kalyanasundaram ascribes these absorbances to higher energy MLCTs.[7]

The determination of the assignments of electronic absorption processes is aided by the use of spectroelectrochemistry.[12,13] It is surprising that to date the only published UV-Vis, near IR spectroelectrochemical study is from 1981.[14] $[Ru(bpy)_3]^z$ is stable in a variety of oxidation states with z = 2 (neutral with $(BF_4)_2$ counterion, 1 (one electron reduction), 0 (two electron

reduction) and -1 (three electron reduction). These results are shown in Figure 1.2 and Table 1.1. (The appropriate reduction potentials were determined by cyclic voltammetry.)

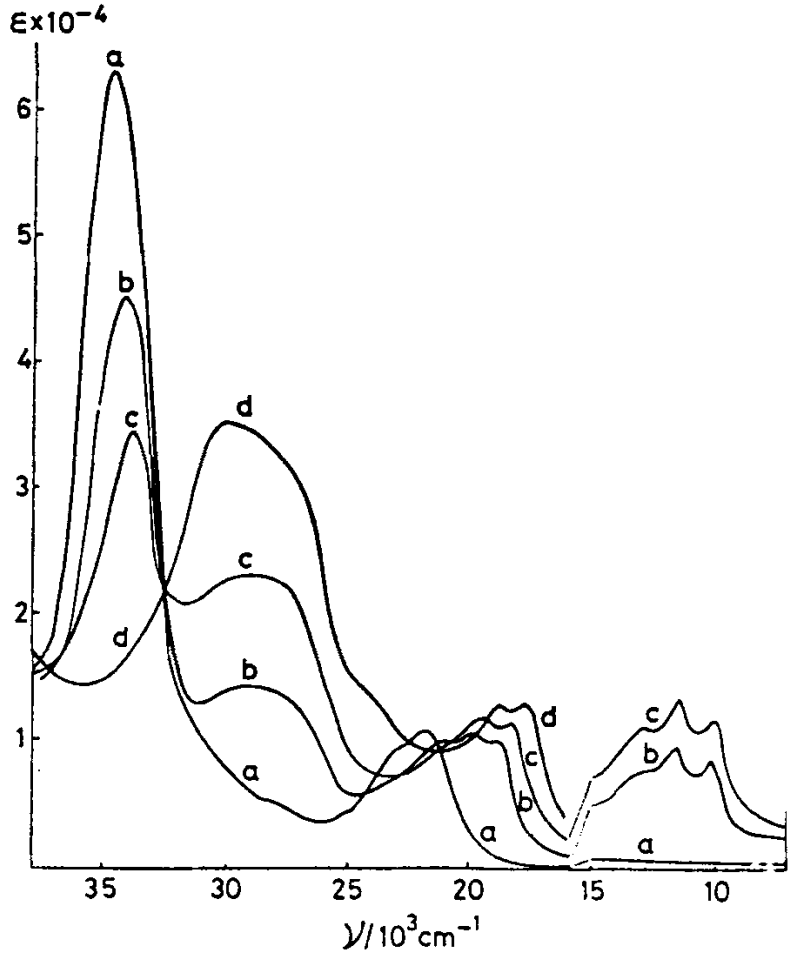

Figure 1.2. Absorption spectra of $[Ru(bpy)_3]^z$ complexes: (a) z = 2+; (b) z = 1+; (c) z = 0; (d) z = 1-; complexes dissolved in dimethyl sulphoxide (UV-Vis region, ε = optical extinction coefficient in mol^{-1} dm^3 cm^{-1}). Heath, G. A.; Yellowlees, L. J.; Braterman, P. S. *J. C. S. Chem. Comm.* **1981**, 287. Reproduced by permission of The Royal Society of Chemistry.

Table 1.1. Cyclic voltammetric data for [Ru(bpy)3](BF4)2 (where bpy = 2,2'-bipyridine).[14]

$E_{1/2}$ (V vs NHE)	Assignment
+1.51	Ru(II)/Ru(III)
-1.07	bpy/bpy^-
-1.26	bpy/bpy^-
-1.53	bpy/bpy^-

The lowest energy transition for ruthenium(II) polypyridyl complexes is typically the Ru ($d\pi$) $\rightarrow$ bpy (π^*) , metal to ligand charge transfer. For $[Ru(bpy)_3]^{+2}$, this occurs at ~450 nm (see Figure 1.1 and 1.2). The location of the higher energy MLCTs cannot be determined by visual inspection of the spectrum of the +2 oxidation state.

The spectroscopy of the +3 oxidation state, Ru(III) adds significant spectral data. Upon oxidation from Ru(II) to Ru(III), the $d\pi$ orbitals are stabilized, if this were not the case, then the subsequent oxidation (+3 to +4) would be potentially observable. As a consequence of the lowering of energy of the $d\pi$ orbitals, the MLCT is shifted out of the UV-Vis window. Therefore, there should be a loss of the 450 nm and 238 nm peaks and the 250 nm shoulder. (Kalyanasundaram proposes that a ligand to Ru(III) charge transfer (LMCT) will be found to the red of the lost MLCT.)[15] The metal- centered, $d\pi \rightarrow d\sigma^*$ shoulders, at 323 nm and 345 nm should also be shifted out of the UV range. The bpy $\pi \rightarrow \pi^*$ transitions, at 288 nm, 205 nm and 185 nm should be slightly red shifted, due to the decreased backbonding, with the lowest energy transition experiencing the greatest red shift.[16]

The spectra of the one electron reduced form $[Ru^{II}(bpy^-)(bpy)_2]^{+1}$ is labeled *b* in Figure 1.2. The newly occupied bpy π^* MO shifts and no longer contributes to the MLCT at 455 nm.

The remaining bpy π^* MOs are destabilized due to increased backbonding. It would seem logical that the new MLCT would be found at a higher energy. The authors assign the lower energy peak at 474 nm as the new MLCT, implying that the metal center is destabilized due to decreased backbonding. The bpy $\pi \rightarrow \pi^*$ transition has red shifted from 286 nm to 292 nm and decreased in intensity, lending further support to the overall destabilization of the metal center and accompanying bpy π MO. The new peak at 342 nm is assigned as a poorly defined bpy^- internal $\pi^* \rightarrow \pi^*$ transition. Upon the second reduction , the MLCT has again red shifted from 474 nm to 481 nm. The peak at 342 nm has increased in intensity and red shifted 3 nm. The bpy $\pi \rightarrow \pi^*$ has red shifted to 296 nm and decreased in intensity.

With the third reduction, each bpy π^* MO has undergone a one electron reduction. This should result in the loss of the MLCT at 481 nm. The authors do not assign an MLCT for this reduction but spectrum *d* shows a peak slightly red shifted from the previously assigned MLCT. In addition to the above assignments, the same authors, in another paper, propose a ligand-ligand inter-valence charge transfer (IVCT), between a reduced bpy π^* and a destabilized, unoccupied bpy π^* MO, at 2220 nm.[17]

In summary, UV-Vis spectroelectrochemistry of a one electron reduced or oxidized form of a complex can confirm the assignment of the lowest energy MLCTs and strongly substantiate the second lowest MLCT. These are the most important transitions in photosensitization applications. The verification of other transitions is less robust. Upon a one electron reduction, the remaining neutral ligand π^* MOs are destablized due to increased

backbonding. This increases the HOMO-LUMO energy gap, thereby creating transitions not usually present in ground state complexes. Thus the results of higher level reductions are very much open to different interpretations and explanations and frequently ask more questions than they answer.

As mentioned above, the lowest energy MLCT is the most significant transition in photochemistry. One extraordinary characteristic of MLCTs is that the resulting excited state molecule is both a better oxidant and reductant than its ground state precursor. Furthermore, the ruthenium polypyridyl complexes are not usually subject to photo-dissociation or ligand substitution in aqueous solutions at room temperature. [18]

The following L*atimer* diagram[19] will be used to illustrate this phenomena.

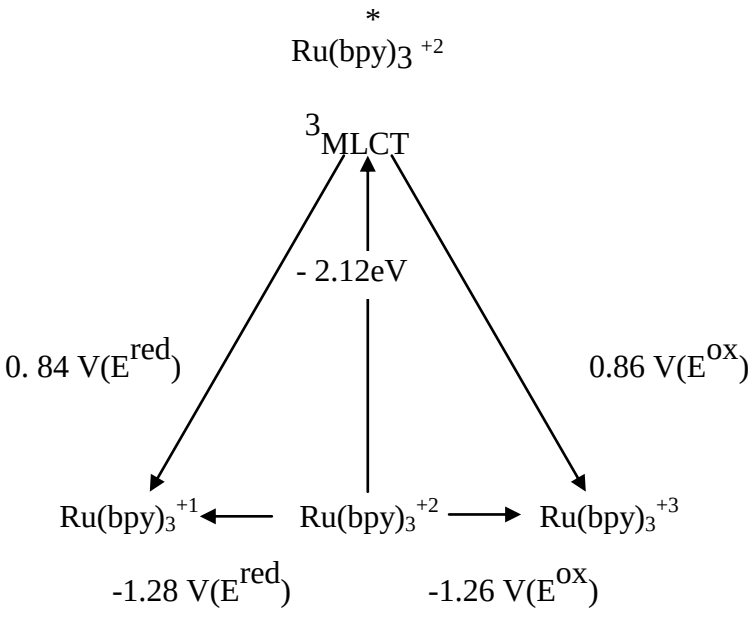

The redox potential of the excited state, $Ru(bpy)_3^{+2}$ cannot be measured directly.

The oxidation potential, $Ru(bpy)_3^{+2*} \rightarrow e^- + Ru(bpy)_3^{+3}$ can be approximated as the sum of the E_{00}, $Ru(bpy)_3^{+2} \rightarrow Ru(bpy)_3^{+2*}$ (2.12 eV) plus the ground state oxidation potential,

$Ru(bpy)_3^{+2} \rightarrow Ru(bpy)_3^{+3} + e^-$ (-1.26V, E^{ox}). Thus the excited state is a stronger reducing agent (0.86V) (E^{ox}) than the ground state $Ru(bpy)_3^{+2}$ (-1.26V)(E^{ox}). The strength of the excited state reduction potential, likewise, follows the same argument.

The first documented photosensitization reaction with $Ru(bpy)_3^{+2}$ was by Adamson and Demas [20] in 1971.

$$Ru(bpy)_3^{+2}$$

$$PtCl_4^{-2} + H_20 \not\longleftarrow \text{No reaction}$$

$$Ru(bpy)_3^{+2}$$

$$PtCl_4^{-2} + H_20 \not\xleftarrow{h\nu} PtCl_3(H_20)^- + Cl^-$$

The $Ru(bpy)_3^{+2}$ acts as a photosensitizer [21] or light absorbing sensitizer [22] (LAS), converting solar energy to available free chemical energy. Two possible mechanisms are possible, energy transfer and outer-sphere electron transfer. The above reaction is one of the few energy transfer quenching reactions, electron transfer reactions being by far the more common.[23]

The best known example of LAS and bi- molecular electron transfer is photosynthesis. It is therefore not surprising that one major thrust of ruthenium polypyridyl research has been in the area of solar energy conversion. The practical and efficient conversion of water into hydrogen and oxygen using $Ru(bpy)_3^{+2}$ as the LAS is a specific area of ongoing research.[24]

An efficient and functioning LAS for photoredox chemistry must fulfill several criteria. (1a) The molecule's absorption spectrum must contain the wavelengths of the MLCTs. (1b) The molar absorptivity must be high. (2) The molecule cannot photodissociate, i.e. there can not be loss of ligands or ligand substitution. (3) The reduction of the ligand and the oxidation of the metal center must be electrochemically reversible. (4) The desired redox reaction must be thermodynamically favorable. (5) The excited state lifetime must be sufficiently long to permit the reaction to occur.[25]

The utility of $Ru(bpy)_3^{+2}$ as a LAS is limited by (1) single electron transfer, (2) a narrow absorption range of the MLCT, and (3) the necessity for bi-molecular collisions.[26] These limitations can be circumvented by the synthesis of multimetallic transition metal systems with polypyridyl bridging ligands and bpy termininal ligands.[27] The four compounds, $[Ru(bpy)(dpb)_2](PF_6)_2$, $[Ru(bpy)_2(dpb)](PF_6)_2$, $[Ru(bpy)_2(dpq)](PF_6)_2$, $[Ru(bpy)(dpb)_2](PF_6)_2$, $[Ru(bpy)(dpq)_2](PF_6)_2$, which are the subject of this thesis, are examples of monometallic LAS, which utilize the bridging ligands 2,3-bis(2-pyridyl)quinoxaline (dpq) and 2,3-bis(2- bipyridyl)benzoquinoxaline (dpb).

The ligand dpq (see Figure 1.3) was first synthesized by Goodwin and Lions in 1959.[28] The mechanism is a Schiff base condensation between the bis-ketone 2,2'-pyridil and the diamine *o*-phenylenediamine. The synthesis of dpb is a modification of the above synthesis in

which *o*- phenylenediamine is substituted by 2,3-diaminonapthalene. Together with the bridging ligand dpp[28], dpq , dpb[29] and the terminal ligand bpy represent a homologous series of diimine ligands.

The incorporation of these ligands within the octahedrally coordinating Ru(II) allows for the tuning of the MLCTs , ligand-centered transitions ($\pi \rightarrow \pi^*$) and excited state lifetimes (according to the energy gap law) [30] as follows. Polypyridyl ligands have nitrogens with lone pairs which form dative bonds with the 6 empty atomic orbitals of ruthenium. The actual nature of the metal ligand bonding is more complex. From a molecular orbital picture, the ligands can donate electron density (σ-donation) and accept electron density (π-backbonding) from the metal center. The degree of stabilization or destabilization is a result of the balance between these two opposing effects. The strength of the σ-donation is reflected in the pKa's of these ligands, for which bpy>dpp>dpq>dpb. The degree of π-backbonding is a function of the extent of conjugation and the presence of empty π^* MOs, with dpb>dpq>dpp>bpy.[31] When the metal center is destabilized by σ-donation or decreased backbonding, the HOMO-LUMO gap is thereby decreased and the absorption wavelength of the MLCT is diminished. The excited state lifetime is concomitantly decreased.

Background on $[Ru(bpy)_2(dpp)](ClO_4)_2$ **:** This compound was first synthesized by Gafney et al. In 1984 [32] by reacting *cis*-$[Ru(bpy)_2Cl_2]$ and dpp in 95% ethanol for 72 hours. The perchlorate salt was precipitated by the addition of aqueous $NaClO_4$ to the hot solution and cooling. The precipitate was recrystallized several times in 1:1 ethanol –water. Elemental analysis showed the compound to have two molecules of hydration. The UV-Vis absorption

spectra showed the typical bpy $\pi \rightarrow \pi^*$ transition (~286 nm) found for $[Ru(bpy)_3]^{+2}$. In the visible region there was one low energy peak at 430 nm and one shoulder at 480 nm. The resonance Raman spectrum confirmed that the shoulder was the Ru ($d\pi$)$\rightarrow$ dpp ($d\pi^*$) MLCT and the 430 nm peak was the Ru ($d\pi$)$\rightarrow$ bpy (π^*) MLCT.

Berger [33] and Gordon and Smith [34] have published the electro-chemistry, spectroelectrochemistry and UV-Vis absorption and emission spectra . From cyclic voltammetry, it was determined that $[Ru(bpy)_2(dpp)]^{+2}$ undergoes one, one electron reversible oxidation (in acetonitrile at +1.45V vs Ag/AgCl) and three reversible, one electron reductions in DMF at –0.91V, -1.32V and –1.56V vs Ag/AgCl.

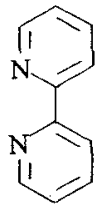

bpy= 2,2'-bipyridine

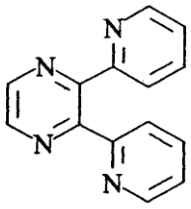

dpp = 2,3-bis(2-pyridyl)pyrazine

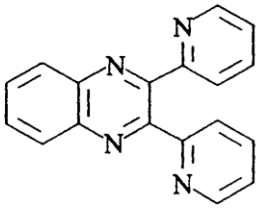

dpq = 2,3-bis(2-pyridyl)quinoxaline

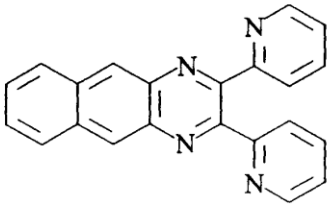

dpb = 2,3-bis(2-pyridyl)benzoquinoxaline

Figure 1.3. Polypyridyl ligands used in this study.

Gordon and Smith found that upon oxidation (+1.5 V) the dpp MLCT at 470 nm was lost and a new lower energy peak at 705 nm grew in, for which they assigned a LMCT . Surprisingly, they do not note that the bpy MLCT at 424 nm is still present after the oxidation, (it should not be present). Furthermore, their spectra of the first reduction was generated at –0.90 V but their recorded CV data finds the reduction to be at –1.06 V (both values vs SCE).

Background on $[Ru(bpy)_2(dpq)](PF_6)_2$: This compound was first synthesized by Rillema and Mack in 1982.[35] $Ru(bpy)_2Cl_2 \bullet 2H_2O$ was reacted with $AgPF_6$ in ~50 ml acetone. After removal of AgCl, dpq was added to the solution and the resulting slurry was refluxed under nitrogen for 24 hours. The resulting solution was reduced in volume and added to an excess of ether. The product was dried under vacuum and purified on an alumina with a 1:1 acetonitrile-methylene chloride mobile phase. Cyclic voltammetry was used to determine the oxidation potential (1.41V vs SSCE) and first two reduction potentials (-0.78 V and –1.41 V vs SSCE). The following assignments were made for the UV-Vis absorption spectra: Ru (dπ) $\rightarrow$ dpq (π^*) MLCT (515 nm, ε=8.1x10^3, Ru (dπ) $\rightarrow$ bpy (π^*) MLCT (427 nm (sh)). Rillema *et al.*[37] have also assigned the shoulders at 391 nm and 350 nm to Ru (dπ) $\rightarrow$ dpq (π_2^*) and Ru (dπ) $\rightarrow$ bpy (π_2^*). The authors did not attempt to distinguish between the dpq $\pi \rightarrow \pi^*$ and the bpy $\pi \rightarrow \pi^*$ transitions.

Gordon *et al.*[36] studied the spectroelectrochemistry of the oxidized form of $[Ru(bpy)_2(dpq)](PF_6)_2$ generated at +1.4V vs SCE and the first reduced form generated at –0.80V vs SCE. Upon oxidation the two lowest energy peaks, 515 nm and 425 nm (sh) disappeared, verifying their assignments of the Ru (dπ) $\rightarrow$ dpq (π^*) MLCT and Ru (dπ)

$\rightarrow$ bpy (π^*) MLCT respectively. In accordance with his data of the oxidation of $[Ru(bpy)_2(dpp)]^{+2}$, Gordon observed a lower energy peak at ~550 nm, having generated $[Ru(bpy)_2(dpq)]^{3+}$, which he assigned as an LMCT transition. Upon reduction of the dpq ligand, the dpq based MLCT was bleached and the remaining bpy based MLCT red shifted due to destabilization of the metal center due to decreased backbonding. He did not use his data to distinguish between bpy vs dpq transitions.

Background on $[Ru(bpy)(dpq)_2](PF_6)_2$ **:** Rillema *et al.*[37] synthesized $[Ru(bpy)(dpq)_2](PF_6)_2$ by reacting two parts dpq and one part $[Ru(bpy)Cl_4]$, in ethylene glycol, for 30 minutes. After filtration of non-dissolved impurities, the product was precipitated by drop-wise addition of saturated $NH_4PF_{6(aq)}$. After collection and drying, the crude product was purified on an alumina column with acetonitrile as the eluent.

Electrochemical measurements were made using differential pulse polarography and cyclic voltammetry. The following half-wave potentials were obtained for $Ru(bpy)(dpq)_2](PF_6)_2$. The oxidation potential was +1.53 V, the first, second and third reduction potentials were –0.66 V, -0.89 V and –1.58 V respectively, vs SSCE.

Electronic transitions were determined from the UV-Vis spectrum and summarized in Table 1.4. The Ru ($d\pi$) $\rightarrow$dpq (π^*) MLCT was found at 512 nm , the Ru ($d\pi$) $\rightarrow$ bpy (π^*) MLCT at 462 nm, a higher energy MLCT Ru ($d\pi$) $\rightarrow$ (π_2^*) at 390 nm (sh) and both dpq $\pi\rightarrow \pi^*$ and bpy $\pi \rightarrow \pi^*$ transitions at 281 nm and shoulders at 256 nm and 330 nm.

The excited state redox potentials were estimated from the emission spectra and ground state redox potentials. Rillema *et al.*[37] concluded that "Ru-BL $^{2+*}$ complexes are poor

reductants relative to $[Ru(bpy)_3]^{+2}$* due to low-energy π^* levels but are good oxidants due to low energy enhanced dπ- π^* interactions."

***Background on $[Ru(bpy)_2(dpb)](PF_6)_2$*:** This compound was first synthesized by Carlson, Wolosh and Murphy in 1991.[38] The protocol for the synthesis is referenced by them as "manuscript in preparation", yet there is no record of this publication on record. The comparative electrochemistry of $[Ru(bpy)_2(dpb)](PF_6)_2$ and $[Ru(dpb)_3](PF_6)_2$ was synthesized and published by Carlson and Murphy in 1991.[39] Brewer *et al.*[40] published the electrochemical properties of $[Ru(bpy)_2(dpb)](PF_6)_2$ in 1992. (see Table 1.2.)

Table 1.2. A comparison of cyclic voltammetric Data for $[Ru(bpy)_2(dpb)](PF_6)_2$ (where bpy = 2,2'- bipyridine and dpb = 2,3-bis(2-pyridyl)benzo-quinaxoline).[a]

$E_{1/2}$ (Brewer)[40] (mV)	$E_{1/2}$ (Murphy)[39]	Assignment
1766	1666	Ru(II)/Ru(III)
-334	-394	dpb/dpb$^-$
-974	-1054	bpy/bpy$^-$
-1314	-1374	bpy/bpy$^-$

[a] Potentials reported in CH_3CN solution with 0.1 M TBAH and converted to a single NHE scale.

Note the 50 to 100 mV discrepancy in values.

The electron absorption characteristics were briefly discussed by Murphy and Carlson. They reported the Ru (π) $\rightarrow$dpb (π^*) MLCT , (at 550 nm) with a molar absorptivity of 8.2 x 10^3 M^{-1} cm^{-1} . Nallas and Brewer more completely correlated the UV-Vis spectra with electronic transitions.[41] (see Table 1.4).

Gordon *et al* [36] studied the spectroelectrochemistry of the oxidation and first reduction of $[Ru(bpy)_2(dpb)](PF_6)_2$ in 1997. Upon oxidation at 1.5V, the Ru (π) $\rightarrow$dpb (π^*) MLCT at 550 nm and Ru (π) $\rightarrow$bpy (π^*) MLCT at 425 nm (sh) were bleached and a new peak appeared at ~ 575 nm; it was assigned as a LMCT. Upon reduction at –0.8 V, the Ru (π) $\rightarrow$dpb (π^*) MLCT was lost and the Ru (π) $\rightarrow$bpy (π^*) MLCT was red shifted to ~ 475 nm. In comparing the assignments of Gordon and Nallas, Gordon identified a shoulder at ~425 nm to which he made the assignment of Ru (π) $\rightarrow$dpb (π^*) MLCT whereas Nallas did not acknowledge the shoulder and assigned the peak at 394 nm for this transition. Gordon thought that this peak at 394 nm was a dpb $\pi \rightarrow \pi^*$ transition. Brewer and Nallas, on the other hand , attributed this transition to a shoulder at 362 nm, which received no assignment by Gordon.

Table 1.3. Summary of Electrochemical Data:

Cyclic voltammetric data for $[Ru(bpy)_2(dpq)](PF_6)_2$, $[Ru(bpy)_2(dpb)](PF_6)_2$, $[Ru(bpy)(dpq)_2](PF_6)_2$ and $[Ru(bpy)(dpb)_2](PF_6)_2$.

COMPOUND	E1/2 (MV) vs NHE	ASSIGNMENT
$[Ru(bpy)_2(dpq)](PF_6)_2$ [35]	1.67	Ru(II)/Ru(III)
in 0.1M TEAP-CH_3CN	-0.54	dpq/dpq^-
at 20 +/- ^oC	-1.17	bpy/bpy^-
		*b*py/bpy^- [d]
$[Ru(bpy)_2(dpb)](PF_6)_2$ [39]	1.67	Ru(II)/Ru(III)
in 0.1 M TBAH-CH_3CN	-0.39	dpb/dpb^-
	-1.05	bpy/bpy^-
	-1.37	bpy/bpy^-
$[Ru(bpy)(dpq)_2](PF_6)_2$ [37]	1.77	Ru(II)/(III)
in 0.1 M TEAP-CH_3CN at	-0.42	dpq/dpq^-
25 +/- ^oC	-0.65	dpq/dpq^-
	-1.34	bpy/bpy^-

[d] An adsorption wave interfered with the determination of this potential.

Table 1.4 Summary of Electronic Absorption Spectroscopy:

The electronic absorption spectroscopy of $[Ru(bpy)_2(dpq)](PF_6)_2$, $[Ru(bpy)_2(dpb)](PF_6)_2$, $[Ru(bpy)(dpq)_2](PF_6)_2$ and $[Ru(bpy)(dpb)_2](PF_6)_2$ in acetonitrile.

Compound	Wavelength	Molar Absorptivity ($M^{-1}\,cm^{-1}$)	Assignment
$[Ru(bpy)_2(dpq)](PF_6)_2$ [37]	517 nm	$8.46x10^3$	$Ru(d\pi)\rightarrow dpq(\pi^*)$MLCT
	426 nm	$8.7x10^3$	$Ru(d\pi)\rightarrow bpy(\pi^*)$MLCT
	391,350 nm (sh)		$Ru(d\pi)\rightarrow (\pi_2)^*$ MLCT
	325 (sh)		$\pi \rightarrow \pi^*$
	284 nm	$7x10^4$	$\pi \rightarrow \pi^*$
$[Ru(bpy)(dpq)_2](PF_6)_2$ [37]	512 nm	$9.6x10^3$	$Ru(d\pi)\rightarrow dpq(\pi^*)$MLCT
	462 nm	$8.3x10^3$	$Ru(d\pi)\rightarrow bpy((\pi^*)$MLCT
	390 nm (sh)		$Ru(d\pi)\rightarrow (\pi_2^*)$ MLCT
	256,330 nm (sh)		$\pi \rightarrow \pi^*$
	281 nm	$6.9x10^4$	$\pi \rightarrow \pi^*$
$[Ru(bpy)_2(dpb)](PF_6)_2$ [36]	550 nm	$8.3x10^3$	$Ru(d\pi)\rightarrow dpb(\pi^*)$MLCT
	425 nm (sh)		$Ru(d\pi)\rightarrow bpy\ (\pi^*)$MLCT
	392 nm(sh)		dpb $\pi \rightarrow \pi^*$
	314 nm	$4.5x10^4$	
	285 nm	$6.8x10^4$	bpy $\pi \rightarrow \pi^*$
	242 nm	$4.5x10^4$	$\pi \rightarrow \pi^*$
$[Ru(bpy)_2(dpb)](PF_6)_2$ [41]	550 nm	$9.5x10^3$	$Ru(d\pi)\rightarrow dpb(\pi^*)$MLCT
	394 nm	$1.4x\ 10^4$	$Ru(d\pi)\rightarrow bpy\ (\pi^*)$MLCT
	362 nm(sh)		dpb $\pi \rightarrow \pi^*$
	286 nm	$7.5x10^4$	bpy $\pi \rightarrow \pi^*$

Statement of Purpose

In summary, the goal of this work is to probe the electrochemical, electron absorption spectroscopic and spectroelectrochemical properties of ruthenium(II) complexes with polyazine bridging ligands, focusing on the dpb ligand. This involved the preparation and study of the new complex $[Ru(bpy)(dpb)_2](PF_6)_2$ as well as the previously reported compounds $[Ru(bpy)(dpq)_2](PF_6)_2$, $[Ru(bpy)_2(dpb)](PF_6)_2$ and $[Ru(bpy)_2(dpq)](PF_6)_2$.

References

1. Cotton, S. A.; Hart, F. A. The Heavy Transition Elements. 1975, 59, Wiley, New York.
2. Sienko, M.; Plane, R. Chemistry: Principles and Properties. 1966, 437, McGraw-Hill, New York.
3. Cotton, F.A.; Wilkinson, G. Advanced Inorganic Chemistry. 1988, 885, John Wiley, New York.
4. Griffith, W. P. The Chemistry of the Rarer Platinum Metals (Os, Ru, Ir and Rh). 1967, 136, John Wiley, New York.
5. Sienko et al. Op. Cit., 437.
6. Paris, J. P.; Brandt, W. W. J. Amer. Chem. Soc. 1959, 5001.
7. Kalyanasundaram, K. Photochemistry of Polypyridine and Porphyrin Complezes. 1992, 107, Academic Press, San Diego.
8. Balzani, V.; Barligelletti, F.; De Cola, L. Top. Curr. Chem. 1990, 158, 31.
9. Roundhill,D.M. Photochemistry and Photophysics of Metal Complexes. 1994, 167, Plenum, New York.
10. Lytle, F. E.; Hercules, D. M. J. Am. Chem. Soc. 1969, 91, 253.
11. Harriman, A. J. Photochem. 1978, 8, 205.
12. Bridgewater, J. S.; Vogler, L. ; Molnar, S.; Brewer, K. Inorg. Chim. Acta. 1993, 179.
13. Scott, S.; Gordon, K. Inorg. Chim. Acta. 1997, 254, 267.
14. Heath, G. A.; Yellowlees, L. J.; Braterman, P. S. J. C. S. Chem. Comm. 1981, 287.
15. Rillema, D. P.; Allen, G. ; Meyer ,T. J.; Conrad, D. Inorg. Chem. 1983, 22, 1617.
16. Nazeeruddin, M. K.; Zakeeruddin, S. M.; Kalyanasundaram, K. J. Phys. Chem. 1993, 97, 9607.
17. Heath, G. A.; Yellowlees, L. J.; Braterman, P. S. Chem. Phys. Lett. 1982, 92, 6, 647.

18. Roundhill, D. M. Op. Cit., 175.

19. Roundhill, D. M. Op. Cit., 175.

20. Demas, J. N.; Adamson, A. W. J. Am. Chem. Soc. 1971, 93, 1800.

21. Kalyanasundaram, K. in Photosensitization and Photocatalysis Using Inorganic and Organometallic Compounds, Ed. By Kalyanasundaram, K.; Gratzel, M., 1993, 113, Kluwer, Norwell MA.

22. Balzani, V.; Maestri, M. in. Photosensitization and Photocatalysis Using Inorganic and Organometallic Compounds, Ed. By Kalyanasundaram, K.; Gratzel, M., 1993, 33, Kluwer, Norwell MA.

23. Kalyanasundaram, Op. Cit., 161.

24. Kalyanasundaram, Op. Cit., 142.

25. Moggi, L. In Photoelectrochemistry, Photocatalysis and Photoreactors, Ed. Schiavello.M. Nato ASI Series.1984, 197-216, Reidel, Boston.

26. Richter, M. M.; Brewer, K. J. Inorg.Chem. 1993, 32, 5762.

27. Roundhill, Op. Cit., 197.

28. Goodwin, H. A.; Lions, F. J. Am. Chem. Soc. 1959, 81, 6415.

29. (a) Biaino, J. A.; Carlson, D.L.; Wolosh, G. M.; DeJesus, D. E.; Knowles, C. F.; Szabo, E. G.; Murphy, W. R. Inorg. Chem. 1990,29, 2327. (b) Stephen , W. I. And Uden, P. C. Anal Chim Acta, 1967, 39, 357. (c) Jensen, R. E. and Pflaum, R. T. J. Heterocycl. Chem 1, 1964, 295. (d) Escuer, A.; Comas, T.; Ribas, J.; Vicente, R. Inorg. Chim. Acta. 1989, 162, 97.

30. Kalyanasundaram, Op. Cit.,20-23.

31. (a) Bridgewater, J. S.;Vogler, L. M.; Molnar, S.M.; Brewer, K. J. Inorg. Chim. Acta. 1993, 208, 179. (b) Richter, M. M.; Brewer, K. J. Inorg. Chem. 1993, 32, 5762.

32. Braunstein, C. H.; Baker, A. D.; Strekas, T. C.; Gafney, H. D. Inorg. Chem, 1984, 23, 857.

33. Berger, R. M. Inorg. Chem. 1990, 29, 1920.

34. Scott, S. M.; Gordon, K. C. Inorg. Chim. Acta. 1997, 254, 267.

35. (a) Rillema, D. P.; Callahan, R. W.; Mack, K. B. *Inorg. Chem.* 1982, 21, 2389. (b) Rillema, D. P.; Mack, K. B. *Inorg. Chem.* 1982, 21, 3849.

35. Scott, S. M.; Gordon, K. C. *Inorg. Chim. Acta.* 1997, 260, 199.

36. Rillema, D. P.; Taghdiri, D. G.; Jones, D. S.; Keller, C. D.; Worl, L. A.; Meyer, T. J.; Levy, H. A. *Inorg. Chem*. 1987, 26, 578.

37. Carlson, D. L.; Wolosh, G. M.; Murphy, Jr. W. R. ?, 1991/1992.

38. Carlson, D. L.; Murphy, W. R. *Inorg. Chim. Acta.* 1991, 181, 61.

39. Molnar, S. M.; Neville, K. R.; Jensen, G. E.; Brewer, K. J. *Inorg. Chim. Acta.* 1993, 206, 69.

40. Nallas, G.N.A. and Brewer, K.J. *Inorg. Chim. Acta.* 1997, 257, 27.

CHAPTER TWO: EXPERIMENTAL METHODS

Materials

HPLC grade acetonitrile was purchased from Mallinckrodt. It was further purified by distillation over $CaCl_2$ chips in a N_2 atmosphere. $RuCl_3 \bullet 3H_2O$ was procured from Johnson Matthey/Alfa Aesar . The terminal ligand 2,2'-bipyridine was purchased from Aldrich. $[Ru(bpy)_2(dpq)](PF_6)_2$ was synthesized by Carla Wibble using a modified synthetic procedure of Rillema and Mack.[1] $[Ru(bpy)(dpq)_2](PF_6)_2$ was synthesized by Carla Wibble using a modified synthetic procedure of Rillema *et al.*[2]

Electronic Absorption Spectroscopy

UV-Vis spectra were recorded at room temperature with A HP 8452A diode array spectrophotometer having 2 nm resolution, using 1cm path length quartz cuvettes. Samples were dissolved in acetonitrile.

Cyclic Voltammetry and Osteryoung Square Wave Voltammetry

All electrochemistry was performed using a Bio Analytical Systems 100 W potentiostat and accompanying software. Analytes were dissolved in acetonitrile containing 0.1M TBAH. A three-electrode system was used, consisting of a BAS Pt wire secondary electrode, BAS epoxy impregnated 1.6 mm Pt working electrode and a BAS Ag/AgCl aqueous reference electrode which was calibrated with ferrocene. The ferrocene to ferrocenium oxidation was used as a reference of 660 mV vs NHE.[3]

Spectroelectrochemistry, Bulk (H-cell) Construction and Operation

The H-cell consisted of a 1 cm quartz cuvette (vertical) fused to a horizontal glass tube with a medium glass frit (constructed by the glass shop)(Figure 2.1).[4] Adjoining the horizontal connecting portion was another vertical glass compartment. The platinum wire counter electrode was immersed in the vertical glass compartment which was filled with solvent and supporting electrolyte. It may contain the analyte to minimize a concentration gradient. The working electrode, which consisted of a platinum gauze, was immersed in the quartz cuvette which contained solvent (acetonitrile), TBAH (supporting electrolyte) and analyte. The reference electrode was positioned above the working electrode and was separated by a medium porosity glass frit. The solution in the quartz cuvette was mixed and deoxygenated by bubbling with argon. The potentials for oxidation and reduction were determined by cyclic voltammetry. The potentials chosen were more negative (for reduction) by approximately 0.2 V and around 0.2V more positive for oxidation. Prior to each spectral acquisition, the argon was turned off. Initially the ground state UV-Vis spectra was taken at 0 V. The potential was then changed and periodic spectra were taken. The current display on the potentiostat decreased as the amount of the electrochemically generated product increased (which implies that the amount of the starting material decreased. The completion of each electrochemical step was determined by both a lack of change in spectra and diminished current. Experience showed that the less concentrated the original solution, the less the analysis time (very profound), therefore very dilute solutions were used. After each electrochemical step, the reversibility of that step was tested by returning to the initial potential. The degree of

reversibility was gauged by the degree of superimposibility between the original and last spectrum.

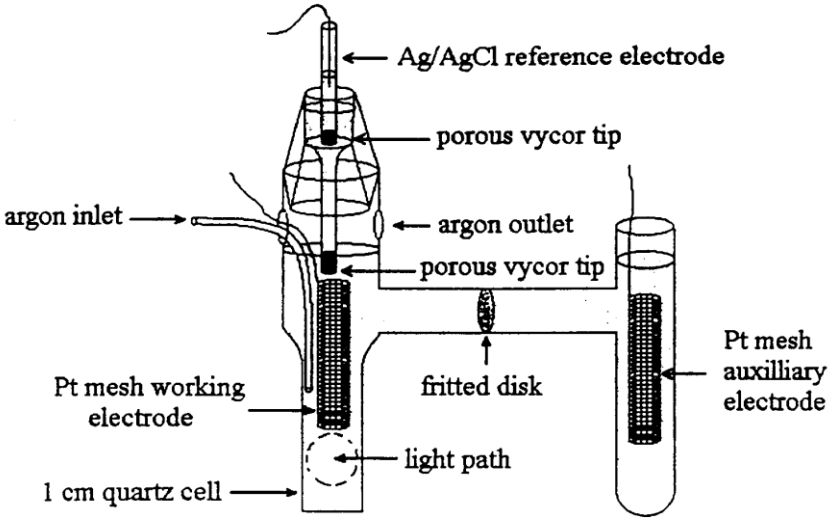

Figure 2.1. H-cell for bulk spectroelectrochemistry.

Optically transparent thin layer cell

The design for the OTTLE cell was a slightly-modified version of Krejcik *et al.* (Figure 2.2).[5] The cell utilized a Perkins-Elmer demountable IR cell. For UV-Vis spectra, quartz windows were substituted for salt optical windows. A three electrode system was sandwiched between two sheets of 6mm polyethylene and fused together with a thermostated hydraulic press. The pseudo-reference was made from three strands of 0.05 mm silver wire wrapped together. The counter electrode was made from a piece of Pt gauze. The working electrode was made from a 100 line/inch gold cloth (Buckbee Mears). Silver paint (Aldrich) was used to join 0.10 mm silver leads to the appropriate electrode. The cell has been modified by extending the polyethylene sheets to where there is a dam with ~1 mm opening between the working and counter electrode. A specially designed platform was built (by physics machine shop) to screw

into the sample-holder base and hold the OTTLE cell so that the optical window and beam path were coincident.

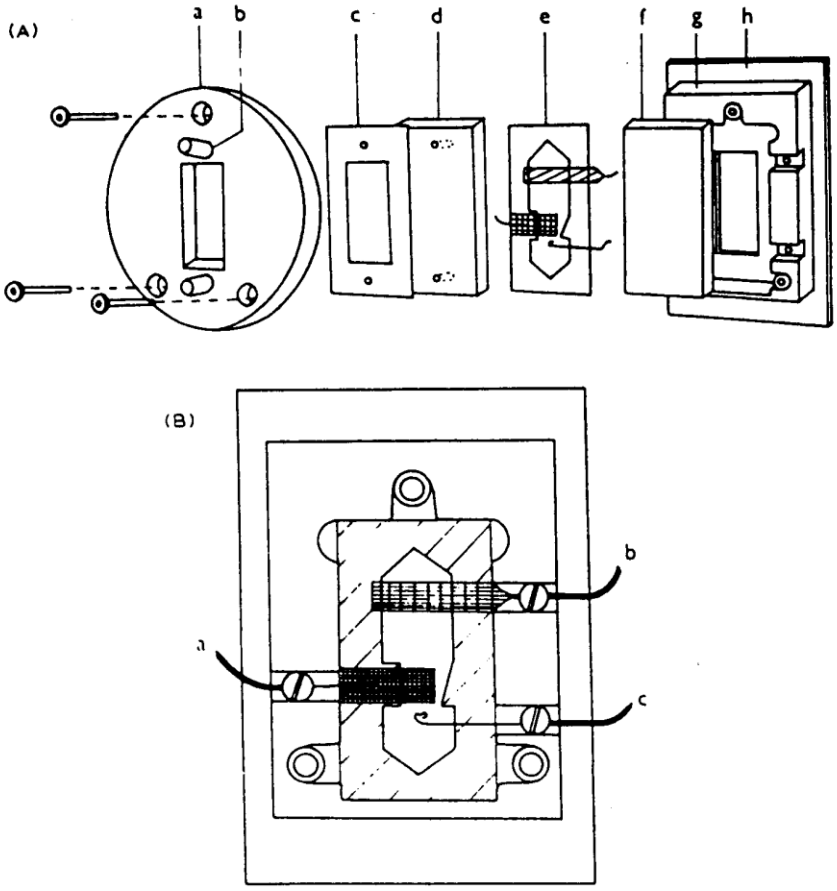

(A) Schematic diagram of the IR OTTLE cell with the three electrode system placed inside the thin layer. (a) Steel pressure plate; (b) inlet; (c) Teflon gasket; (d,f) front and back KBr windows; (e) polyethylene spacer with melt-sealed electrodes; (g) Teflon holder; (h) back plate. (B) Front view of the cell composed of the parts (e)-(h) of (A) showing the position of the electrodes and their soldered contacts with Cu conductors fixed by screws. (a) Au minigrid working electrode with

Figure 2.2. The OTTLE cell of Krejcik *et al.*[5]
Reprinted from *Journal of Electroanalytical Chemistry,* Vol 317, Krejcik, M.; Danek, M.; Hartl, J., pp179, 1991, with permission of Elsevier Science".

Prior to mounting the OTTLE cell in the platform cell, the blank sample (0.1M TBAH in deoxygenated CH_3CN) was syringed into the cell via one Luer port. Air and excess solution came out from the opposite port. Once free of air bubbles, the ports were capped. The cell was mounted and appropriate electrode leads were connected. The short optical path length (~0.17 mm) of the OTTLE cell necessitated a more concentrated solution as compared to the H-cell. Due to the small volume and large ratio of the surface area of the working electrode to volume, the analysis time was greatly shortened. Complete reductions or oxidations were completed in one to three minutes. The experimental procedures for the spectral acquisition of spectroelectrochemical data was similar to the protocol for the H-cell.

Mass Spectroscopy

Mass spectra were determined with a Fisions Instruments VG Quattro Triple Stage Quadrapole Mass Spectrometer. Although commonly called Fast Atom Bombardment, in positive ion mode, (FAB+), Liquid Secondary Ionic Mass Spectroscopy (LSIMS) is a more accurate acronym. The sample molecules, dissolved in a matrix of glycerol or nitro- benzyl alcohol, are ionized by collision with a beam of cesium ions which are accelerated by a 20 kV bias.

Synthesis

TBAH

Tetrabutyammoniumhexafluorophosphate (TBAH). Single batches were made by combining Bu_4NBr (Aldrich) (50.0g, 231 mmol in 600 mL deionized water) and KPF_6 (Aldrich) (31.0g, 168 mmol in 50 mL DI water). The precipitate, $TBAH_{(s)}$, was separated

from $KBr_{(aq)}$ (supernatant) by vacuum filtration. The TBAH was then dissolved in 800 ml hot ethanol. DI water was then added to make a saturated solution (~400ML). The solution was cooled to facilitate crystallization. Two to three additional recrystallizations were performed. The product was vacuum dried at ~87 ^{o}C and analyzed by cyclic voltammetry for purity. Figure 2.3 shows a representative CV. Note that there is no superoxide peak at ~-0.8 V and no reduction of hydrogen (from water contamination) at the –1.8 V.

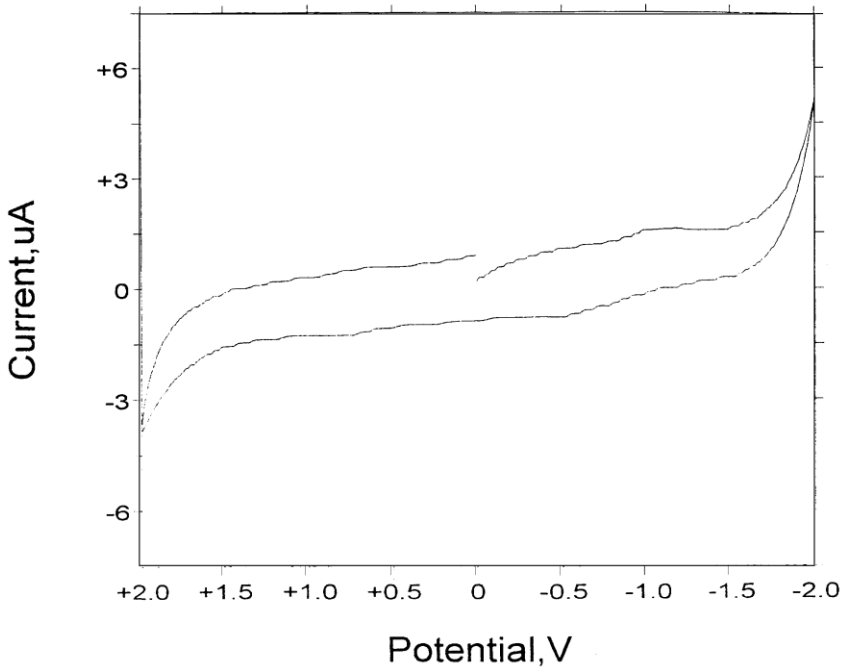

Figure 2.3. Background CV of 0.1 M TBAH in acetonitrile at room temperature using a Ag/AgCl reference electrode.

2,3-bis(2-pyridyl)quinoxaline (dpq)

The synthesis was a modification of Goodwin and Lions [6] . *O*-phenylenediamine (Aldrich)(2.16 g, 20.0 mmol) and 2,2'-pyridil (4.24 g, 20.0 mol) were dissolved in 50 ml 100% ethanol and heated for 2 hours. The product was recrystallized 5 times in 100% ethanol.

2,3-bis(2-pyridyl)benzoquinoxaline (dpb)

The synthesis was a modification of Goodwin and Lions.[6] 2,3-diaminonapthalene (2.498 g, 15.78 mmol) and 2,2'-pyridil (3.393 g, 15.98 mmol) were dissolved in 125 ml 100% ethanol and refluxed for 5 hours and cooled overnight.

The precipitate was recrystallized in ~30 ml 100% ethanol and dried by evaporation. Yield was 2.1 g or 41%. The product was further purified on an alumina column with methylene chloride as eluent. The final purified product was analyzed for purity by absence of C=O stretch from 1690 to 1760 cm^{-1} in IR spectra. Analysis by cyclic voltammetry and UV-Vis spectroscopy were also performed.

Bis(2,2'-bipyridine) ruthenium(II) dichloride. [$Ru(bpy)_2Cl_2$]

The synthesis was according to Sullivan *et al.*[7] $RuCl_3 \bullet 3H_2O$ (4.73 g, 180 mmol), 2,2'-pyridyl (bpy)(5.62 g, 36.0 mmol), LiCl (3.79 g, 90.0 mmol) were dissolved in 35 mL DMF and heated for 7.5 hours. After addition of a liberal amount of acetone, the solution was cooled in the refrigerator overnight. The product was then isolated by vacuum filtration with a glass frit. The filtrate was washed with a copious amount of DI water and diethyl ether and then dried in a dessicator with CaH_2 chips.

2,2'-bipyridine ruthenium(II) tetrachloride.[$Ru(bpy)Cl_4$]

The synthesis was described by Krause.[8] $RuCl_3 \bullet 3H_2O$ (5.15g, 19.7 mmol) and 2,2'-bipyridyl (3.75g, 24.0 mmol) were combined with 25 ml 1N HCl . The components were left in covered

beaker for ~2.5 months. The product was collected by vacuum filtration with a glass frit and dried over P_2O_5. The product was analyzed by LSIMS. See Appendix Figure 3.8.

Bis(2,2'-bipyridine)2,3-bis(2'-pyridyl)benzoquinoxaline)ruthenium(II) Hexafluorophosphate.

$[Ru(bpy)_2(dpb)](PF_6)_2$

$Ru(bpy)_2Cl_2$ (0.258 g, 0.532 mmol) and

dpb (0.174 g, 1.11 mmol) were dissolved in 30 mL ethanol and 15 mL DI water and refluxed for 2.5 hours. The product was precipitated by the addition of 100 mL saturated KPF_6 and isolated by vacuum filtration with a glass frit. Product was washed with ethanol and diethyl ether. Final product was dried in a dessicator for 2 days. Yield was 0.486 g or 88.1% .

(2,2'-bipyridine)(2,3-bis(2-pyridyl)quinoxaline)ruthenium(II) Hexafluorophosphate.

$[Ru(bpy)(dpq)_2](PF_6)_2$:

This synthesis is a modification of the literature synthesis of Rillema *et al.*[2] $Ru(bpy)Cl_4$ (0.223 g, 0.853 mmol) and dpq (0.382 g, 1.34 mmol) were combined with 30 ml 95% ethanol and heated for ~ 5 days under argon. An 80 ml saturated solution of KPF_6 was diluted with 40 ml DI water and added to the reacted solution. The mixture was cooled in the refrigerator and stored therein for further purification.

(2,2'-bipyridine)(2,3-bis(2-pyridyl)benzoquinoxaline)ruthenium(II) Hexafluorophosphate.

$[Ru(bpy)(dpb)2](PF6)_2$

Ru(bpy)Cl4 (0.209 g,mmol) and dpb (0.345g, 1.03 mmol) were combined with 40mL 95% ethanol and 15 ml DI water. This as heated under water, argon for ca. 5 days. An 80 ml saturated solution of KPF6 was diluted with 40 ml DI which was then added to the round

bottom flask and refrigerated for several days. The products were collected by vacuum filtration, with a glass frit and dried with ca. 150 ml diethyl ether. Ethanol was mistakenly added to the drying product which resulted in some loss of product as indicated by the eluent changing color from clear to purple. The dried product was analyzed with LSIMS (see Figure 3.4) and purified by alumina chromatography. The dpb (yellow band) was first eluted using 1:2, acetonitrile/toluene . The remaining purple band was removed from the column and added as a slurry on a shorter column to speed purification, using 2:1 acetonitrile/toluene. Two bands were collected, the first, dark purple and the second, dark pink. The first band was evaporated to precipitate the product. This product was dissolved in a minimal amount of acetonitrile and run through another alumina column (smaller bore, shorter length) with 2:1 acetonitrile/toluene mobile phase. From this dark purple band, three eluents were collected, evaporated under vacuum and dissolved in pure acetonitrile. The final product (actually three) was flash precipitated by addition of diethyl ether, filtered and dried.

References

1. Rillema, D. P.; Mack, K. B. *Inorg. Chem.* 1982, 21, 3849.
2. Rillema, D. P.; Taghdiri, D. G.; Jones, D. S.; Keller, C. D.; Worl, L. A.; Meyer, T. J.; Levy, H. A. *Inorg. Chem*. 1987, 26, 578.
3. Gagne, R. R.; Koval, C. A.; Lisensky, G. C. *Inorg. Chem*. 1980, 19, 2855.
4. Jones, S. W. Ph.D. Thesis, p 50. Virginia Tech, 1999.
5. Krejcik, M.; Danek, M.; Hartl, J. *J. Electroanal. Chem.* 1991, 317, 179.
6. Goodwin, H. A.; Lions, F. *J. Am. Chem. Soc.* 1959, 81, 6415.
7. Sullivan, B. P.; Salmon, D. J.; Meyer, T, J. *Inorg. Chem.* 1978, *17*, 3334.
8. Krause, R. A. *Inorgica Chimica Acta.* 1977, 22, 209.

CHAPTER THREE: RESULTS

The four ruthenium polyazine bridging ligand complexes were prepared according to a similar two step synthetic strategy whereby (1) the terminal ligand, bpy, was first bound to the ruthenium metal center and (2) the bridging ligand was bound to the metal center of the intermediate. After purification on neutral alumina, compounds were analyzed for identity and purity.

Identification using Liquid Secondary Ion Mass Spectroscopy

Elemental analysis was not performed on our polyazine complexes of ruthenium (II) because of its inability to clearly distinguish monometallic mixed ligand complexes and bimetallic complexes.[1] For example, when comparing $[Ru(bpy)_2(dpq)](PF_6)_2$ and $\{[Ru(bpy)_2]_2(dpq)\}(PF_6)_4$, the % (N / total N, C, H) is 18.8 % and 18.7% respectively. The % (C/ total C, N, H) is 56 % vs 54 %. For H the % is 5 % vs 6 % . Furthermore, solvents of crystallization are a common complicating factor.

Instead, identifications were determined with FAB^+-MS (more precisely LSIMS) Accurate mass spectral interpretation requires that the LSIMS of matrices, starting materials and intermediates be known. The LSIMS of the two matrices used, glycerol (MW 92+1) and nitro-benzyl alcohol (MW 153+1) are seen in Appendix Figures 3.1 and 3.2. The LSIMS of the free ligands bpy, dpq and dpb are shown Appendix Figures 3.3, 3.4, 3.5. The LSIMS of $[Ru(bpy)Cl_4]$ (MW 399) , as seen in Appendix Figure 3.6, does not indicate that the molecular ion is present. In fact, peaks at 449 m/z and 414 m/z could be $[Ru(bpy)_2Cl]^+$ and $[Ru(bpy)_2]^+$ respectively. Note the peak at 207 m/z, this may be evidence of the unreacted reactant $RuCl_3$ minus the three waters of hydration. The mass spectrum of the final product

$[Ru(bpy)_2(dpb)](PF_6)_2$ (MW 1038), is shown in Figure 3.1. The peak at 892 m/z is $[Ru(bpy)_2(dpb)](PF_6)^+$. The peak at 750 m/z represents $[Ru(bpy)_2(dpb)]^+$. The mass spectrum of $[Ru(bpy)_2(dpq)](PF_6)_2$ (MW 988) is shown in Figure 3.2. The mass peak at 842 m/z is the $[Ru(bpy)_2(dpq)](PF_6)^+$ cation, the peak at 695 m/z is $[Ru(bpy)_2(dpq)]^+$. The peak at 412 m/z represents $[Ru(bpy)_2]^+$. The mass spectrum of $[Ru(bpy)(dpq)_2](PF_6)_2$ (MW 1117) is seen in Figure 3.3. The peaks at 973 m/z and 826 m/z are the cations $[Ru(bpy)(dpq)_2](PF_6)^+$ and $[Ru(bpy)(dpq)_2]^+$ respectively. The $LSIMS^+$ mass spectrum of $[Ru(bpy)(dpb)_2](PF_6)_2$ (MW 1217) is displayed in Figure 3.4. The mass peaks at 1071 m/z and 926 m/z are the cations $[Ru(bpy)(dpb)_2](PF_6)^+$ and $[Ru(bpy)(dpb)_2]^+$ respectively. The mass peak centered at 1104 m/z may implicate a chloride adduct.

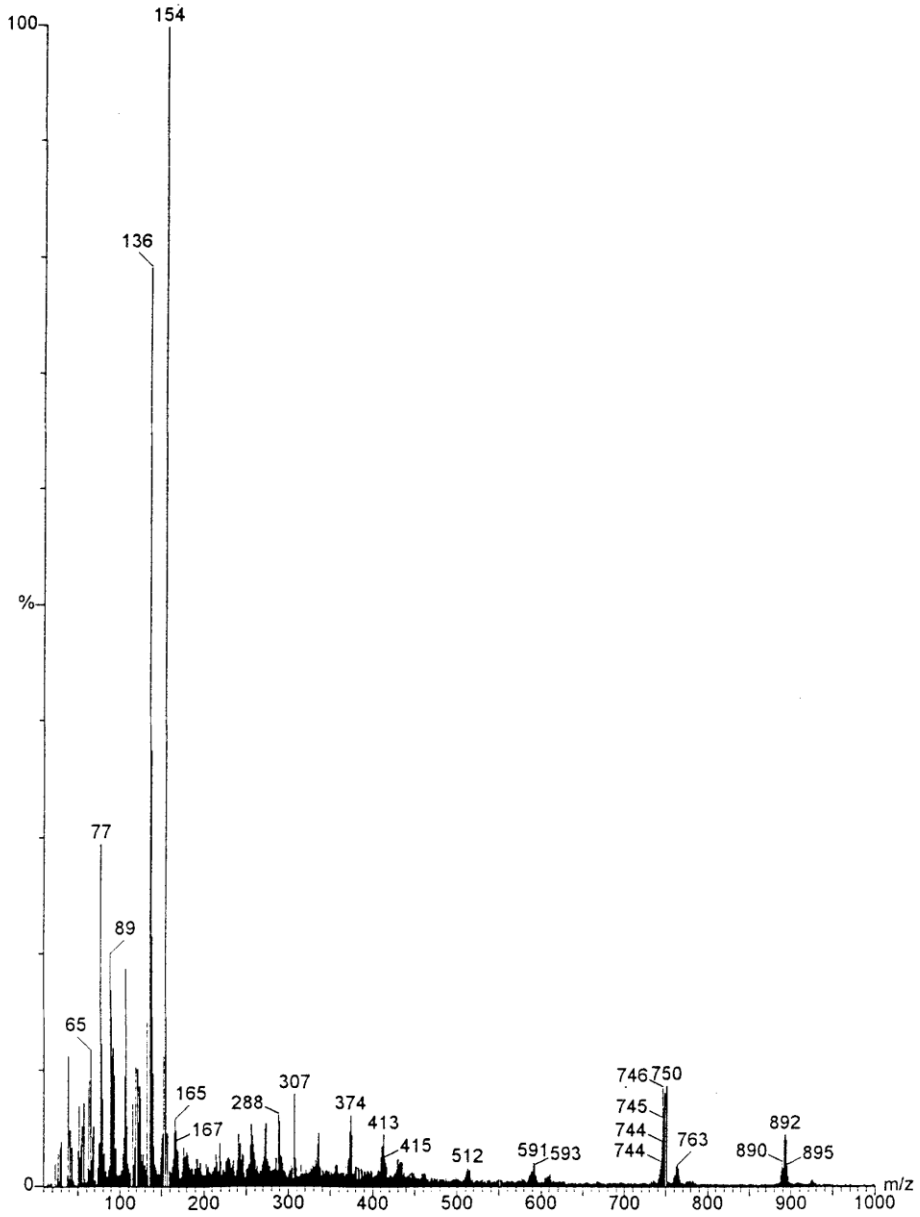

Figure 3.1. LSIMS of $[Ru(bpy)_2(dpb)](PF_6)_2$

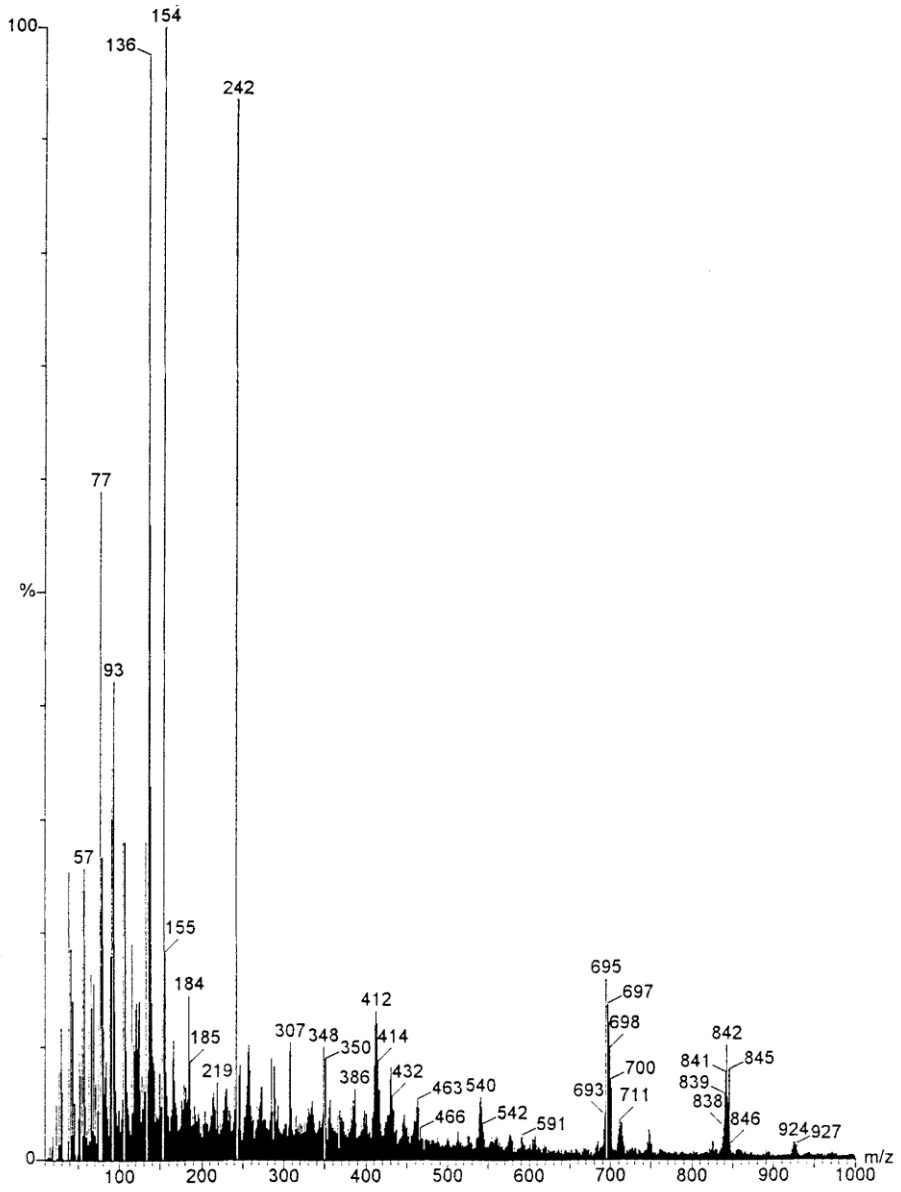

Figure 3.2. LSIMS of $[Ru(bpy)_2(dpq)](PF_6)_2$.

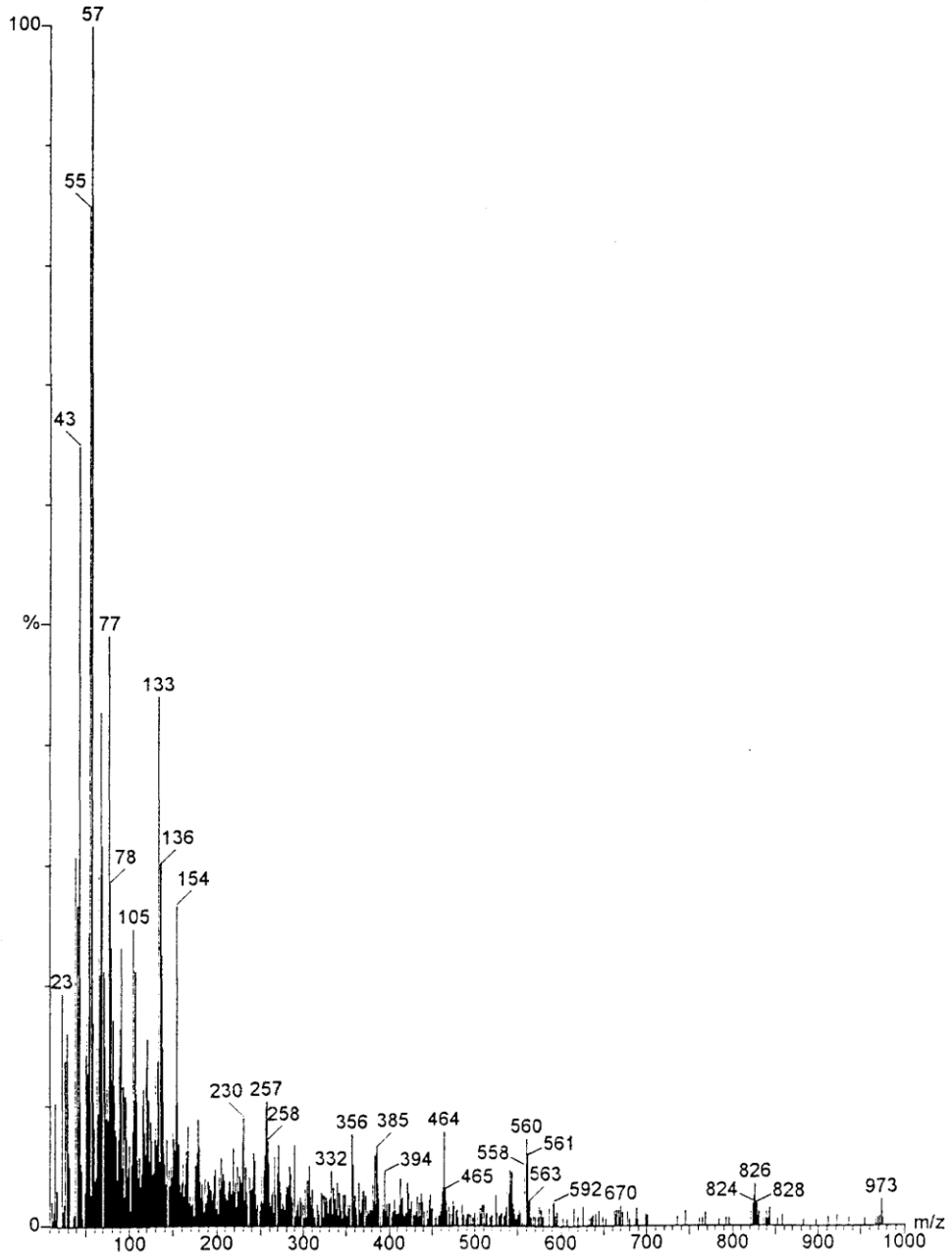

Figure 3.3. LSIMS of $[Ru(bpy)_2(dpq)](PF_6)_2$.

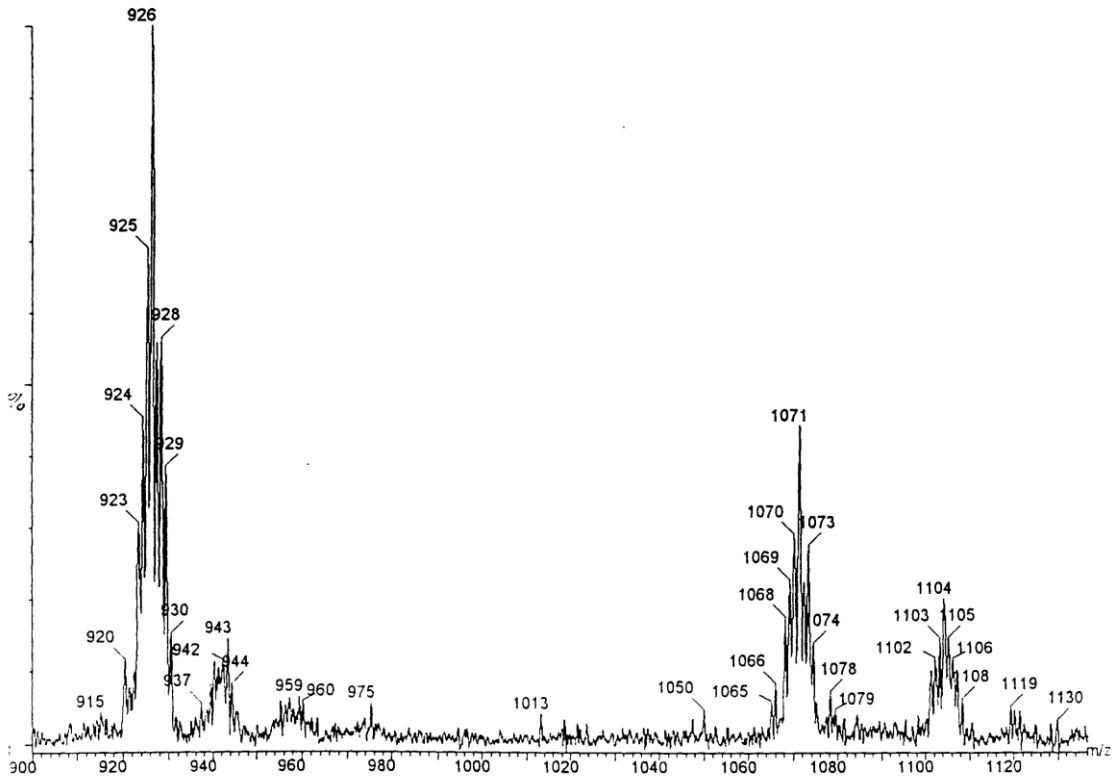

Figure 3.4. LSIMS of $[Ru(bpy)(dpb)_2](PF_6)_2$.

Electrochemistry of Background Electrolyte and Ligands

Accurate data acquisition with the three electrode electrochemical system requires a good background provided by pure electrolyte (TBAH) and both dry and well deoxygenated solvent (acetonitrile). Figures 2.3, 3.5, and 3.6 are representative CV and OSWV of the solvent electrolyte system. For purposes of comparison, the Ag/AgCl reference electrode is standardized vs ferrocene/ferrocenium which is known to be 665 mv vs NHE .[1] Additionally, this well established, fully reversible one electron oxidation/reduction can be used as a reference for Nernstian reversibility. Theoretically ΔE_p, (where $\Delta E_p = |E_p^{anodic} - E_p^{cathodic}|$) should be 59 mV for a reversible one electron transfer.[2] Using resistance compensation, an ΔE_p of 56 mV was obtained with a platinum electrode (Figure 3.7) was achieved .[3] Figure 3.8

shows how a highly concentrated solution gives an exaggerated peak separation of 462 mV. (IR compensation will not eliminate this exaggerated peak separation).

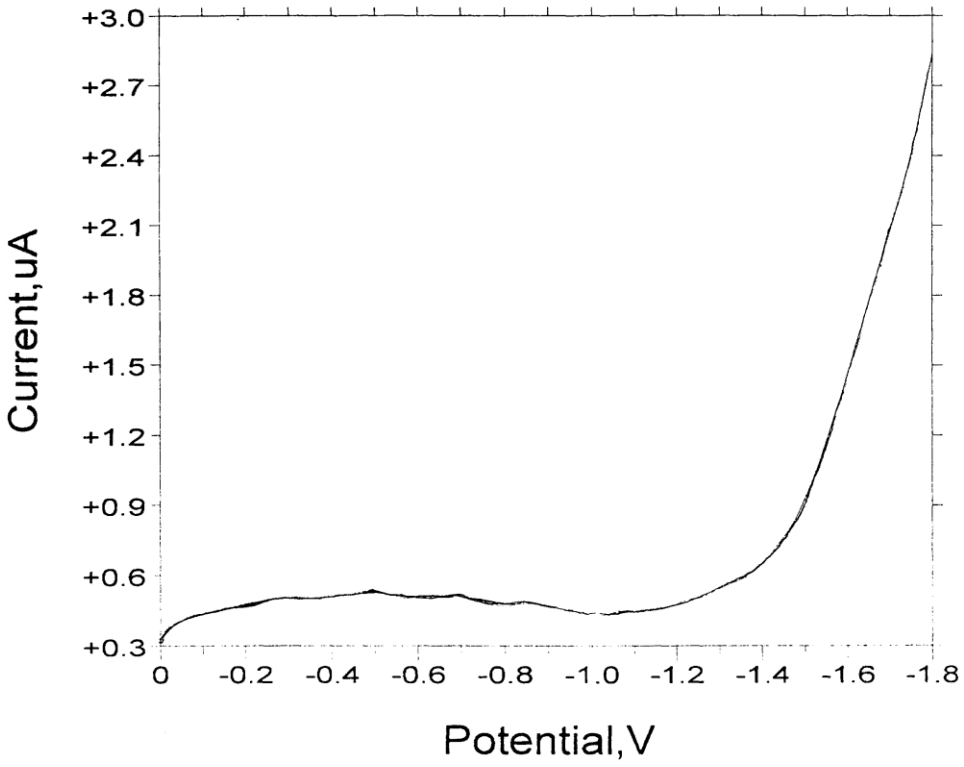

Figure 3.5. OSWV of background electrolyte, 0 to –1.8 V. 0.1 M TBAH in acetonitrile.

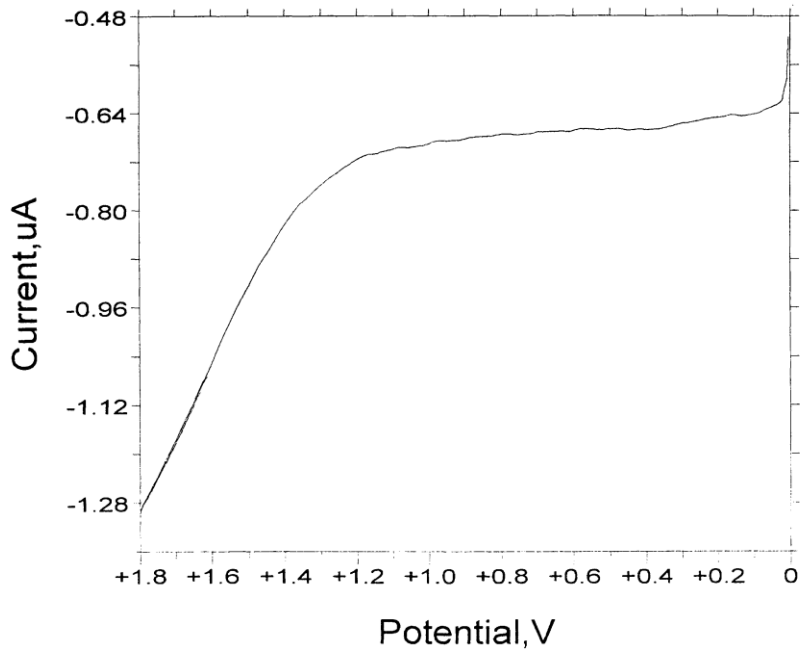

Figure 3.6. OSWV of background electrolyte, 0 to 1.8 V. 0.1 M TBAH, in acetonitrile.

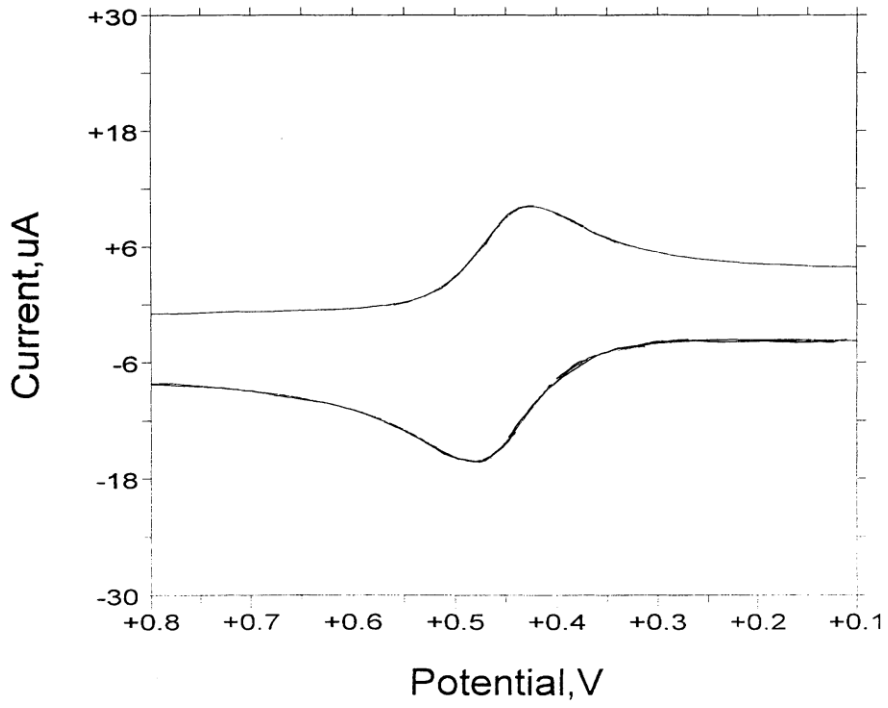

Figure 3.7. CV of ferrocene oxidation with IR (internal resistance) compensation and platinum electrode in acetonitrile. ΔE_p = 56 mV.

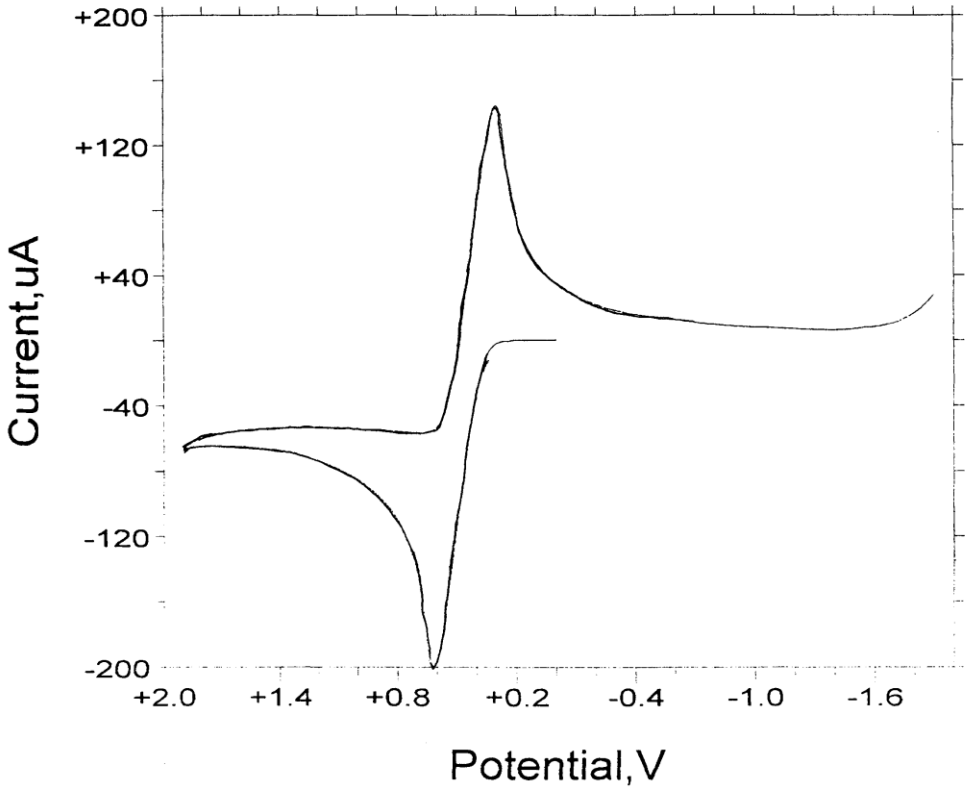

Figure 3.8. CV of a high concentration of ferrocene with no IR compensation in acetonitrile. ΔE_p = 462 mV

Electrochemistry-OSWV

The Osteryoung square wave voltammagram of $[Ru(bpy)_2(dpb)]\ (PF_6)_2$ is shown in Figure 3.9. The OSWV of $[Ru(bpy)_2dpq)](PF_6)_2$ shown in Figure 3.10. The OSWV of $[Ru(bpy)(dpq)_2]\ (PF_6)_2$ is seen in Figure 3.11. The OSWV of $[Ru(bpy)(dpb)_2](PF_6)_2$ Figure 3.12. The OSWV of $[Ru(bpy)_3](PF_6)_2$ as seen in Figure 3.13.

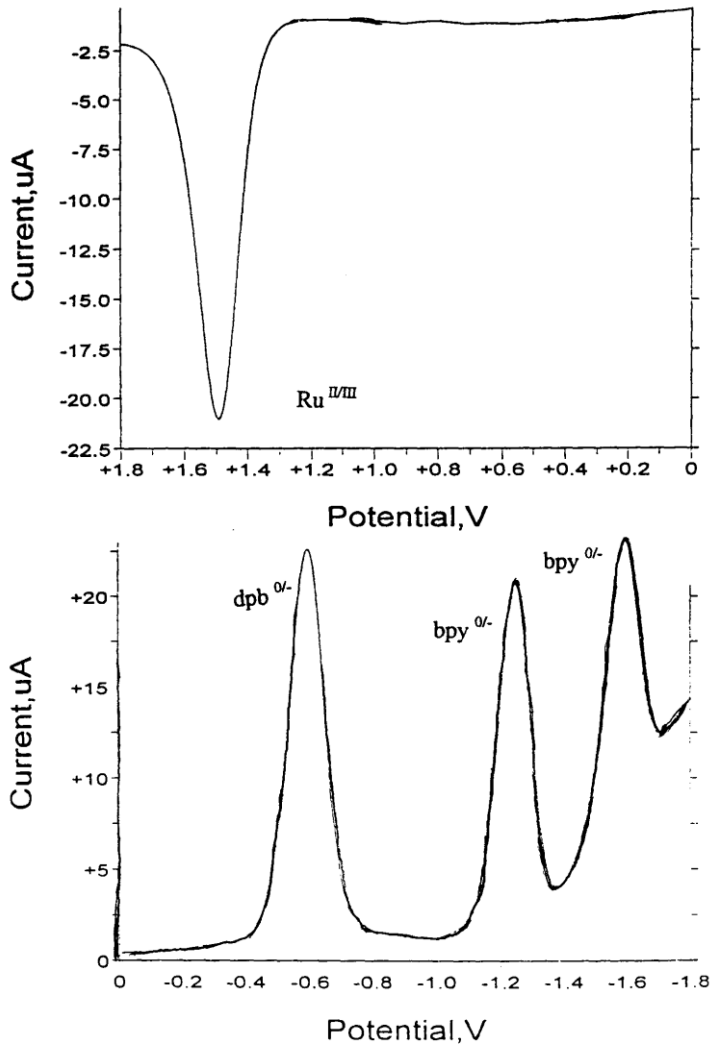

Figure 3.9. Osteryoung square wave voltammogram of $[Ru(bpy)_2(dpb)](PF_6)_2$ (where bpy= 2,2' bipyridine, dpb= 2,3-bis(2-pyridyl)benzoquinoxaline and using a Ag/AgCl reference electrode).

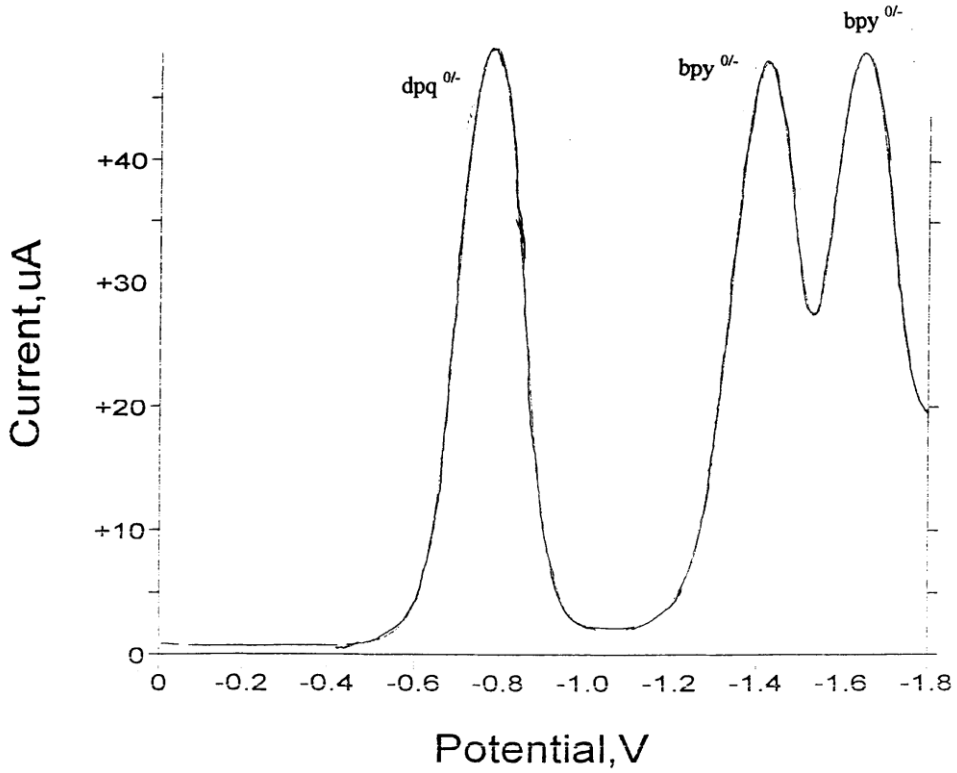

Figure 3.10. Osteryoung square wave voltammogram of $[Ru(bpy)_2(dpq)](PF_6)_2$ (where bpy= 2,2' bipyridine, dpq= 2,3-bis(2-pyridyl)quinoxaline and using a Ag/AgCl reference electrode).

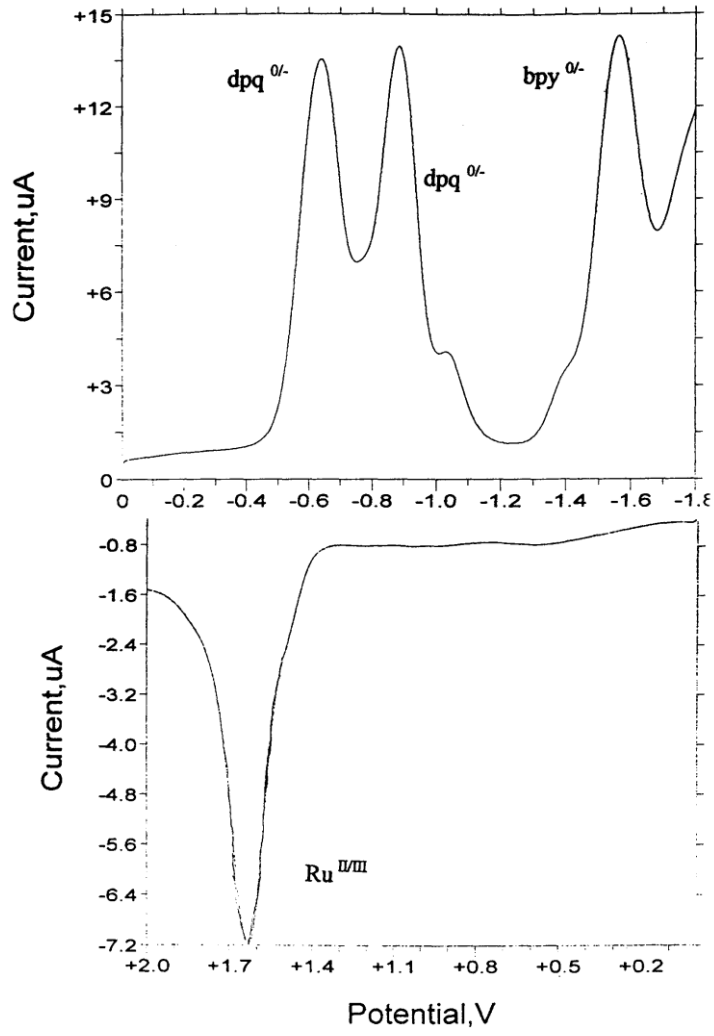

Figure 3.11. Osteryoung square wave voltammogram of $[Ru(bpy)(dpq)_2](PF_6)_2$ (where bpy= 2,2' bipyridine, dpq= 2,3-bis(2-pyridyl)quinoxaline and using a Ag/AgCl reference electrode).

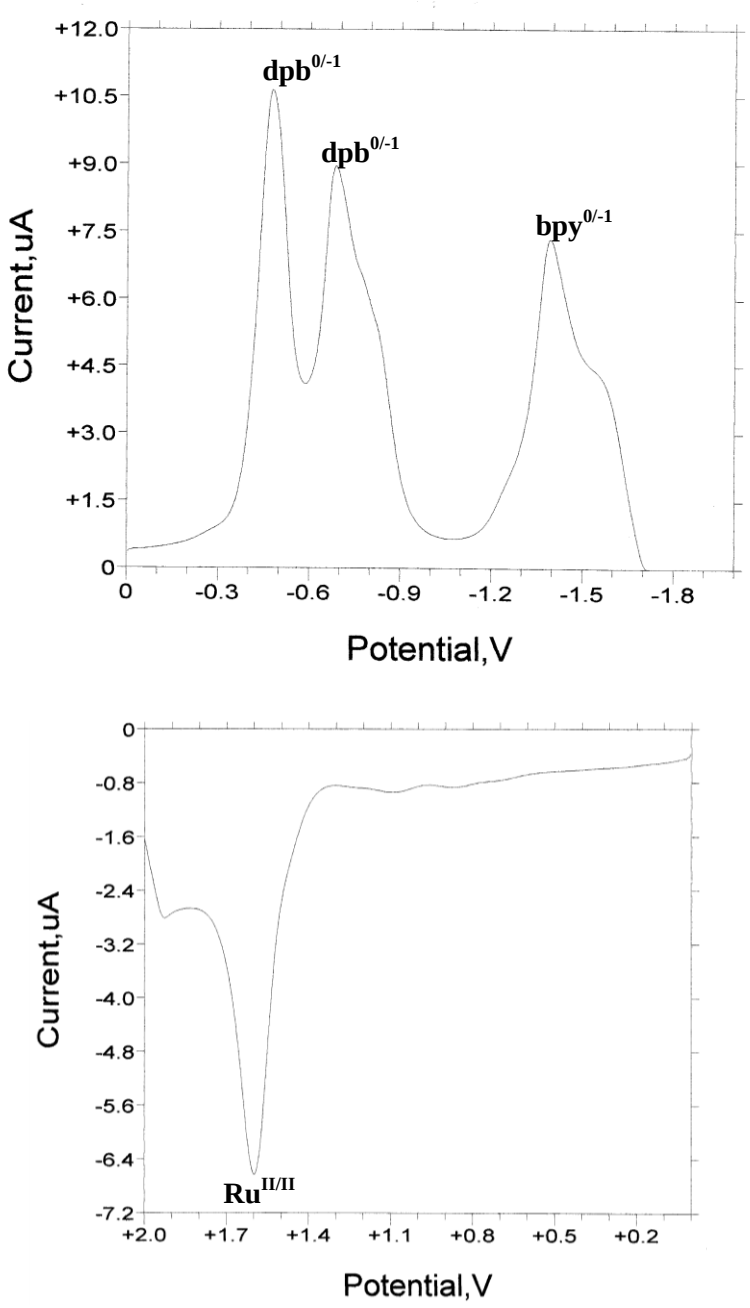

Figure 3.12. Osteryoung square wave voltammogram of $[Ru(bpy)(dpb)_2](PF_6)_2$ (where bpy= 2,2' bipyridine, dpb = 2,3-bis(2-pyridyl)benzoquinoxaline and using a Ag/AgCl reference electrode).

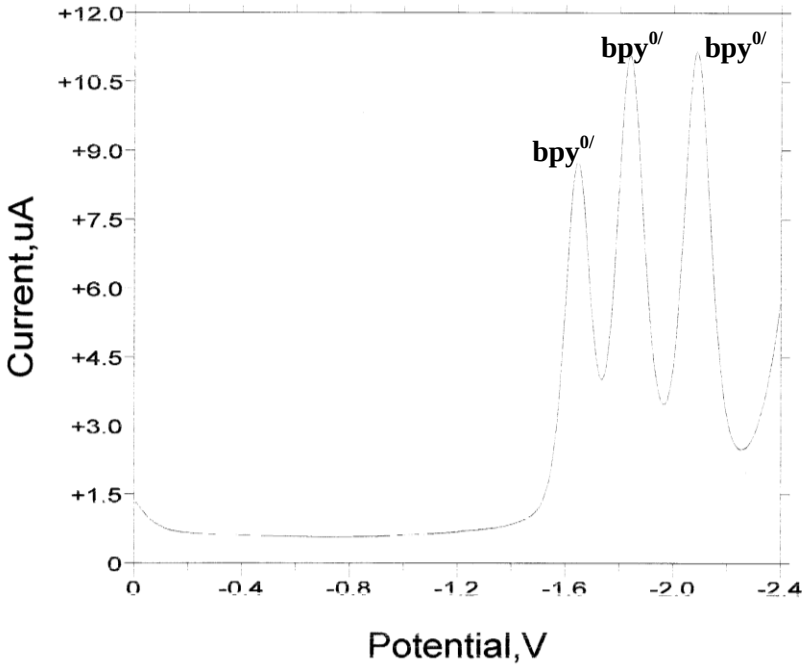

Figure 3.13. Osteryoung square wave voltammogram of $[Ru(bpy)_3](PF_6)_2$ (where bpy = 2,2' bipyridine and using a Ag/AgCl reference electrode).

Electrochemistry-Cyclic Voltammetry

The CV's of $[Ru(bpy)_2(dpq)](PF_6)_2$, $[Ru(bpy)_2dpb)](PF_6)_2$ and $Ru(bpy)(dpq)_2](PF_6)_2$ are shown in Figures 3.14, 3.15 and 3.16. The CV of $[Ru(bpy)(dpb)_2](PF_6)_2$ is shown in Figure 3.17. Table 3.1 summarizes the oxidative and reductive potentials, relative to NHE, of the compounds $[Ru(bpy)_2(dpq)]$ $(PF_6)_2$, $[Ru(bpy)_2(dpb)](PF_6)_2$, $[Ru(bpy)(dpq)_2](PF_6)_2$, and $[Ru(bpy)(dpb)_2](PF_6)_2$.

Table 3.1. Cyclic voltammetric data for a series of ruthenium (II) complexes incorporating polypyridyl ligands (where bpy = 2,2'-bipyridine, dpq = 2,3-bis(2-pyridyl)quinoxaline , dpb =2,3-bis(2-pyridyl)benzoquinoxaline).[a]

Compound	**$E_{1/2}$ oxid**	**$E_{1/2}$ red(1)**	**$E_{1/2}$ red(2)**	**$E_{1/2}$ red (3)**
$[Ru(bpy)_2(dpq)](PF_6)_2$	1700	-510	-1150	-1370
$[Ru(bpy)_2(dpb)](PF_6)_2$	1760	-330	-1020	-1410
$[Ru(bpy)(dpq)_2](PF_6)_2$	1850	-410	-650	-1350
$[Ru(bpy)(dpb)_2](PF_6)_2$	~1900	-250	-470	~-1280
$[Ru(bpy)_3](PF_6)_2$	1600	-1010	-1200	-1430
$[Ru(dpb)_3](PF_6)_2$ [1]	1910	-240	-410	-640

[a] Potentials measured in CH_3CN solution with 0.1 M TBAH and Ag/AgCl reference electrode with a scan rate of 200 mV/sec and converted to a NHE scale.

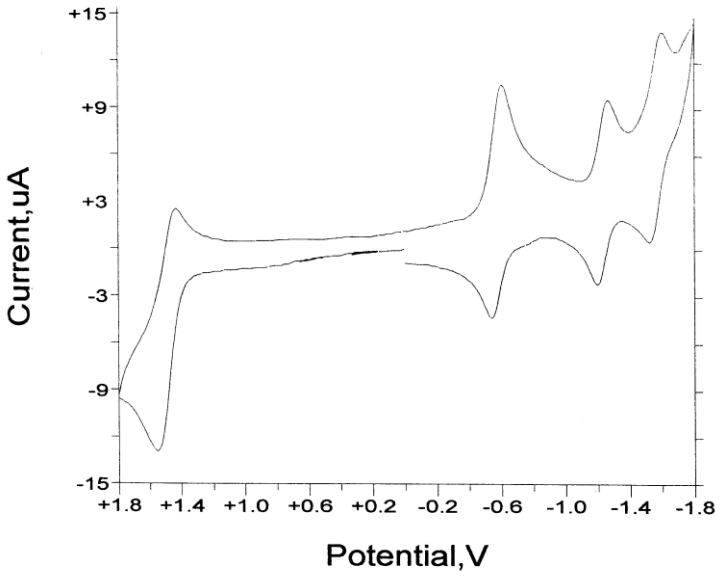

Figure 3.14. Cyclic voltammogram of $[Ru(bpy)_2(dpq)](PF_6)_2$ (where bpy= 2,2'-bipyridine, dpq = 2,3-bis(2-pyridyl)quinoxaline and using a Ag/AgCl reference electrode with a scan rate of 200 mV/sec).

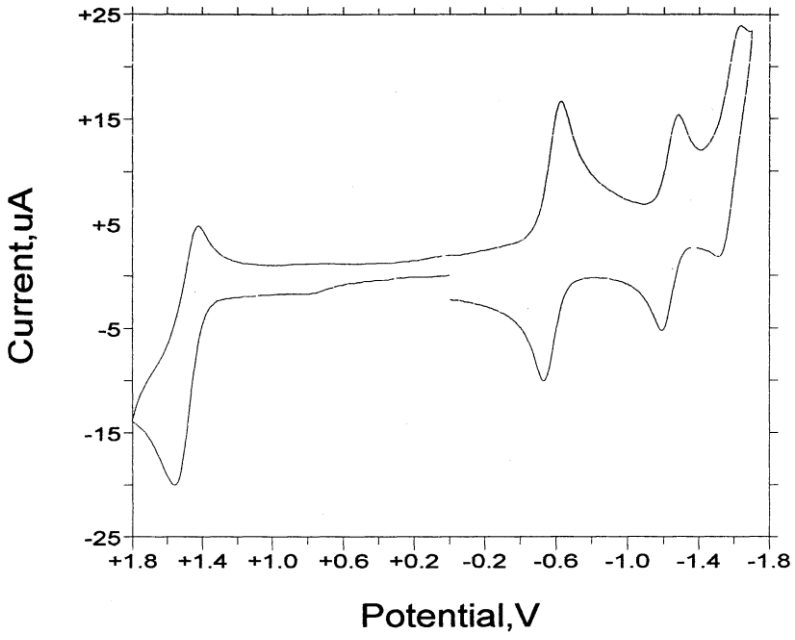

Figure 3.15. Cyclic voltammogram of $[Ru(bpy)_2(dpb)](PF_6)_2$ (where bpy= 2,2'-bipyridine, dpb = 2,3-bis(2-pyridyl)benzoquinoxaline and using a Ag/AgCl reference electrode with a scan rate of 200 mV/sec).

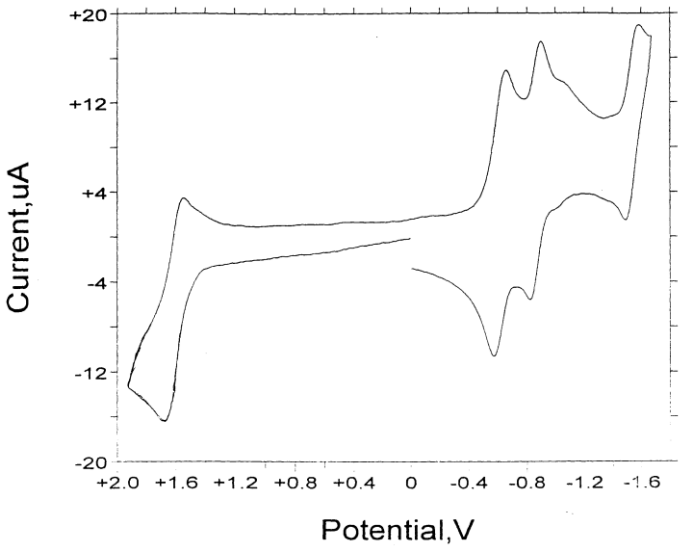

Figure 3.16. Cyclic voltammogram of $[Ru(bpy)(dpq)_2](PF_6)_2$ (where bpy= 2,2'-bipyridine, dpq = 2,3-bis(2-pyridyl)quinoxaline and using a Ag/AgCl reference electrode with a scan rate of 200 mV/sec).

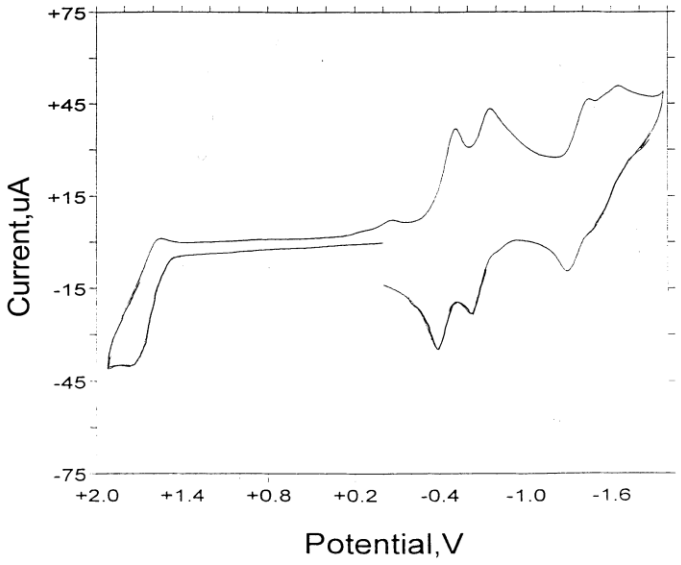

Figure 3.17. Cyclic voltammogram of [Ru(bpy)(dpb)2](PF6)2 (where bpy = 2,2'-bipyridine, dpb = 2,3-bis(2-pyridyl)benzoquinoxaline and using a Ag/AgCl reference electrode with a scan rate of 200 mV/sec).

UV-Vis Spectroscopy

Ligands- The UV-Vis electronic absorption spectra of the ligands bpy, dpq and dpb are shown in Figure 3.18 (molar absorptivity vs wavelength).

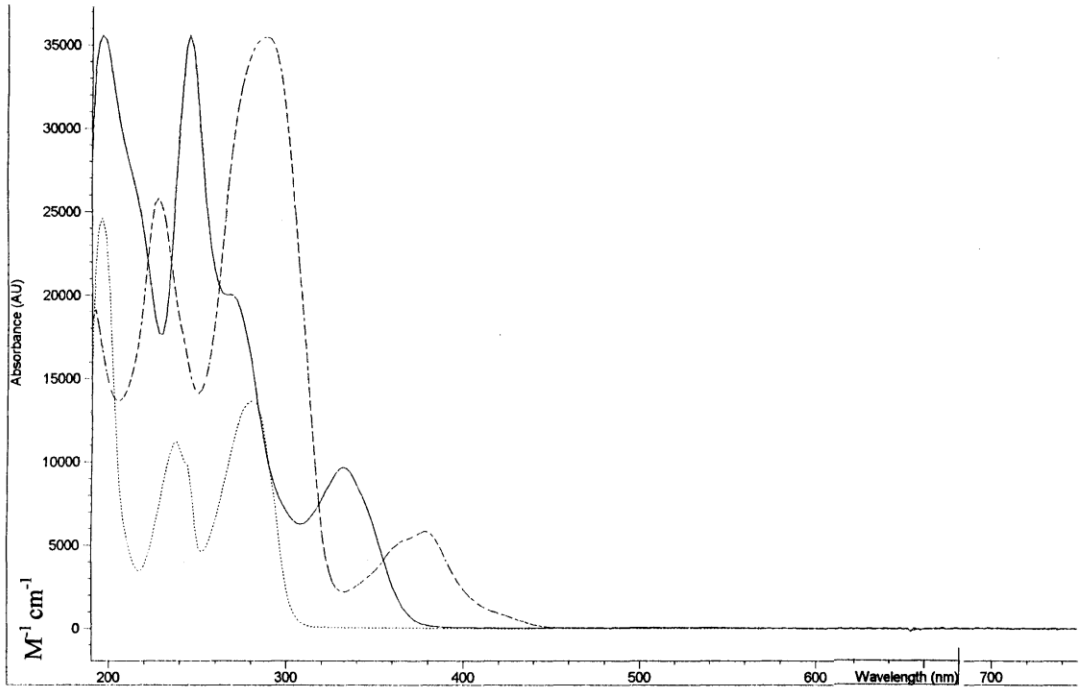

Figure 3.18. The comparative UV-Vis spectra (molar absorptivity vs wavelength) of the ligands bpy (….), (where bpy = 2,2'-bipyridine) dpq (___), (where dpq =2,3-bis(2-pyridyl)quinoxaline) and dpb (_ _ _), (where dpb =2,3-bis(2-pyridyl)benzoquinoxaline).

Monometallic Ruthenium Complexes

The UV-Vis spectra of $[Ru(bpy)_2(dpq)](PF_6)_2$, $[Ru(bpy)_2(dpb)](PF_6)_2$, $[Ru(bpy)(dpq)_2](PF_6)_2$ and $[Ru(bpy)(dpb)_2](PF_6)_2$ are shown in Figure 3.19.

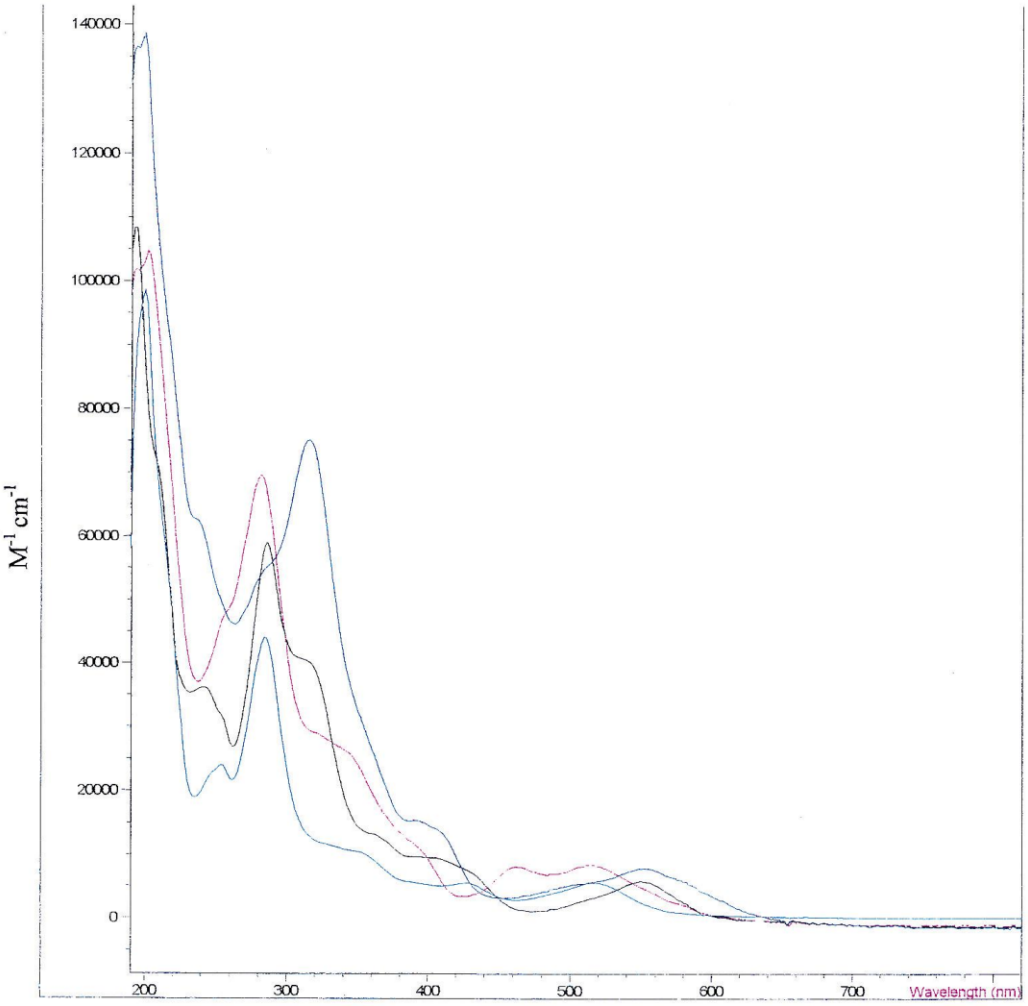

Figure 3.19. The comparative electronic absorption spectra of $[Ru(bpy)_2dpq](PF_6)_2$ (light blue), $[Ru(bpy)_2(dpb)](PF_6)_2$ (dark blue), $[Ru(bpy)(dpq)_2](PF_6)_2$ (black) and $[Ru(bpy)(dpb)_2](PF_6)_2$ (red) in acetonitrile at room temperature. (Where bpy = 2,2'-bipyridine, dpq = 2,3-bis(2-pyridyl)quinoxaline) and dpb = 2,3-bis(2-pyridyl) benzoquinoxaline).

Spectroelectrochemistry

Initially, spectroelectrochemical data were obtained using an H-cell apparatus. See Figure 2.1. The difficulty in obtaining reversible oxidations from compounds previously reported to display reversible behavior prompted the employment of an OTTLE cell.[4] See Figure 2.2. As ferrocene/ferrocenium has served as the model, one-electron reversible oxidation, the spectra of its electrochemical oxidation (1.71V) and reduction (-0.25V) to the original species are shown in Appendix Figure 3.7.

$[Ru(bpy)_2(dpq)](PF_6)_2$

The oxidation (at 1.89 V) and regeneration of the parent complex (at –0.25 V) with the H-cell are shown in Figure 3.20. The oxidative spectra obtained with the OTTLE cell are seen in Figure 3.21. The one electron reduction of the complex at –1.00 V lead to irreversible behavior with the H-cell, (see Figure 3.22). The reductive process was reversible with the OTTLE cell as seen in Figure 3.23. The graph of the first, second and third reductions is shown in Figure 3.24. The second and third reductions were not reversible.

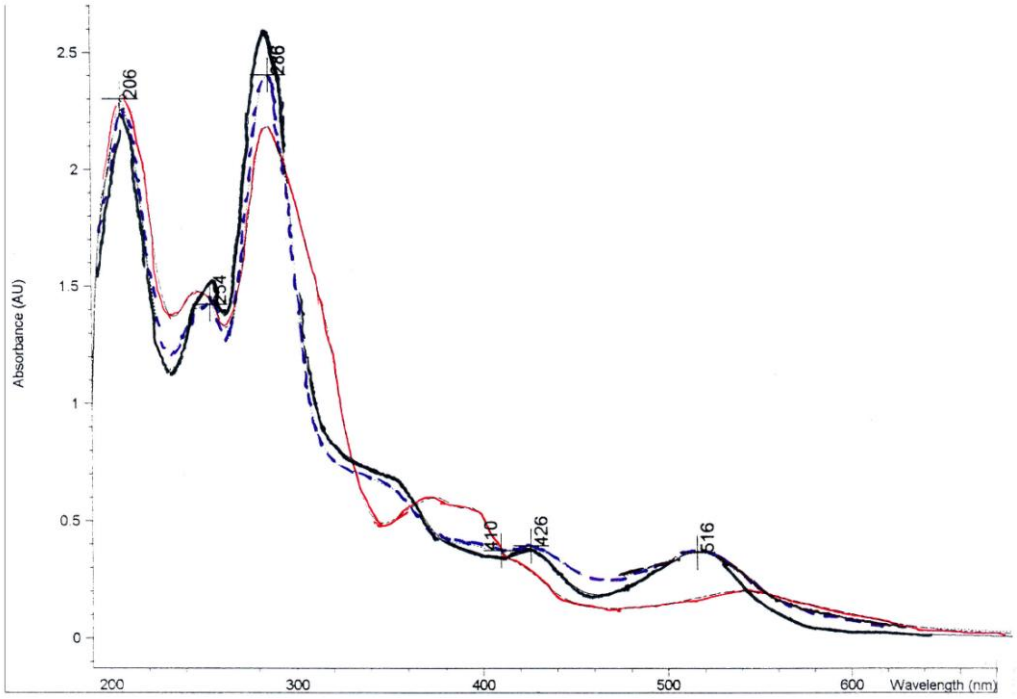

Figure 3.20. Oxidative spectroelectrochemistry of $[Ru(bpy)_2(dpq)](PF_6)_2$ with H-cell. (___= 0V, _ _ _ = 1.89V, ….. = -0.25V). (Where bpy = 2,2'-bipyridine, dpq = 2,3-bis(2-pyridyl)quinoxaline). 0.1M TBAH in CH_3CN at room temperature.

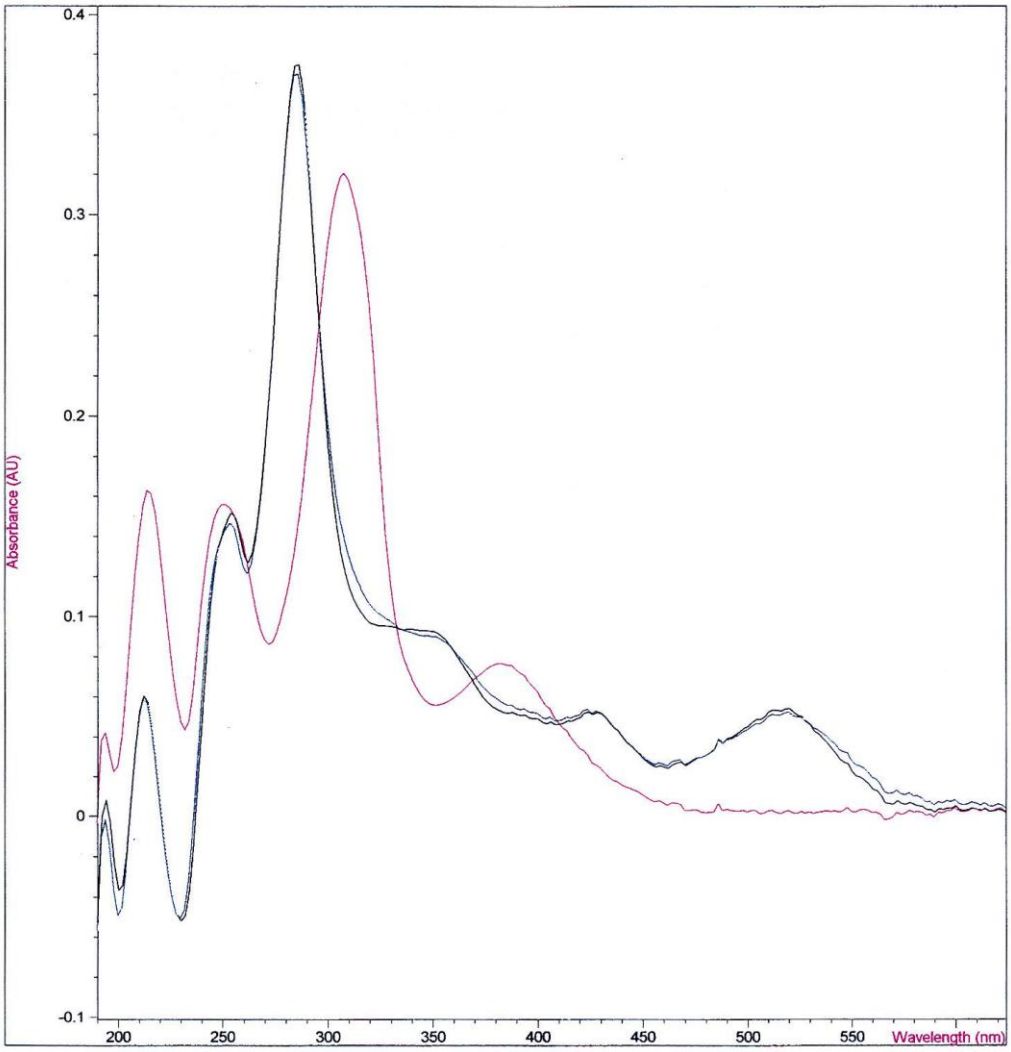

Figure 3.21. Oxidative spectroelectrochemistry of $[Ru(bpy)_2(dpq)](PF_6)_2$ with OTTLE cell. (Black = 0V, red = 1.90V, blue = 0V). (Where bpy = 2,2'-bipyridine, dpq = 2,3-bis(2-pyridyl)quinoxaline). 0.1M TBAH in CH_3CN at room temperature.

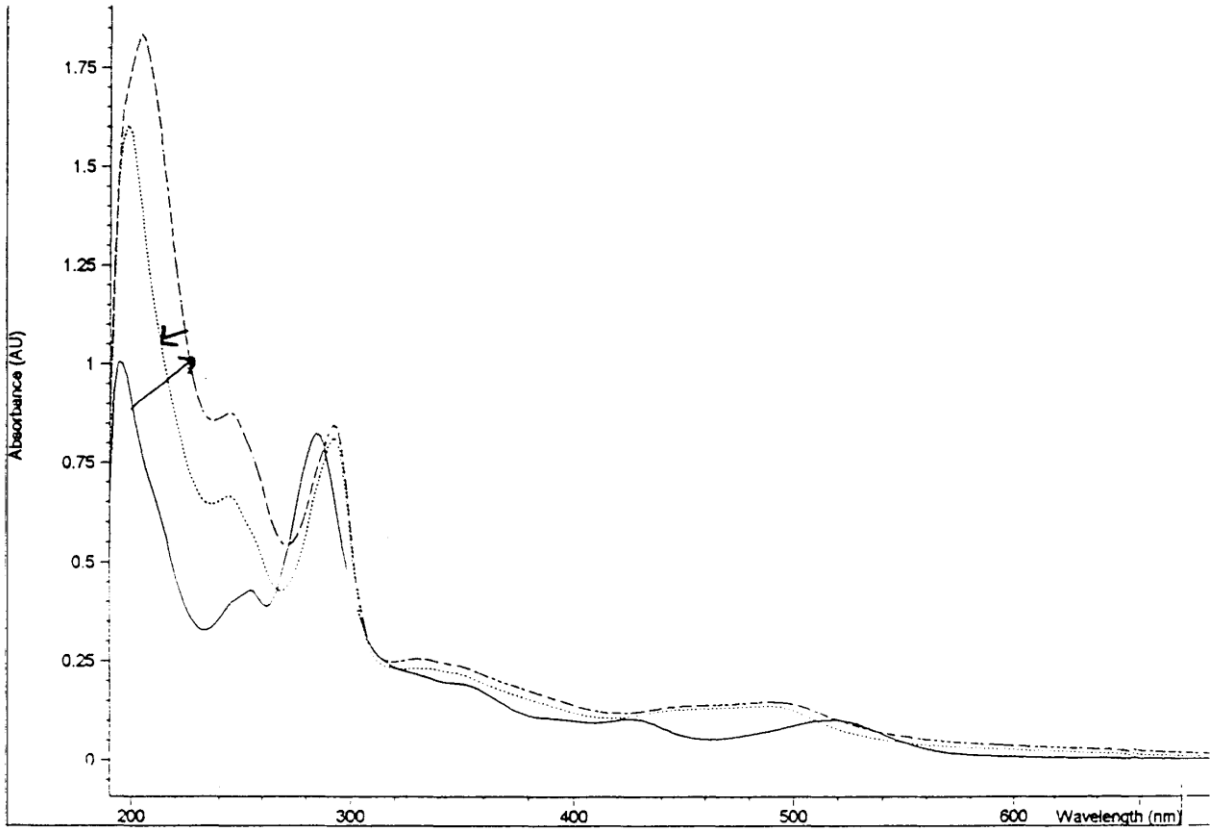

Figure 3.22. First reduction of $[Ru(bpy)_2(dpq)](PF_6)_2$ with H-cell. (___ = 0V, _ _ _= -1.00V, …. = 0.25V). (Where bpy= 2,2'-bipyridine, dpq = 2,3-bis(2-pyridyl)quinoxaline). 0.1M TBAH in CH_3CN at room temperature.

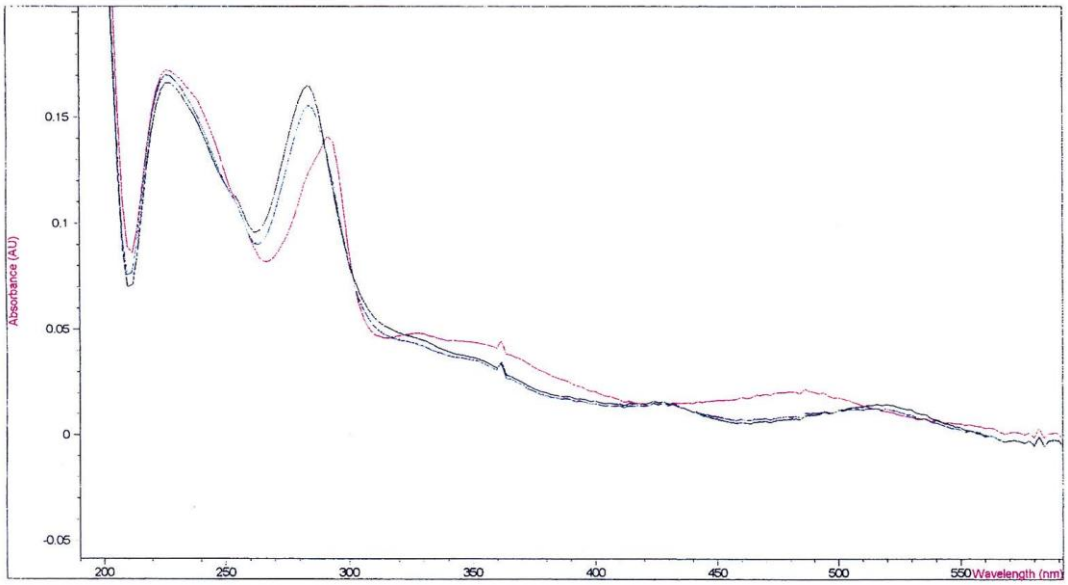

Figure 3.23. First reduction of $[Ru(bpy)_2(dpq)](PF_6)_2$ with OTTLE cell. (Black = 0V, red = -1.00V, blue = 0V). (Where bpy = 2,2'-bipyridine, dpq = 2,3-bis(2-pyridyl)quinoxaline). 0.1 M TBAH in CH_3CN at room temperature.

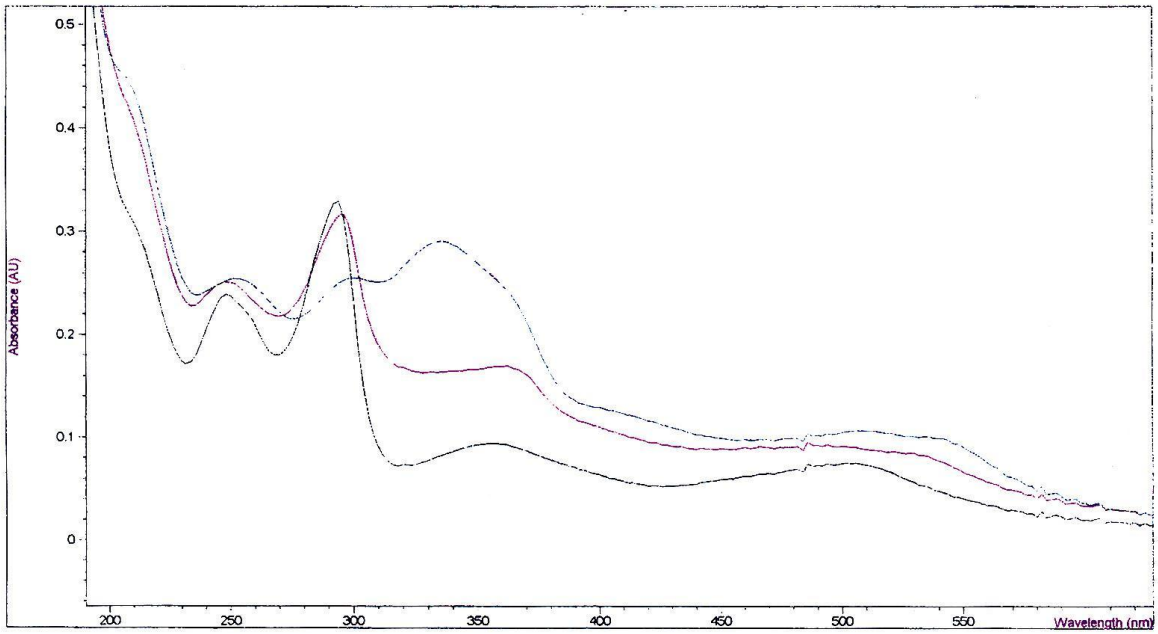

Figure 3.24. First, second and third reduction of $[Ru(bpy)_2(dpq)](PF_6)_2$ with the OTTLE cell. (Where bpy = 2,2'-bipyridine, dpq = 2,3-bis(2-pyridyl)quinoxaline). (Black = -1.00V, red = -1.55V, blue = 1.90V). 0.1 M TBAH in CH_3CN at room temperature.

[Ru(bpy)(dpq)$_2$](PF$_6$)$_2$

The oxidation (1.80 V) and reduction to generate the parent complex seen in Figure 3.25. The first reduction (-0.70 V) and oxidation to generate the parent complex are shown in Figure 3.26. The reduction is not fully reversible. Further reduction (-1.00V) leads to loss of reversibility. See Figure 3.27.

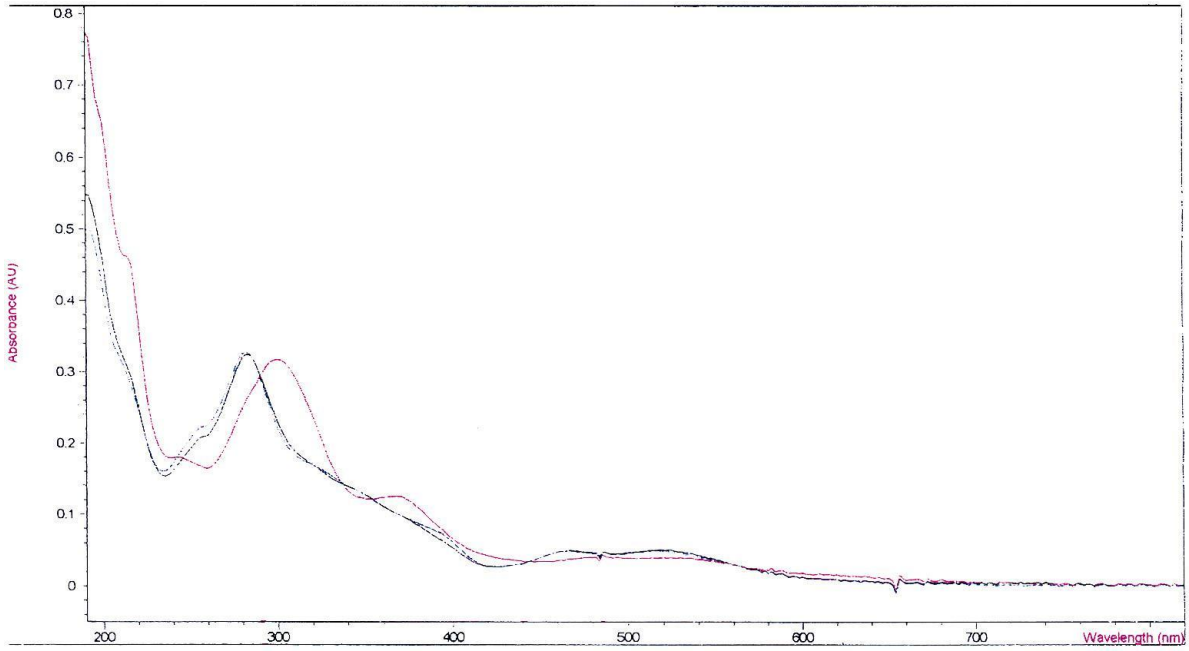

Figure 3.25. Oxidative spectroelectrochemistry of [Ru(bpy)(dpq)2](PF6)2 with OTTLE cell. (Where bpy= 2,2'-bipyridine, dpq = 2,3-bis(2-pyridyl)quinoxaline). (Black = 0 V, red = 1.80 V, blue = 0 V). 0.1 M TBAH in CH3CN at room temperature.

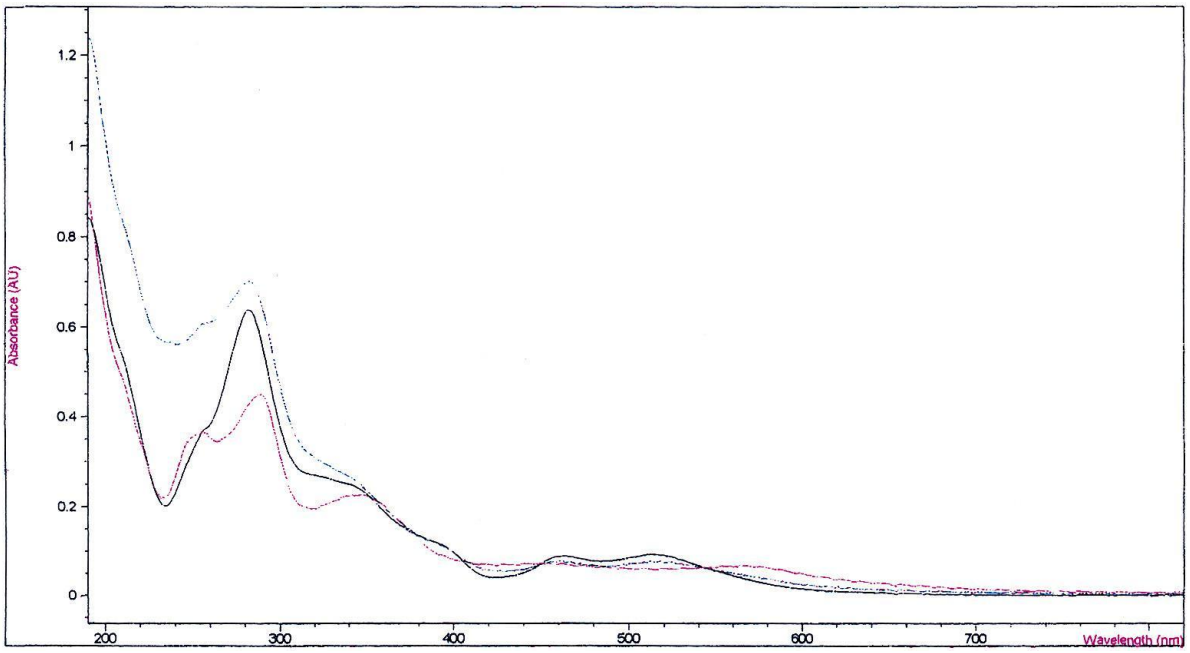

Figure 3.26. First reductive spectroelectrochemistry of $[Ru(bpy)(dpq)_2](PF_6)_2$ with OTTLE cell. (Where bpy = 2,2'-bipyridine, dpq = 2,3-bis(2-pyridyl)quinoxaline). (Black = 0 V, red = -0.70 V, blue = 0V). 0.1 M TBAH in CH_3CN at room temperature.

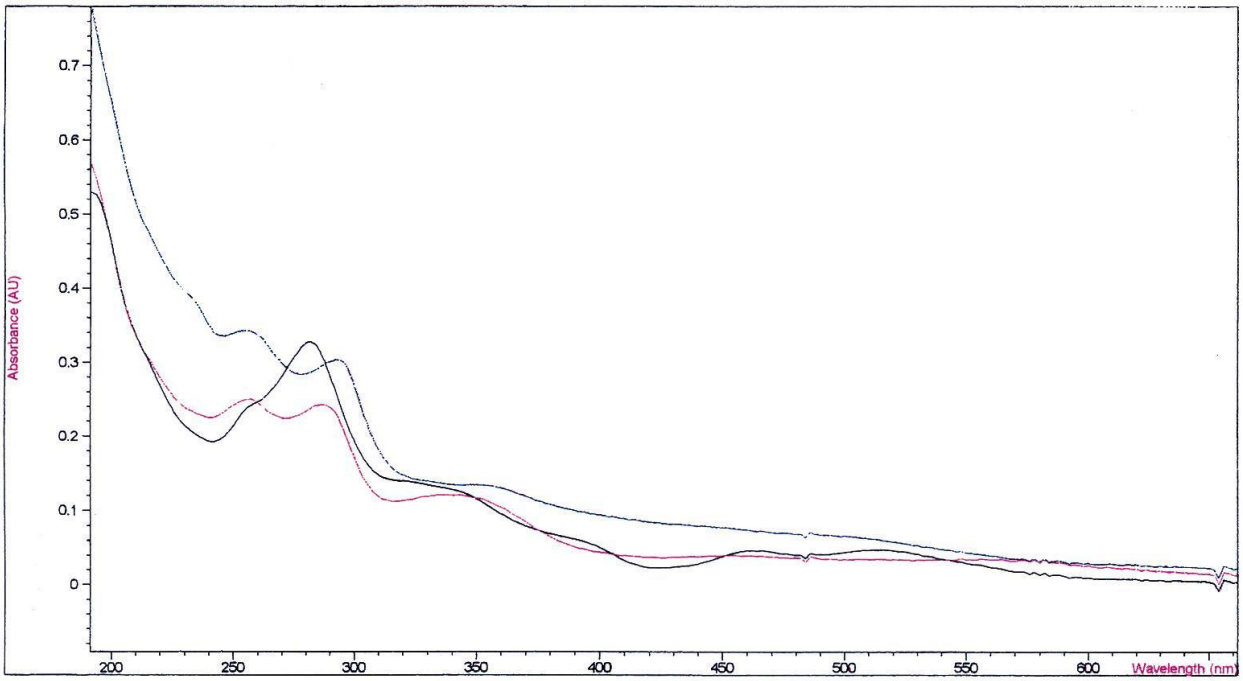

Figure 3.27. First and second reductive spectroelectrochemistry of [Ru(bpy)(dpq)2](PF6)2 with OTTLE cell. (Where bpy = 2,2'-bipyridine, dpq = 2,3-bis(2-pyridyl)quinoxaline). Black = 0 V, red = -0.70 V, blue = -1.00 V. 0.1 M TBAH in CH3CN at room temperature.

[Ru(bpy)(dpb)$_2$](PF$_6$)$_2$

The spectral data for this compound were acquired with the OTTLE cell. The oxidation at 1.75 V and reduction to the parent compound are shown in Figure 3.28. The reduction at –0.50 V and oxidation to the parent compound are seen in Figure 3.29. The composite of subsequent reductions at –0.60 V, -1.00 V and –1.75 V is shown in Figure 3.30. The reductions at –1.00 V and –1.75 V were irreversible.

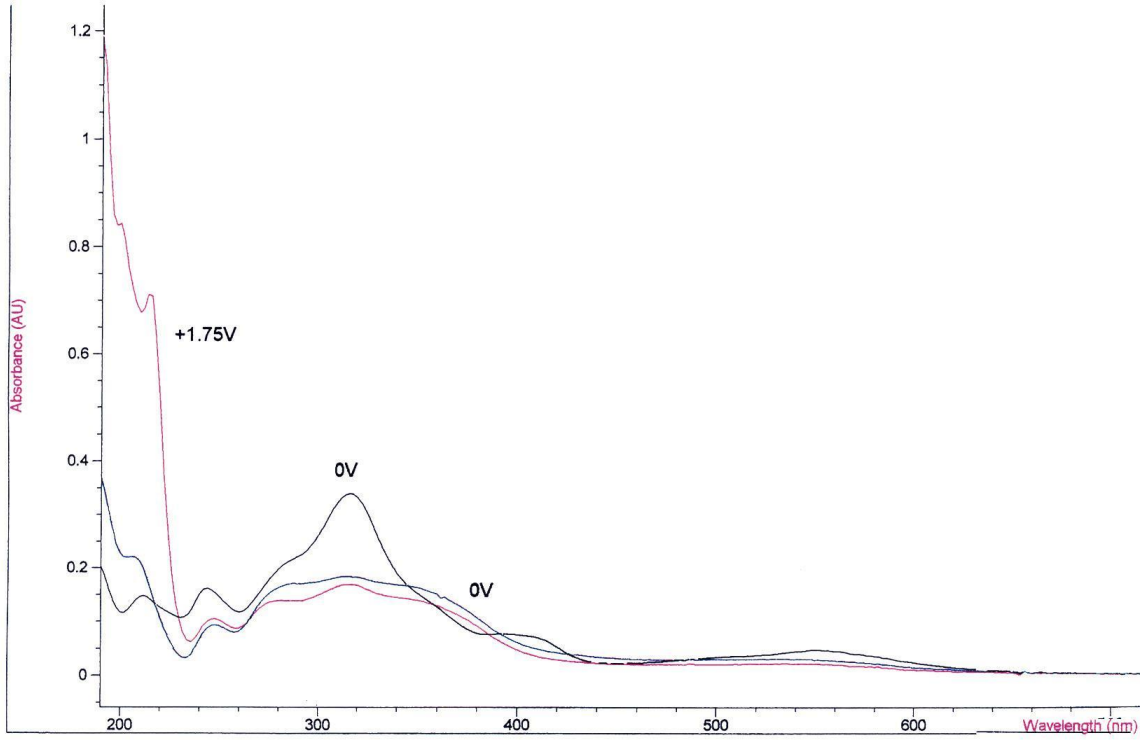

Figure 3.28. The oxidative spectroelectrochemistry of [Ru(bpy)(dpb)$_2$](PF$_6$)$_2$ with the OTTLE cell. (Black = 0 V, red = 1.75 V, blue = 0 V). 0.1M TBAH in CH$_3$CN at room temperature.

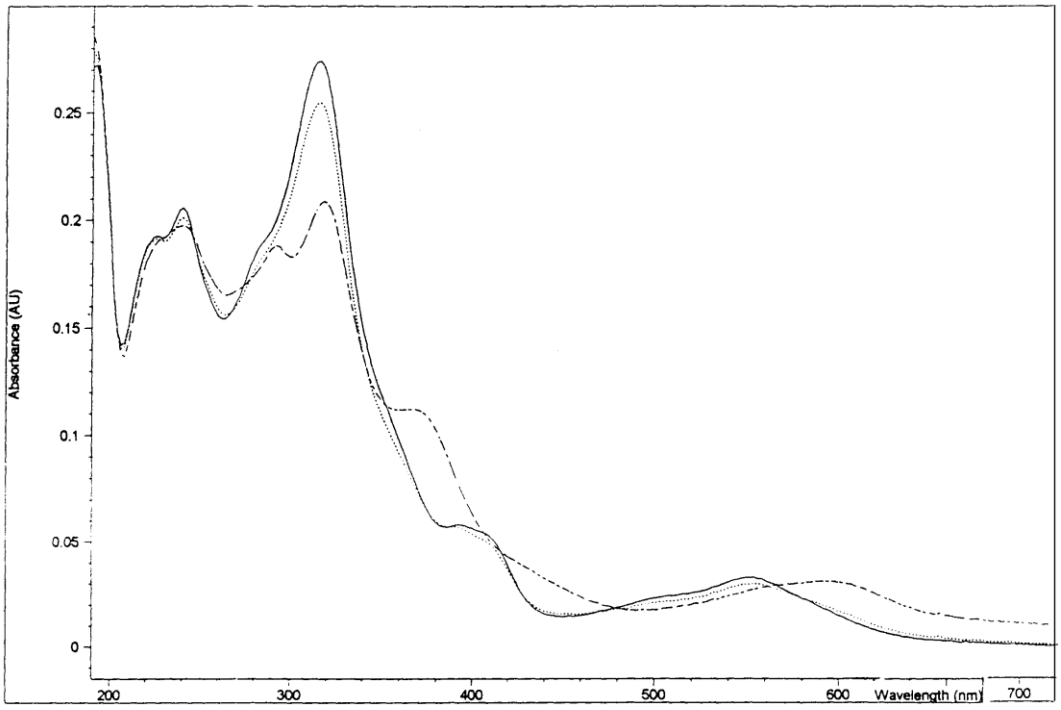

Figure 3.29. The first reductive spectroelectrochemistry of $[Ru(bpy)(dpb)_2](PF_6)_2$ with the OTTLE cell. (Solid line = 0 V, dash and dots = -0.50 V, dots = 0 V). 0.1 M TBAH in CH_3CN at room temperature.

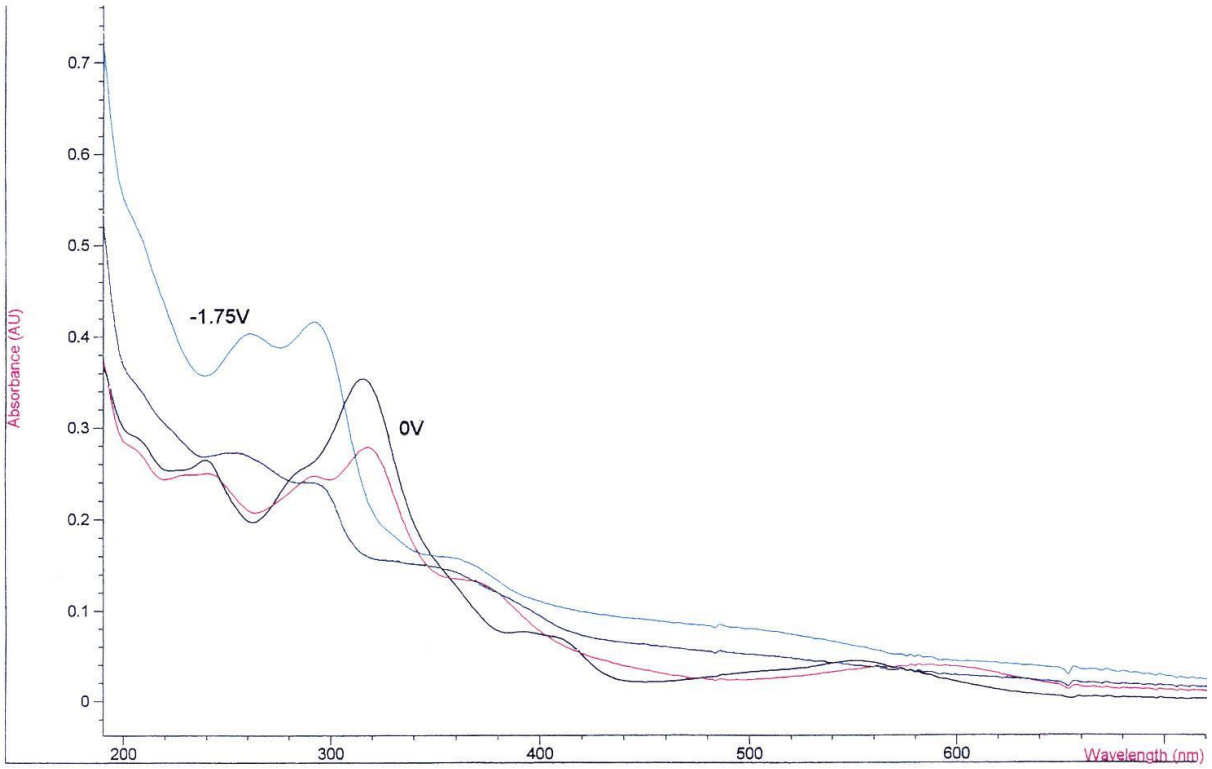

Figure 3.30. Composite of parent complex, first, second and third reduction spectroelectrochemistry of $[Ru(bpy)(dpb)_2](PF_6)_2$ with the OTTLE cell.(Black = 0 V, red = -0.50 V, blue =-1.00 V, light blue = -1.75 V). 0.1 M TBAH in CH_3CN at room temperature.

References

1. Carlson, D. L.; Murphy, W. R. *Inorg. Chim. Acta.* 1991, 181, 61.

CHAPTER FOUR: DISCUSSION

Synthesis and Purification

Monoruthenium mixed polypyridyl complexes can be prepared by two different synthetic strategies. (1) The bridging ligand is combined with $RuCl_3 \bullet 3H_20$ in ethanol/water to yield $[Ru(BL)_xCl_{6-2x}]$. This yield is often low due to the formation of the polymeric systems. To minimize this, the bridging ligands can be protected on one side and deprotected after binding to the metal.[1] In either case the terminal ligand bpy is then added via a substitution for the remaining chlorides. (2) The somewhat simpler synthetic route is to add the terminal ligand bpy to the $RuCl_3 \bullet 3H_20$ and then add the bridging ligand. This is the chosen method for the complexes synthesized in this study. Purification by adsorption chromatography on alumina was effective in removing impurities (unreacted starting materials, bimetallic and polymetallic complexes, and complexes with unwanted BL/bpy stoichiometries) for $[Ru(bpy)_2(dpq)](PF_6)_2$, $[Ru(bpy)(dpq)_2](PF_6)_2$, and $[Ru(bpy)_2(dpb)](PF_6)_2$. Purification was less effective for the new compound $[Ru(bpy)(dpb)_2](PF_6)_2$. After two alumina chromatographs, there remained ca 1% electroactive impurities as determined by OSWV.

The major difference between the protocol used by the Brewer[3] group and Rillema,[2] for the synthesis of the ruthenium dpq complexes, was the choice of solvent. The Brewer protocol uses an ethanol/ water solvent mixture, whereas Rillema used acetone (for the synthesis of $[Ru(bpy)_2(dpq)](PF_6)_2$) and ethylene glycol (for the synthesis of $[Ru(bpy)(dpq)_2](PF_6)_2$). Additionally, Rillema removed the chlorides from $[Ru(bpy)Cl_4]$ with the addition of $AgPF_6$ prior to the addition of the dpq ligand.

Identification of Products

As illustrated in the results section, page 35, elemental analysis is not an effective method of identification for these types of complexes. Liquid secondary ion mass spectroscopy (LSIMS),on the other hand, will accurately confirm the identity of the parent ion. (Most ions formed will have +1 charge). LSIMS will not determine the purity of the compound since these complexes fragment extensively due to collisions with accelerated cesium atoms.

The mass spectra of all compounds analyzed herein show the loss of one PF_6^- counterion. The relative intensity of the parent ion minus one PF_6^- is not of diagnostic importance, as most of the sample is fragmented into lower mass ions. The crucial factor is that the parent ion is present. The LSIMS results, pages 37-40, confirm the identity of the four synthesized compounds.

Determination of Purity

Osteryoung square wave voltammetry is a sensitive method for detecting electroactive impurities.[4] It is well known that the observed oxidation for each of the four compounds being studied represents the $Ru^{II/III}$ couple. Typically, reductions are ligand centered and bridging ligands (dpq and dpb) reduce before the terminal ligand bpy.

The OSWVs of the following three complexes $[Ru(bpy)_2(dpb)](PF_6)_2$ (as seen in Figure 3.9), $[Ru(bpy)_2(dpq)](PF_6)_2$ (as seen in Figure 3.10) and $Ru(bpy)(dpq)_2](PF_6)_2$, (as seen in Figure 3.11), show no detectable electroactive impurities. Figure 3.12 is the OSWV of the same compound (synthesized by the author). The small peak at 1.9 V may be evidence water. The small shoulder at –1.6 V is indicative of a small amount of polypyridyl

impurity. For the sake of comparison, the OSWV of $[Ru(bpy)_3](PF_6)_2$ is seen in Figure 3.13. The compound shows no detectable impurities. It is interesting that whereas $[Ru(bpy)(dpq)_2](PF_6)_2$ was synthesized and purified satisfactorily, $[Ru(bpy)(dpb)_2](PF_6)_2$ was not. This can be explained both in terms of increased steric hindrance and decreased sigma donation of the dpb ligand.[2c]

Curiously, the level of purity in $[Ru(bpy)(dpb)_2](PF_6)_2$ decreased with more than two runs through neutral alumina . This would suggest that there may be some degradation of the product due to interaction with the neutral alumina or an increased retention of the desired product. Silica and *Florisil* magnesium hydrogen silicate) were also tried but the compounds irreversibly adsorbed to these adsorbents. This dilemma begged the following question. Could the starting materials and intermediate compounds be further purified?

Cyclic Voltammetry

The monometallic ruthenium polypyridyl complexes are known to undergo a one electron, metal based oxidation and multiple ligand based reductions.[5] The potential of the first reduction reflects the relative energy of the lowest lying, most stable π^* ligand molecular orbital (MO). The ease of reduction for the free ligands (least negative $\Delta E_{1/2}$ vs NHE) is dpb (-0.85 V) >dpq (-1.14 V) >bpy(-1.99 V). The ratio of peak currents ($I_p^a/I_p^c \cong$ and the symmetry of the reductive and oxidative peaks indicates reversible electron transfer. The $E_p^a - E_p^c \cong 59$ mV rule of thumb for Nernstian behavior suggests a one electron transfer.[6]

Many factors impact the signal to noise ratio and detectability of impurities in ruthenium complexes. The cyclic voltammogram varies with the purity of the compound and the purity of the solvent/electrolyte system. Water contamination can lead to a lower solvent

window and can obscure the third reduction peak for systems of this type. The presence of oxygen will introduce an irreversible reduction peak at ~ -1.0V which represents the reduction of oxygen to superoxide radical. The cyclic voltammogram of $[Ru(bpy)(dpb)_2](PF_6)_2$ shows more impurity and a narrower solvent window as compared to the other compounds.

A comparison between the reductive peaks of the free ligands and the first reductive peaks of the complexes (Table 4.1) reveals the stabilization of the ligand π^* upon coordination to the ruthenium metal center. The ease of reduction of the ligand (less negative $\Delta E_{1/2}$) follows the same order as in the ruthenium complexes (dpb>dpq>bpy). The substantial stabilization of the ligands upon complexation, implies a decrease in electron density due to sigma donation to the metal center.[7] When comparing mono vs bis- bridging ligands complexes (dpq and dpb) the bis-bridging ligand complex is always easier to reduce by about 80 mV. This effect may be rationalized by the decrease in σ-donation (from bis-bpy vs mono-bpy) to Ru which stabilizes the metal center and consequently stabilizes the bridging ligand. Alternatively, the presence of two bridging ligands gives two systems with enhanced metal to ligand backbonding to be shared thereby reducing the destabilization on each bridging ligand.

Table 4.1. Reduction potentials vs NHE in acetonitrile with 0.1 M TBAH at room temperature for a series of polypyridyl ligands and ruthenium complexes.

Complex or ligand	$\Delta E_{1/2}$ (mV)
$[Ru(bpy)_2(dpq)](PF_6)_2$	-505
$[Ru(bpy)(dpq)_2](PF_6)_2$	-415
$[Ru(bpy)_2(dpb)](PF_6)_2$	-335
$[Ru(bpy)(dpb)_2](PF_6)_2$	-250
bpy[8]	-2280
dpq[8]	-1430
dpb[8]	-1140

bpy = 2,2'-bipyridine

dpq = 2,3-bis(2-pyridyl)quinoxaline

dpb = 2,3'-bis(2-pyridyl)benzoquinoxaline

The second and third reduction potentials are impacted by the fact that a prior reduction has occurred. Many bis-bridging ligand complexes have degenerate π^* orbitals, one based on each equivalent bridging ligand. A one electron reduction will populate the π^* orbital of one of the BLs, resulting in the destabilization of the other BL based π^* orbital. The $\Delta E_{1/2}$ for $[Ru(bpy)(dpq)_2](PF_6)_2$ is -415 mV, but the reduction of the second bridging ligand occurs at -650 mV. Reduction of the first bridging ligand, hinders backbonding to that BL and results in enhanced backbonding to the remaining bridging ligand.[8] Additionally, the different reduction potentials for equivalent polypyridyl ligands could result from electronic coupling of the two polypyridyl ligands as facilitated by the ruthenium metal center.[8]

The trends for the second and third reduction potentials follow a similar pattern to that seen for the first reductions with dpb reducing prior to dpq and bpy. The third reductive couples are quasi-reversibility. This often results when the adsorption of the electrochemically generated neutral analyte onto the electrode surface is possible.

The oxidation potential for these types of complexes reflects the electron density on the ruthenium metal center since this oxidation represents the $Ru^{II/III}$ couple. Ligands which donate electron density to the metal destabilize metal based orbitals and decrease the oxidation potential. The order of σ-donation of the three ligands is bpy > dpq > dpb. Ligands which accept electron density from the metal stabilize the metal based orbitals and increase the oxidation potential. The order of metal to ligand π^* backbonding is dpb > dpq > bpy. Both π and σ effects contribute to the observed oxidation potential. These effects are illustrated by the following data: $\Delta E_{1/2}$ oxidation for $[Ru(dpb)_3]^{+2}$ (1910 mV)[9] > $[Ru(bpy)(dpb)_2](PF_6)_2$ (1900 mV) > $[Ru(bpy)(dpq)_2](PF_6)_2$ (1850 mV) > $[Ru(bpy)_2(dpb)](PF_6)_2$ (1755 mV > $[Ru(bpy)_2(dpq)](PF_6)_2$ (1700 mV). This trend suggests that the increased degree of π-backbonding dominates the $\Delta E_{1/2}$ oxidation potential observed.

Electronic Absorption Spectroscopy and Spectroelectrochemistry

The assignment of electronic transitions is of key importance in the characterization of compounds which act as photosensitizers. UV-Vis absorption spectroscopy gives the energy and extinction coefficients of these electronic transitions. Spectroelectrochemistry is a method often used to verify these assignments in systems of this type possessing many acceptor orbitals with well defined redox behavior. Additionally, spectroelectrochemistry probes the

electrochemical reversibility of the redox processes on a time scale of minutes. To date, there has not been a complete and unambiguous characterization of the electron absorption spectrum of any ruthenium bridging ligand polypyridyl complex.

Ruthenium polypyridyl bridging ligand complexes are expected to display a number of electronic transitions. For $[Ru\ (L_n)(BL_{3-n})]^{+2}$ complexes, the lowest energy visible transition will a Ru (dπ)→ BL (π_1*) charge transfer transition. If the complex contains three of the same BLs or three bpys, then there will be only one low energy MLCT observed. It is expected that the molar absorptivity for this MLCT would be higher than for a bis-BL complex or bis-bpy complex due to the increased transition probability. Higher energy MLCTs, Ru (dπ)→ BL ($\pi_{2,3\ldots}$*) are expected to occur, but are often difficult to locate and assign. For mixed-ligand complexes of the formula $[Ru\ (BL)_2(bpy)]^{+2}$ and $[Ru(BL)(bpy)_2]^{+2}$, a second low energy MLCT, Ru (dπ)→ bpy (π_1*) will be seen at energies higher than the Ru (dπ)→ BL (π_1*) charge transfer transition.

Intraligand transitions (IL) are also expected for each polypyridyl ligand, they can be more difficult to assign. It is known from comparisons of the electronic absorption spectroscopy of similar complexes that the bpy π → π_1^* transition occurs at ca 286 nm. A BL based π → π_1* transition will be of lower energy than a bpy π→ π_1* transition. A BL based n → π_1* transition should be found at a lower energy than the BL based π → π_1* transition. Higher energy intraligand manifolds also exist, such as bpy π → π_2*. Furthermore, transitions are not always seen as distinct peaks, shoulders from one transition frequently are superimposed upon peaks from another transition.

Metal centered (or ligand field) transitions represent the excitation of an electron from the Ru ($d\pi$) to the Ru ($d\sigma^*$) orbital. For the complexes in this study, these transitions are seen in the UV portion of the spectrum.

The complex nature of the electronic absorption spectrum of these systems indicates the potential utility of spectroelectrochemistry to unravel the nature and energy of the observed transitions. As seen in the discussion above, many electronic transitions are possible for these types of complexes.

In order to clearly probe the impact of the redox change on the electronic spectroscopy observed, one needs to consider the nature of the optical transitions and redox processes. Table 4.2 gives a list of possible electronic transitions as well as the expected impact on each transition as a result of metal oxidation or ligand reduction. The first column in Table 4.2 lists possible electronic transitions for polyazine complexes of ruthenium.

Table 4.2. Electronic transitions of polyazine complexes of ruthenium and the impact of metal oxidation or ligand reduction upon these transitions.

Type of Electronic transition	Expected impact of $Ru^{II/III}$ oxidation	Expected impact of 1^{st} $BL^{0/-1}$ reduction
Ru (dπ)→ BL (π_1^*) CT	blue shift out of visible	blue shift out of visible
Ru (dπ)→ BL ($\pi_{2,3,\ldots}^*$) CT	blue shift out of visible	blue shift
Ru (dπ)→ 2^{nd} BL (π_1^*) CT	blue shift out of visible	red shift
Ru (dπ)→2^{nd} BL ($\pi_{2,3,\ldots}^*$) CT	blue shift out of visible	red shift
Ru(dπ)→ bpy (π_1^*) CT	blue shift out of visible	red shift
Ru(dπ)→ bpy ($\pi_{2,3..}^*$) CT	blue shift	red shift
1^{st} BL π→π_1^* IL	slight red shift	blue shift out of visible
1^{st} BL π→$\pi_{1,2,3,\ldots}^*$ IL	slight red shift	blue shift
2^{nd} BL π→π_1^* IL	slight red shift	slight red shift
2^{nd} BL π→$\pi_{2,3,\ldots}^*$ IL	slight red shift	slight red shift
1^{st} BL n→π_1^* IL	slight red shift	blue shift out of visible
1^{st} BL n→$\pi_{1,2,3,\ldots}^*$ IL	slight red shift	blue shift
2^{nd} BL n→π_1^* IL	slight red shift	slight red shift
2^{nd} BL n→$\pi_{2,3,\ldots}^*$ IL	slight red shift	slight red shift
bpy π→ π_1^* IL	slight red shift	slight red shift
bpy π→ $\pi_{2,3\ldots}^*$ IL	slight red shift	slight red shift
LF or metal centered	blue shift	red shift

This table of predictions is based on others work and orbitals involved the processes. The second column of Table 4.2 lists the spectral changes expected upon the $Ru^{II/III}$ oxidation. MLCTs will be strongly blue shifted, out of the visible and possibly UV due to the stabilization of the Ru (dπ) orbitals upon oxidation. Gordon *et al.*[10] propose that a new LMCT

appears at low energy as a result of the electrochemical generation of the Ru(III) species. The ligand based $\pi \rightarrow \pi^*$ transitions will be red shifted after ruthenium oxidation due to decreased backbonding stabilizing the π^* orbitals.

The third column of Table 4.2 lists the expected spectral changes resulting from a one electron reduction of the 1st BL, which results in the occupation of the BL π^* orbital. The lowest energy MLCT involving this BL π^* acceptor orbital in the parent complex is shifted to higher energy out of the observed window. If the complex is of a bis-BL type, the second still unreduced BL will retain an unoccupied low energy π^* orbital resulting in a red shifted MLCT. The reduction of the first BL destabilizes the remaining BL and bpy π^* orbitals slightly and more drastically destabilizes the ruthenium based $d\pi$ orbitals. This leads to a red shift of the other MLCT transitions based on other acceptor ligands.

The lowest energy BL (n or π) $\rightarrow \pi_1^*$ transition should be blue shifted out of the visible range upon reduction of that ligand. The remaining BL and bpy based $\pi \rightarrow \pi_1^*$ transitions can also be impacted by the increased electron density on the metal center by BL reduction. This could yield a minor red shift of these IL transitions. Metal centered transitions ($d \rightarrow d$ or LF) are LaPorte forbidden giving rise to their low intensity. Their location in our BL complexes, should be blue shifted in comparison to $[Ru(bpy)_3]^{+2}$ due to the decrease in σ-donation and increase in π-acceptance of the BLs as compared to bpy. These transitions should be impacted more by metal oxidation than BL reduction.

UV-Vis Spectra of $[Ru(bpy)_2(dpq)](PF_6)_2$

As mentioned in the introduction, this compound was first synthesized by Rillema and Mack in 1982.[2b] Rillema's electronic absorption assignments were based on UV-Vis data from the Ru(II) complex. See Table 4.3.

Table 4.3. UV-Vis electronic absorption spectra of $[Ru(bpy)_2(dpq)](PF_6)_2$, in acetonitrile, at T = 20+/- ^oC, according to Rillema and Mack.[2b]

Compound	λ_{max} (nm)	ε (M^{-1} cm^{-1})	Assignment[a]
$[Ru(bpy)_2(dpq)](PF_6)_2$	517	$8.5x10^3$	$Ru(d\pi)\rightarrow dpq(\pi_1^*)$ MLCT
	426	$8.7x10^3$	$Ru(d\pi)\rightarrow bpy(\pi_1^*)$ MLCT
	391(sh), 350(sh)		$Ru(d\pi)\rightarrow (\pi_2)^*$ MLCT
	325 (sh)		$\pi \rightarrow \pi^*$
	284	$7x10^4$	$\pi \rightarrow \pi^*$

[a] If ligand is not specified, then assignment could be BL or bpy.

The UV-Vis spectra of $[Ru(bpy)_2(dpq)](PF_6)_2$ are seen in Figure 3.20-3.24, recorded in CH_3CN. The lowest energy transition at 516 nm has been assigned as Ru $(d\pi)\rightarrow$ dpq (π^*) MLCT by Rillema and Mack.[2b] The second lowest energy peak at 426(sh) nm has been assigned Ru $(d\pi)\rightarrow$ bpy (π^*) MLCT. Rillema *et al.*[2c] have postulated that the shoulders at 390 nm and 350 nm are higher energy MLCTs of the $d\pi \rightarrow \pi_2^*$ type. Additionally, there were high intensity peaks at 200, 254 and 284 nm which were assigned intra-ligand $\pi \rightarrow \pi^*$ transitions. These could be based on BL or bpy.

Spectroelectrochemistry of $[Ru(bpy)_2(dpq)](PF_6)_2$

Gordon *et al.*[10] published the UV-Vis spectra accompanying the $Ru^{II/III}$ oxidation and $dpq^{0/-1}$ reduction. From these results he has made the following assignments shown in Table 4.4.

Table 4.4. UV-Vis absorption spectra of $[Ru(bpy)_2(dpq)](PF_6)_2$, in acetonitrile, at T= 25 ^oC, according to Gordon *et al.*[10]

Compound	λ_{max} (nm)	ε (M^{-1} cm^{-1})	Assignment[a]
$[Ru(bpy)_2(dpq)](PF_6)_2$	515	$8.1x10^3$	$Ru(d\pi)\rightarrow dpq(\pi_1^*)$ MLCT
	425		$Ru(d\pi)\rightarrow bpy(\pi_1^*)$ MLCT
	284	$6.8x10^4$	$\pi \rightarrow \pi^*$

This study has revealed some interesting aspects of the spectroscopy of these types of complexes. It was not clearly indicated which electrochemical processes were reversible, which hinders interpretation of the resultant species. There are two shoulders present in the spectrum between 300 and 400 nm which have not been assigned. Upon oxidation of the metal center Gordon *et al.* assigned the peak at 544 nm as a LMCT and observed a new unassigned peak at 375 nm.

The following spectra were obtained in this study, the interpretations and assignments were made in light of the current data and previously cited papers.

Impact of Oxidation at 1.90 V

In Figures 3.20 and 3.21 the peaks at 520 nm and 424 nm are lost upon the oxidation of Ru(II) to Ru(III) at 1.90V. The shoulder at ~350 nm is lost, while a peak at 382 nm appears.

The fate of the shoulder at ~390 nm is unclear due to the new peak at 382 nm. The peak at 286 nm is lost and a peak at 308 nm appears. Note that a peak at ~540 nm formed with the H-cell (Figure 3.20), but not with the OTTLE cell (Figure 3.21).

This oxidation of the ruthenium center is > 99% reversible with the OTTLE cell as seen in Figure 3.21.

Interpretation

The loss of the 520 nm and 424 nm peak, upon ruthenium oxidation, supports the assignments Ru (dπ) → dpq (π_1^*) and Ru (dπ) → bpy (π_1^*) MLCT transitions, respectively. The red shift in the peak from 286 to 308 nm, tentatively assigned bpy $\pi \rightarrow \pi_1^*$ supports the hypothesis that the stabilization of the ruthenium dπ orbitals upon oxidation decreases the extent of backbonding with the ligands and decreases the π^* energy.

The peak at 382 nm likely represents a red shifted dpq based $\pi \rightarrow \pi_1^*$ transition. This transition would then originate at the shoulder ca 350 nm in the parent complex. The ca 390 nm shoulder, which was lost upon oxidation, lends support to Rillema's [2c] assignment of a higher energy MLCT. Significantly, the energy peak at 540 nm that was observed by Gordon *et al.*[10] and by this author (using the H-cell) is absent in the OTTLE oxidation experiment. This suggests that the supposed LMCT at 540 nm results from incomplete oxidation.

As mentioned above, this oxidation of the ruthenium center is > 99% reversible with the OTTLE cell as seen in Figure 3.21. The isobestic points at ~332 nm , ~370 nm and ~405 nm are indicative of a clean conversion with absence of any light absorbing degradation products.

Impact of First Reduction at –1.00 V

(see Figure 3.22 for H-cell and Figure 3.23 for OTTLE cell). The reduction is 94% reversible with the OTTLE cell as seen in Figure 3.23. Several isobestic points are present. Upon a one electron reduction at –1.00 V to reduce the dpq ligand, the peaks at 516 nm and 424 nm lost. Peaks at 328 nm and 483 nm are formed. The peak at 286 nm is red shifted to 292 nm. The peak at 226 nm does not change.

Interpretation

(Gordon did not discuss the results of the dpq reduction.) As a result of a one electron reduction at –1.00 V, the dpq π^* orbital is occupied. This shifts the lowest energy MLCT, Ru (dπ) → dpq (π_1^*) at 516 nm and the dpq $\pi \rightarrow \pi_1^*$ IL beyond the high energy window at 200 nm. The Ru (dπ) → bpy (π_1^*) MLCT and bpy $\pi \rightarrow \pi^*$ transitions should only experience minor shifts. The absence of the 424 nm peak and appearance of the peak at 483 nm is consistent with a red shifted Ru (dπ) → bpy (π_1^*) MLCT. This author finds this shift surprising as it would be expected that increased backbonding would destabilize the bpy π^* and cause a blue shift of transitions using this acceptor orbital. The experimental result suggests that the metal centered orbitals must be significantly destabilized by the dpq reduction and decreased backbonding. This is further supported by the fact that this MLCT is red shifted 59 nm, whereas the bpy $\pi \rightarrow \pi_1^*$ is red shifted only 6 nm (from 286 to 292 nm). The new peak at 328 nm is neither a Ru (dπ) → dpq (π_1^*) MLCT nor dpq $\pi \rightarrow \pi_1^*$ IL. An assignment as a Ru (dπ)

→ bpy (π_2^*) MLCT is reasonable. This would suggest that its location prior to reduction would have been slightly to the blue, it exact location being obscured by the large peak at 286 nm.

Impact of Second Reduction at –1.55 V

(see Figure 3.24). The second reduction was not reversible. The previously assigned bpy $\pi \rightarrow \pi_1^*$ transition (286 nm) red shifts to 296 nm on the second reduction. The Ru (dπ)→ bpy (π_1^*) at ~ 500 nm is not prominent and a subtle shoulder at ~530 nm has appeared. The peak at 360 nm has red shifted to 370 nm.

Interpretation- (There are no examples of the second reductive spectra of this complex in the literature.) The reduction at –1.55 V should result in the loss of the Ru (dπ) → dpq (π_1^*) MLCT and one Ru (dπ) → bpy (π_1^*) MLCT. The lowest energy transition at ~ 530 nm should be the Ru (dπ) →2nd bpy (π_1^*). The peak at 370 nm should be the Ru (dπ) → dpq (π_2^*) or bpy (π_2^*) MLCT. The bpy $\pi \rightarrow \pi_1$ transition red shifts (to 296 nm) as expected.

Table 4.5. Summary for The UV-Vis electronic absorption spectra of $[Ru(bpy)_2(dpq)](PF_6)_2$ in acetonitrile at room temperature**.**

λ_{max} (nm)	ε ($M^{-1}\,cm^{-1}$)	Assignment	Source
517	$8.5x10^3$	$Ru(d\pi)\rightarrow dpq(\pi_1^*)$ MLCT	Rillema
426	$8.7x10^3$	$Ru(d\pi)\rightarrow bpy(\pi_1^*)$ MLCT	Rillema
391 (sh)		$Ru(d\pi)\rightarrow (\pi_2)^*$ MLCT	Rillema
350 (sh)		$Ru(d\pi)\rightarrow (\pi_2)^*$ MLCT	Rillema
		$dpq\ \pi \rightarrow \pi_1^*$	Duchovnay
325 (sh)		$dpq\ \pi \rightarrow \pi_1^*$	Rillema
		$dpq\ \pi \rightarrow \pi_2^*$	Duchovnay
284	$7x10^4$	$bpy\ \pi \rightarrow \pi_1^*$	Rillema
250		d→d	Duchovnay

The UV-Vis Spectrum of $[Ru(bpy)(dpq)_2](PF_6)_2$

As mentioned in the introduction, this compound was first synthesized by Rillema *et al.*[2c] in 1986. Rillema's electronic absorption assignments were based on the UV-Vis spectra for the parent Ru(II) complex. See Table 4.6.

Table 4.6. UV-Vis electronic absorption spectra of $[Ru(bpy)(dpq)_2](PF_6)_2$, in acetonitrile, at T= 20+/-1 ^oC, According to Rillema *et al.*[2c]

Compound	λ_{max} (nm)	ε (M^{-1} cm^{-1})	Assignment[a]
$[Ru(bpy)(dpq)_2](PF_6)_2$	512	$9.6x10^3$	Ru(dπ)→dpq(π_1^*) MLCT
	462	$8.3x10^3$	Ru(dπ)→bpy(π_1^*) MLCT
	390 (sh)		Ru(dπ)→(π2*) MLCT
	330 (sh)		$\pi \rightarrow \pi_1^*$
	281	$6.9x10^4$	$\pi \rightarrow \pi_1^*$
	256 (sh)		$\pi \rightarrow \pi_2^*$

[a] If ligand is not specified, then assignment could be BL or bpy.

The UV-Vis spectra of $[Ru(bpy)(dpq)_2](PF_6)_2$, synthesized by the Brewer group, is seen in Figures 3.25 to 3.27. Rillema *et al.*[2c] made the following assignments. The Ru (dπ) →dpq (π_1^*) MLCT was found at 512 nm , Ru (dπ)→ bpy (π_1^*) MLCT at 462 nm, a higher energy MLCT Ru (dπ)→π_2^* at 390 nm (sh) and both dpq $\pi \rightarrow \pi_1^*$ and bpy $\pi \rightarrow \pi_1^*$ transitions at 330 (sh) nm, 281 nm and 256 (sh) nm.

Spectroelectrochemistry of $[Ru(bpy)(dpq)_2](PF_6)_2$

Rillema did not publish any spectroelectrochemical data on this compound. Nor did Gordon. The following results are therefore the first presented spectroelectrochemical data on $[Ru(bpy)(dpq)_2](PF_6)$.

Impact of Oxidation at 1.80 V

See Figure 3.25 . The oxidation($Ru^{II/III}$) was ~97% reversible. The two MLCTs at 512 nm and 462 nm are gone, but a small plateau still remains in this visible wavelength range. The peak at 282 nm red shifts to 300 nm. There is a small shoulder peak at ~260 nm which is lost and a small peak at ~245 nm which develops. There are also two shoulders at around 330 nm and 390 nm which are lost while a distinct peak at 368 nm appears.

Interpretation

The interpretations presented are made in light of our data, Rillema's spectroscopic assignments and the spectroelectrochemical properties of the above discussed $[Ru(bpy)_2(dpq)](PF_6)$. Oxidation removes one electron from the metal and transforms the ruthenium d^6 to d^5. This will lower the energy of the Ru (dπ) orbitals and shift the Ru (dπ) dpq (π_1^*) MLCT and Ru (dπ) bpy (π_1^*) MLCT out of the visible range. Thus it would be reasonable to assign the Ru (dπ) $\rightarrow$dpq (π_1^*) MLCT to the 520 nm peak and the 466 nm peak to the Ru (dπ) $\rightarrow$bpy (π_1^*) MLCT in the spectrum of the parent complex. If the shoulders at 390 nm represents a higher energy MLCT, it would be expected that they would shift out of the visible upon metal oxidation, which is slightly discernable from the spectra . As with the prior compound, the bpy $\pi \rightarrow \pi_1^*$ is red shifted (from 292 nm to 300 nm) due to reduced backbonding of the metal center. The peak at 368 nm is the red shifted dpq $\pi \rightarrow \pi_1^*$ transition. The shoulder at ~260 nm is clearly gone, but whether it is blue-shifted to ~245 nm is not certain.

Impact of the First Reduction at –0.70 V

See Figure 3.26. Reduction by one electron results in the occupation of the π^* orbital on one of the dpq ligands. The reduction was 85% reversible. The previously assigned bpy $\pi \rightarrow \pi_1^*$ at 282 nm is red shifted to 288 nm upon dpq reduction. The shoulder at ~256 nm is now a distinct peak at 256 nm. The shoulder from 320 nm to 350 nm is transformed into a distinct peak at 344 nm. The shoulders from 380 nm to 400 nm and the MLCT at 514 nm and 462 nm are lost. Weak shoulders appear at 564 nm and 448 nm.

Interpretation

The first, one electron reduction (-0.70 V) should reduce one of the two dpq ligands. This should shift the lowest energy Ru ($d\pi$)$\rightarrow$dpq (π_1^*) MLCT out of the visible region. The remaining unreduced dpq ligand should have a π_1^* orbital that is destabilized due to increased backbonding from the more electron rich metal center. As in $Ru(bpy)_2(dpq)](PF_6)_2$, the ruthenium $d\pi$ should also be destabilized due to decreased backbonding. The resulting Ru ($d\pi$) $\rightarrow$ dpq (π_1^*) MLCT will be shifted according to which destabilization is greater. The resulting dpq MLCT should also be of reduced intensity because there is now only one LUMO dpq acceptor orbital available. If the pattern seen in $[Ru(bpy)_2(dpq)](PF_6)_2$ applies with this analog, the resulting Ru ($d\pi$) $\rightarrow$ dpq (π_1^*) MLCT will be red shifted. The new shoulder at ca 564 nm is the logical location for this transition. The Ru ($d\pi$) $\rightarrow$ bpy (π_1^*) MLCT was at 463 nm prior to reduction. This MLCT should be red shifted. Its location is not obvious from the spectra. The dpq $\pi \rightarrow \pi_1^*$ should be red shifted, thus explaining the new peak at 350 nm. The appearance of a more distinct peak at 256 nm is interesting. If this is a bpy $\pi \rightarrow \pi_2^*$ transition,

then it implies that only the bpy π_1^* is destabilized and that the bpy π_2^* is unchanged, which is unlikely. The peak newly revealed by dpq reduction is most likely a metal centered transition.

Impact of the Second Reduction at –1.00 V

See Figure 3.27. Reduction by a second electron should result in the occupation of the π_1^* orbital of the second dpq ligand. This reduction was not reversible. After reduction, there are no distinct peaks at wavelengths greater than 360 nm. There are one or two small peaks from 335 nm to 355 nm. The bpy $\pi \rightarrow \pi_1^*$ transition is red shifted from 288 nm to 294 nm. The enigmatic peak at 256 nm blue shifts to 252 nm and doubled in intensity.

Interpretation

The second, one electron reduction should shift the Ru ($d\pi$) $\rightarrow$(π_1^*) dpq MLCT transition out of the visible region due to the occupation of both dpq π_1^* orbitals. The dpq $\pi \rightarrow \pi_1^*$ transition should also be shifted out of the observable range. The Ru ($d\pi$) $\rightarrow$bpy (π_1^*) MLCT should be the lowest energy transition. Its presence is not discernable. The large increase in intensity may indicate degradation of the analyte. The blue shift of the 256 nm peak to 252 nm is consistent with the metal centered (LF) assignment.

Table 4.7. Summary of UV-Vis electronic absorption spectra of $[Ru(bpy)(dpq)_2](PF_6)_2$ in acetonitrile.

λ_{max} (nm)	ε (M^{-1} cm^{-1})	Assignment[a]	Source
512	$9.6x10^3$	Ru(dπ)→dpq(π^*) MLCT	Rillema
462	$8.3x10^3$	Ru(dπ)→bpy(π^*) MLCT	Rillema
390 (sh)		Ru(dπ)→ (π_2)* MLCT	Rillema
330 (sh)		(dpq) $\pi \rightarrow \pi_1^*$	Rillema
281	$6.9x10^4$	(bpy) $\pi \rightarrow \pi_1^*$	Rillema
256 (sh)		$\pi \rightarrow \pi_2^*$	Rillema
		d→ d	Duchovnay

[a] If ligand not specified, it could be BL or bpy.

Comparison between $[Ru(bpy)_2(dpq)](PF_6)_2$ and $[Ru(bpy)(dpq)_2](PF_6)_2$:

The Ru (dπ) →dpq (π_1^*) MLCT occurs at 5 nm higher energy for the bis-dpq complex vs the bis-bpy complex. The $\Delta E_{1/2}$, $Ru^{II/III}$- $dpq^{0/-1}$ is the same for both compounds. The Ru (dπ) →bpy (π_1^*) MLCT is at a lower energy (462 nm) for $[Ru(bpy)(dpq)_2](PF_6)_2$ than $[Ru(bpy)_2(dpq)](PF_6)_2$ (424 nm). This result is logical, there is less backbonding with the bpy due to the bis-dpq BL. The Ru (dπ) →(π_2^*) MLCT occurs at the 390 nm shoulder for both complexes. (It is not presently possible to determine which is the acceptor ligand, bpy or dpq). According to Rillema's assignments, the dpq $\pi \rightarrow \pi_1^*$ for bis-dpq was a 330 nm shoulder vs a 325 nm shoulder for the bis-bpy compound. In this study, the bis-bpy complex dpq $\pi \rightarrow \pi_1^*$ was assigned to the shoulder at 350 nm. Thus the compound with the higher energy metal to bridging ligand MLCT also has a higher energy dpq $\pi \rightarrow \pi_1^*$ transition. The same pattern is

seen with the bpy $\pi \rightarrow \pi_1^*$ transition, where the bis-dpq compound had a peak at 281 nm vs 284 nm for the bis-bpy analog. A comparison of the metal centered transition shows that the bis-dpq complex has a lower energy transition (a shoulder at 256 nm) vs a shoulder at 250 nm for the bis-bpy analog. ($[Ru(bpy)_3](PF_6)_2$ also has a metal centered transition at 250 nm.) In the light of these results no explanation is offered as to the small differences in the absorption peaks of metal centered transitions. A comparison of the molar absorptivities of the Ru ($d\pi$) $\rightarrow$dpq (π_1^*) MLCT is interesting. It would be expected that if these transitions are largely localized then the bis- dpq compound should have double the molar absorptivity due to the presence of two degenerate bridging ligand based acceptor orbitals. The data from Rillema *et al.* Shows that the bis-dpq compound's $\varepsilon = 9.6 \times 10^3\ M^{-1}\ cm^{-1}$ whereas the mono-dpq compound's $\varepsilon = 8.4 \times 10^3\ M^{-1}\ cm^{-1}$.

The reversibilities of the oxidation and first reduction spectra of $[Ru(bpy)_2(dpq)](PF_6)_2$ were very high, 100% and 94% respectively. In contrast, for $[Ru(bpy)(dpq)_2](PF_6)_2$, the oxidation spectra was ~97% reversible but the first reduction spectra was only 85% reversible. The reproducibility of reversibility was inconsistent and varied with individual attempts. The lack of reversibility for the second and third reductions was consistent.

UV-Vis Spectrum of $[Ru(bpy)_2(dpb])(PF_6)_2$

(see Figure 3.19). As mentioned in the introduction, this compound was first synthesized by Murphy *et al.*[9] in 1991. They assigned the lowest energy peak at 550 nm to Ru ($d\pi$)$\rightarrow$dpb (π_1^*) MLCT. Gordon *et al.*[10] (1997) looked at the spectroelectrochemistry of the $Ru^{II/III}$ oxidation and the one electron reduction of this complex. Their assignments are shown in Table 4.8.

Table 4.8. UV-Vis electronic absorption spectra of $[Ru(bpy)_2(dpb)](PF_6)_2$ in acetonitrile at 25°C by Gordon *et al.*[10]

Compound	λ_{max} (nm)	ε (M^{-1} cm^{-1})	Assignment
$[Ru(bpy)_2(dpb)](PF_6)_2$	550	$8.3x10^3$	Ru(dπ)→dpq(π_1^*) MLCT
	425 (sh)		Ru(dπ)→bpy(π_1^*) MLCT
	392 (sh)		dpb π → π_1^*
	314	$4.5x10^4$	
	285	$6.8x10^4$	bpy π → π_1^*
	242	$4.5x10^4$	π → π_2^*
			(BL or bpy)

A low energy shoulder at 425 (sh) nm was assigned as a Ru (dπ)→bpy (π_1^*) MLCT. The shoulder at ~392 nm was assigned as a dpb π →π_1^* intra-ligand transition. The bpy π →π_1^* transition occurs at 285 nm. A higher energy intra-ligand π →π^* transition was found at 242 nm.

(The spectroelectrochemistry of $[Ru(bpy)_2(dpb)](PF_6)_2$ was not performed with the OTTLE cell due to time constraints).

Gordon *et al*.[10] studied the spectroelectrochemistry of the oxidation and first reduction of $[Ru(bpy)_2(dpb)](PF_6)_2$ in 1997. Upon oxidation at 1.5 V, the Ru (π) →dpb (π^*) MLCT at 550 nm and Ru (π) →bpy (π_1^*) MLCT at 425 nm (sh) were bleached and a new peak appeared at ~ 575 nm; it was assigned as a LMCT. Upon reduction at –0.8 V, the Ru (π) →dpb (π_1^*) MLCT was lost and the Ru (π) →bpy (π_1^*) MLCT was red shifted to ~ 475 nm.

UV-Vis Spectra of [Ru(bpy)(dpb)$_2$](PF$_6$)$_2$

This new compound was determined by OSWV to be ca 99% pure. See Figure 3.12. The Ru(II) spectra in Figures 3.28, 3.29 and 3.30 show the peak at 552 nm, but only in Figure 3.30 can the peak at 500 nm be clearly resolved. All figures show shoulders from 380-420 nm and a smaller shoulder at ca 450 nm. The next transition is a strong peak at 316 nm. There is a shoulder at ~ 280 nm and a noticeable peak at 242 nm.

Spectroelectrochemistry of [Ru(bpy)(dpb)$_2$](PF$_6$)$_2$:

Impact of Oxidation at 1.75 V

(see Figures 3.28). The oxidation at this potential generates the Ru(III) species. The reversal of the oxidation was incomplete, ca 10%. After oxidation, the peaks at 552 nm, 500 nm, and shoulder from 394 nm to 415 nm, were absent.

There may be a shoulder at ~360 nm which remains after oxidation. The most prominent peak, at 316 nm, is reduced in intensity by ~ 50% upon oxidation. There is a shoulder at ~ 280 nm which appears to blue shift slightly. A substantial peak at 242 nm red shifts to 248 nm and is reduced in intensity by 33%. The reversal of the oxidation was incomplete.

Interpretation

The Ru (dπ)$\rightarrow$dpb (π_1^*) MLCT should shift out of the visible region upon oxidation. Indeed, the lowest energy peak at 552 nm is not seen after oxidation. Likewise the Ru (dπ)$\rightarrow$bpy (π_1^*) MLCT should also shift out of the visible region, this transition is assigned to the 500 nm peak which is no longer visible. The shoulder from 394 nm to 415 nm is not seen upon oxidation, this region should contain higher energy MLCTs, which also should shift out

of the visible after oxidation of the metal center. The dpb $\pi \rightarrow \pi_1^*$ and bpy $\pi \rightarrow \pi_1^*$ should be assignable, with the dpb transition being of lower energy. The bpy $\pi \rightarrow \pi_1^*$ transition has in prior compounds been seen at ~ 286 nm. This peak is seen here as a shoulder, being obscured by the large absorption at 316 nm.

Impact of the First Reduction at –0.50 V

(see Figure 3.29). Reduction by one electron leads to the reduction of one of the two dpb ligands. The reduction was > 90% reversible. The lowest energy transitions at 554 nm and 500 nm are lost and a new peak at 590 nm appears. The significant shoulder at ~390 nm may be blue shifted to ~378 nm. The intense peak at 316 nm has red shifted to 318 nm and decreased in intensity. Prior to reduction, a small shoulder at 280 nm was superimposed upon the 316 nm peak. This small peak became more clearly defined upon the diminishment of the dominant peak. The noticeable peak at 240 nm did not change.

Interpretation

The first, one electron reduction should reduce one of the dpb ligands. This should shift both the Ru (dπ)$\rightarrow$dpb (π_1^*) MLCT and dpb $\pi \rightarrow \pi_1^*$ intra-ligand transition out of the visible region. A destabilization of the dpb based orbital on the second ligand is also expected. Destabilization of the Ru (dπ) orbitals upon ligand reduction red shifts the remaining Ru (dπ)$\rightarrow$dpb (π_1^*) MLCT to 590 nm. The Ru (dπ)$\rightarrow$bpy (π_1^*) MLCT should also red shift from 500 nm, but its location is not obvious. This transition and the remaining Ru (dπ)$\rightarrow$dpb (π_1^*) MLCT are probably overlapping. A shoulder appears at ca 380 nm and is of unknown origin. The shoulder at ~ 286 nm, which is the bpy $\pi \rightarrow \pi_1^*$ transition, remains relatively

unaffected. The peak at 316 nm is not likely to be dpb $\pi \rightarrow \pi_1^*$ because the dpq $\pi \rightarrow \pi_1^*$ in the bis-dpq analog is seen at 330 nm. It could be a higher energy IL transition, dpb $\pi \rightarrow \pi_2^*$.

Impact of the Second Reduction at –1.0 V

(see Figure 3.30). The second reduction led to a species in which both dpb ligands are reduced by one electron. This reduction was not reversible. Generation of the two electron reduced species gives a low intensity shoulder at 360 nm. This is about an 18 nm blue shift from the first reduction peak location. The prominent peak at 318 nm is gone. The peak at ~286 nm remains. A new peak at ~ 258 nm appears. The peak at 240 nm is gone.

Interpretation

After two one electron reductions, the only Ru ($d\pi$)$\rightarrow$ (π_1^*) MLCT likely is the Ru ($d\pi$)$\rightarrow$bpy (π_1^*) MLCT. This transitions location is obscured in a region of multiple absorbance peaks. The (lowest energy) dpb $\pi \rightarrow \pi_1^*$ transition is shifted out of the observable range. The second dpb $\pi \rightarrow \pi_1^*$ transition is similarly shifted. This data suggests that the 318 nm peak in the parent species is the dpb $\pi \rightarrow \pi_2^*$ transition. It is not clear if the 240 nm peak has red shifted to ~258 nm or whether the former is lost and the latter represents a different transition. In lieu of the similarity between this complex and the three previously discussed complexes, the assignment of d $\rightarrow$d for the transition at 240 nm in the parent species would be reasonable.

Table 4.9. Summary of UV-Vis electronic absorption spectra of $[Ru(bpy)(dpb)_2](PF_6)_2$, in acetonitrile, at room temperature**.**

λ_{max} (nm)	Assignment (Duchovnay)
552	Ru (dπ)→dpb (π_1^*) MLCT
500	Ru (dπ)→bpy (π_1^*) MLCT
ca 425 (sh)	Ru (dπ)→bpy or dpb (π_2^*) MLCT
ca 390 (sh)	dpb π → π_1^*
316	dpb π → π_2^*
285	bpy π → π_1^*
242	d → d

Comparison between $[Ru(bpy)_2(dpb)](PF_6)_2$ and $[Ru(bpy)(dpb)_2](PF_6)_2$

The Ru (dπ) →dpb (π_1^*) MLCT occurs at the same wavelength, 550 nm, for both complexes. The Ru (dπ) →bpy (π_1^*) MLCT peak is seen at 500 nm for the bis- dpb complex and 425 nm (sh) in the bis-bpy complex. This pattern was also seen in the two dpq analogs.The dpb π→ π_2^* IL transition was assigned to the peak at 316 nm for the bis-dpb complex by this author. The location of the dpb π → π_1^* was obscured by overlapping absorbance peaks in the 390 nm region. Gordon et al.[10] assigned the 392 nm (sh) to the dpb π → π_1^* for the bis-bpy complex. The bpy π → π_1^* transition (~286 nm) seems to be consistent for both complexes. Both complexes have peaks at 242 nm, which has been designated as d → d by this author as compared to π→ π_1^* IL by Gordon et al.[10] In light of these comparisons the following summary of the electronic transitions for the bis-bpy complex is shown in Table 4.10.

Table 4.10. Summary of UV-Vis electronic absorption spectra of [Ru(bpy)2(dpb)](PF6)2 in acetonitrile.

λ_{max} (nm)	ε (M^{-1} cm^{-1})	Assignment	Source
550	$8.3x10^3$	Ru(dπ)→dpq(π_1^*) MLCT	Gordon
425 (sh)		Ru(dπ)→bpy(π_1^*) MLCT	Gordon
392 (sh)		dpb $\pi \rightarrow \pi_1^*$	Gordon
314	$4.5x10^4$	????	Gordon
	$4.5x10^4$ (Gordon)	dpb $\pi \rightarrow \pi_2^*$	Duchovnay
285	$6.8x10^4$	bpy $\pi \rightarrow \pi_1^*$	Gordon
242	$4.5x10^4$	$\pi \rightarrow \pi_2^*$ (BL or bpy)	Gordon
	$4.5x10^4$	d→ d	Duchovnay

Comparison between [Ru(bpy)(dpq)2](PF6)2 and $Ru(bpy)(dpb)2](PF6)_2$

The Ru (dπ) →dpb π^* MLCT is lower in energy for the dpb complex, 552 nm vs 512 nm for the dpq complex. This is an expected result as the dpb π^* acceptor orbital is lower in energy compared to the dpq counterpart. The Ru (dπ) →bpy π^* MLCT is lower in energy for the dpb complex, 500 nm vs 462 nm for the dpq complex. This result is consistent with decreased backbonding between the metal center and the bpy π^* acceptor orbital in the bis-dpb complex. The same pattern follows for higher energy MLCTs, 420 nm for the dpb complex vs 390 nm for the dpq complex. All IL transitions are lower in energy for the dpb complex, as is the d → d transition.

References

1. Denti, G.; Campagna, S.; Sabatino, L.; Scolastica, S.; Ciano, M.; Balzani, V.*Inorg. Chem.* 1990, 29, 4750.
2. (a) Rillema, D. P.; Callahan, R. W.; Mack, K. B. *Inorg. Chem.* 1982, 21, 2389. (b) Rillema, D. P. and Mack, K. B. *Inorg. Chem.* 1982, 21, 3849. © Rillema, D. P.; Taghdiri, D. G.; Jones, D. S.; Keller, C. D.; Worl, L. A.; Meyer, T. J.; Levy, H. A. *Inorg. Chem*. 1987, 26, 578.
3. (a) Bridgewater, J. S.; Vogler, L. ; Molnar, S.; Brewer, K. *Inorg. Chim Acta*. 1993, 208, 179. (b) Richter, M. M.; Brewer, K. J. *Inorg.Chem*. 1993, 32, 5762.
4. Wang, J. *Analytical Electrochemistry*, 1994, 53, VCH Publishers, New York.
5. (a) Bridgewater, J. S.;Vogler, L. M.; Molnar, S.M.; Brewer, K. J. *Inorg. Chim. Acta.* 1993, 208, 179. (b) Richter, M. M.; Brewer, K. J. *Inorg. Chem*. 1993, 32, 5762.
6. Bard, A.; Faulkner, L. *Electrochemical Methods.* 1980, 229, John Wiley, New York.
7. Vogler, L. M., Ph.D. Dissertation. YEAR? 63.
8. Donohue, R. J.; Tait, C. D.; DeArmond, M. K.; Wertz, D. W. *Spectrchim. Acta.* 1986, 42, 233.
9. Carlson, L. C. and Murphy, W. R. Jr. *Inorg. Chim. Acta.* 1991, 181, 61.
10. Scott, S.; Gordon, K. *Inorg. Chim. Acta*. 1997, 254, 267.

CHAPTER FIVE: CONCLUSIONS AND FUTURE WORK

This work is composed of synthetic, electrochemical and spectroelectrochemical studies. A new compound, $[Ru(bpy)(dpb)_2](PF_6)_2$ has been prepared and its purity and identity were analyzed with OSWV and LSIMS. Purification was difficult, with a ca 1% impurity remaining after repeated alumina adsorption chromatographs. The spectroscopic and redox properties of the new complex and three related dpb and dpq systems were probed with cyclic voltammetry, electronic absorption spectroscopy, and spectroelectrochemistry. The spectroelectrochemical studies were conducted with both a bulk H-cell and OTTLE cell. The significant conclusions of this study are highlighted.

Synthesis

(1) The new compound $[Ru(bpy)(dpb)_2](PF_6)_2$ was synthesized.

(2) LSIMS verified its identity.

(3) OSWV indicated presence of ca 1% electroactive impurity after repeated alumina adsorption chromatographs.

(4) The previously studied compounds $[Ru(bpy)_2(dpb)](PF_6)_2$, $[Ru(bpy)_2(dpq)](PF_6)_2$, and $[Ru(bpy)(dpq)_2](PF_6)_2$ were prepared for more detailed analysis.

(5) An attempt was made to probe the purity and identity of the starting material $RuCl_3 \bullet 3H_20$ and intermediate $Ru(bpy)Cl_4$. The LSIMS of the starting material $RuCl_3 \bullet 3H_20$ (see Appendix Figure 3.8) did not reveal the parent ion. The peak at m/z=137 is evidence of $RuCl^+$. The LSIMS of $Ru(bpy)Cl_4$ (see Appendix Figure 3.6) did not contain the parent ion, m/z = 400, and thus did not confirm the composition. Upon washing $Ru(bpy)Cl_4$ with ethanol, two fractions were produced, a soluble brown filtrate and a relatively insoluble black solid. The

UV-Vis spectra of these two fractions , as seen in Appendix Figure 3.9, are significantly different. Anderson and Seddon[1] determined by elemental analysis that Krause's[2] synthesis, used herein, produces $Ru(bpy)Cl_3$ (thus implying polymeric form), whereas the protocol of Dwyer *et al.*[3] yielded $Ru(bpy)Cl_4$. Although the identity of this intermediate was not determined in this study, its utility as a precursor in the synthesis of $[Ru(bpy)(dpq)_2](PF_6)_2$ and many other mixed ligand complexes has been demonstrated. Future work should explore alternative chromatographic methods, such as HPLC and cation exchange chromatography, which may yield a more pure product.

Electrochemistry

(1) OSWV was used to ascertain purity by detection of electroactive impurities, with a detection limit of approximately 0.3%.

(2) Cyclic voltammetry was used to probe electrochemical reversibility, and $E_{1/2}$ values.

(3) Contamination by water and oxygen leads to poor electrochemical reversibility, so an anaerobic electrochemical cell with internal desiccant was constructed. Further testing of this new cell will be part of my proposed future research.

(4) One important piece of information gained by electrochemical studies is the order of ligand reductions for mixed ligand complexes like $[Ru(bpy)(dpb)_2](PF_6)_2$. Typically each dpb ligand will reduce by one electron followed by a one electron reduction of any bpy ligands. Some aspects of the electrochemistry of $[Ru(bpy)(dpb)_2](PF_6)_2$ seem to suggest the $dpb^{-/2-}$ couple may occur prior to the bpy reduction. The lack of reversibility in the spectroelectrochemistry did not allow the assignment of this third reduction. Low temperature studies may be used in the future to address this question.

Spectroelectrochemical Experimental Design

(1) Spectroelectrochemical analysis requires good electronic spectroscopy as well as high electrochemical conversion and reversibility. Several studies were undertaken to achieve these criteria. To enhance reversibility, an OTTLE cell (a modification of the Hartl cell[4]) was constructed and used. A typical H-cell was also used for comparison. (a) Electrochemical reversibility is significantly different between the two methods, the OTTLE cell facilitating better reversibility, as high as 99% as compared to 50% with the H-cell. (b) The time needed for analysis is shorter with the OTTLE cell, 1 minute for the OTTLE vs 15 minutes for the H-cell.

(2) The impact of analyte concentration on spectroelectrochemical studies was explored. It was found that (a) the resolution of shoul ders is enhanced with increasing concentration and (b) the time of analysis and degree of irreversibility increase with increased analyte concentration. The protocol for (a) requires high concentrations whereas the protocol for (b) necessitates low concentrations.

Summary of Spectroelectrochemistry Conclusions

(1) The electronic transitions of the new complex $[Ru(bpy)(dpb)_2](PF_6)_2$ have been presented in Table 4.9. The spectroelectrochemistry of the metal oxidation, first and second one electron reduction of the BL has been presented. The oxidation was only 10% reversible whereas the 1st reduction was 90% reversible. The poor reversibility of the oxidation was unexpected and warrants further research. Although the 2nd reduction was not reversible, spectral results provided valuable information supporting assignment of the peak at 316 nm as dpb $\pi \rightarrow \pi_2^*$.

(2) The electronic transitions, supported by spectroelectrochemical analysis, of the related bis-BL complex $[Ru(bpy)(dpq)_2](PF_6)_2$ have been presented in Table 4.10. The spectroelectrochemical oxidation of the metal center was 97% reversible. The 1st one electron reduction of the BL was 85% reversible. The 2^{nd} one electron reduction of the 2^{nd} BL was not reversible.

(3) When complete oxidation of the metal center of $[Ru(bpy)_2(dpb)](PF_6)_2$, $[Ru(bpy)_2(dpq)](PF_6)_2$, $[Ru(bpy)(dpb)_2](PF_6)_2$ and $[Ru(bpy)(dpq)_2](PF_6)_2$ is achieved, using the OTTLE cell, no low energy transitions are left. This indicates that this transition which Gordon *et al.*[6] assigned as a LMCT is likely a residual. This highlights the importance of careful and complete electrochemical conversions in spectroelectrochemical studies. As LMCTs are reasonable further studies aimed at locating them (possibly in the NIR) are warranted.

(4) This study has assigned the peak at ca 240-260 nm to a d → d metal- centered transition. Rillema and Gordon assign these peaks to IL transitions.

(5) A comparison of the transitions of the two bis-BL complexes shows that the electronic transitions of the bis-dpb complex are of lower energy than the corresponding transitions of the bis-dpq complex.

(6) The Ru ($d\pi$) → dpb (π_1^*) MLCT for both dpb BL complexes occurred at the same wavelength, 550 nm. In contrast, the corresponding MLCT for the bis-dpq

BL complex was seen at 512 nm as opposed to 517 nm for the mono-dpq complex. Thus no specific conclusion can be made concerning the effect one or two BLs on the MLCT.

This is surprising in light of the fact that the corresponding MLCTs for the tris-BL complexes are higher in energy than their corresponding bis-BL counterparts.

(7) The Ru (dπ) → bpy (π_1^*) MLCT is of lower energy for the bis-BL complexes vs the corresponding mono-BL complexes.

(8) It has been assumed that second lowest energy transition of the parent complex is Ru (dπ) → bpy (π_1^*) MLCT and that the third lowest energy peak is a higher energy Ru (dπ) → BL (π_2^*) MLCT. It is possible that the Ru (dπ) → bpy (π_1^*) MLCT is in reality the 3rd peak and the Ru (dπ) → BL (π_2^*) is the 2nd peak. This dilemma can not be resolved with the presently available spectroelectrochemical data. The clarification of this question warrants further research.

(9) The bpy π →π^* IL transition is least affected by the number and identity of the BL when comparing the four analogs.

Future Work

Synthesis: The complex [Ru(bpy)(dpq)(dpb)]$(PF_6)_2$ would a challenging compound to synthesize.

Purification: Alternative methods of purification should be explored, such as HPLC and cation exchange chromatography.

Electrochemistry*:* Electrochemical data, using CV and OSWV, need to be obtained with the new anaerobic cell. Low temperature studies, using the anaerobic cell, also need to be conducted.

Spectroelectrochemistry: (1) The spectroelectrochemistry of [Ru$(bpy)_2$(dpb)$(PF_6)_2$ needs to be done. (2) Location of shoulders (weak absorbance peaks) needs to be re-evaluated by using

high concentrations of analyte. With this additional data, spectroelectrochemical studies of the four complexes needs to repeated. (3) The low reversibility of the electrochemical oxidation of the new complex $[Ru(bpy)(dpb)_2](PF_6)_2$ needs to be re-evaluated. (4) The reason for the lack of reversibility of the 2nd and 3rd electrochemical reductions needs to be explored. (5) The assumption that the 2nd lowest energy peak is a Ru ($d\pi$) $\rightarrow$bpy (π_1^*) MLCT warrants future research. (6) The spectroelectrochemical analysis of the tris-BL ruthenium complexes will yield valuable additional information. (7) A low temperature OTTLE cell needs to be built. (8) A NIR OTTLE spectroelectrochemical cell needs to be designed and built for the analysis of LMCTs, interligand transitions and intraligand transitions of reduced ligand complexes. It is the hope of this author that the reader has gained some appreciation of the challenges faced in obtaining and interpreting spectroelectrochemical data. The opportunity for future research is abundant.

References

1. Seddon, K.R.; Anderson, S. *J. Chem. Res. (Synopsis)*. 1979, 2, 74.
2. Krause, R. A. *Inorg. Chim. Acta*. 1977, 22, 209.
3. Dwyer, F. P.; Goodwin, H. A.; Gyarfas, E. C. *Aust. J. Chem.* 1962,
4. Krejcik, M.; Danek, M.; Hartl, J. *J. Electroanal. Chem.* 1991, 317, 179.
5. (a) Rillema, D. P.; Callahan, R. W.; Mack, K. B. *Inorg. Chem.* 1982, 21, 2389. (b) Rillema, D. P.; Callahan, R. W.; Mack, K. B. *Inorg. Chem.* 1982, 21, 3849. (c) Rillema, D. P.; Taghdiri, D. G.; Jones, D. S.; Keller, C. D.; Worl, L. A.; Meyer, T. J.; Levy, H. A. *Inorg. Chem*. 1987, 26, 578.
6. Scott, S.; Gordon, K. *Inorg. Chim. Acta*. 1997, 254, 267.
7. Richter, M. M. Ph.D. Dissertation. 1993, 147.

Appendix Figure 1.1. Diasteriomers of $[Ru(bpy)(dpb)_2]^{+2}$. Each diasteriomer has an enantiomer.

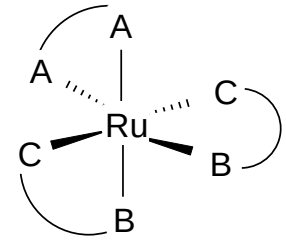

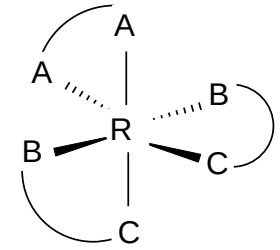

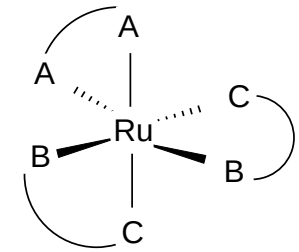

A= N of terminal ligand 2,2' bipyridine
B= N of pyridine of bridging ligand
C= N of pyrazine portion of bridging ligand

Appendix Figure 3.1. LSIMS^{+} of the matrix glycerol. MW 92+1.

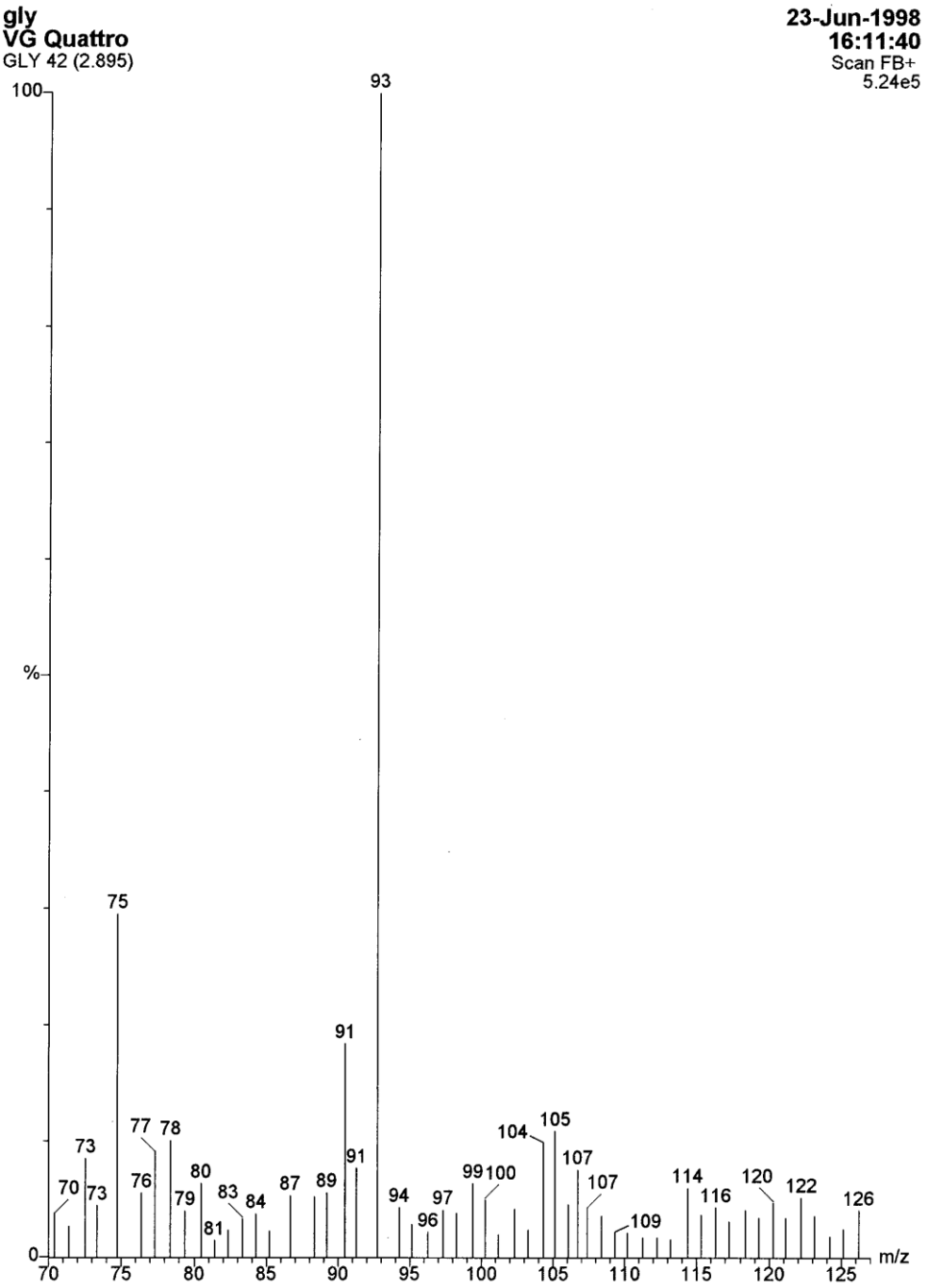

Appendix Figure 3.2. LSIMS^{+} of the matrix nitro-benzyl alcohol. MW 153+1

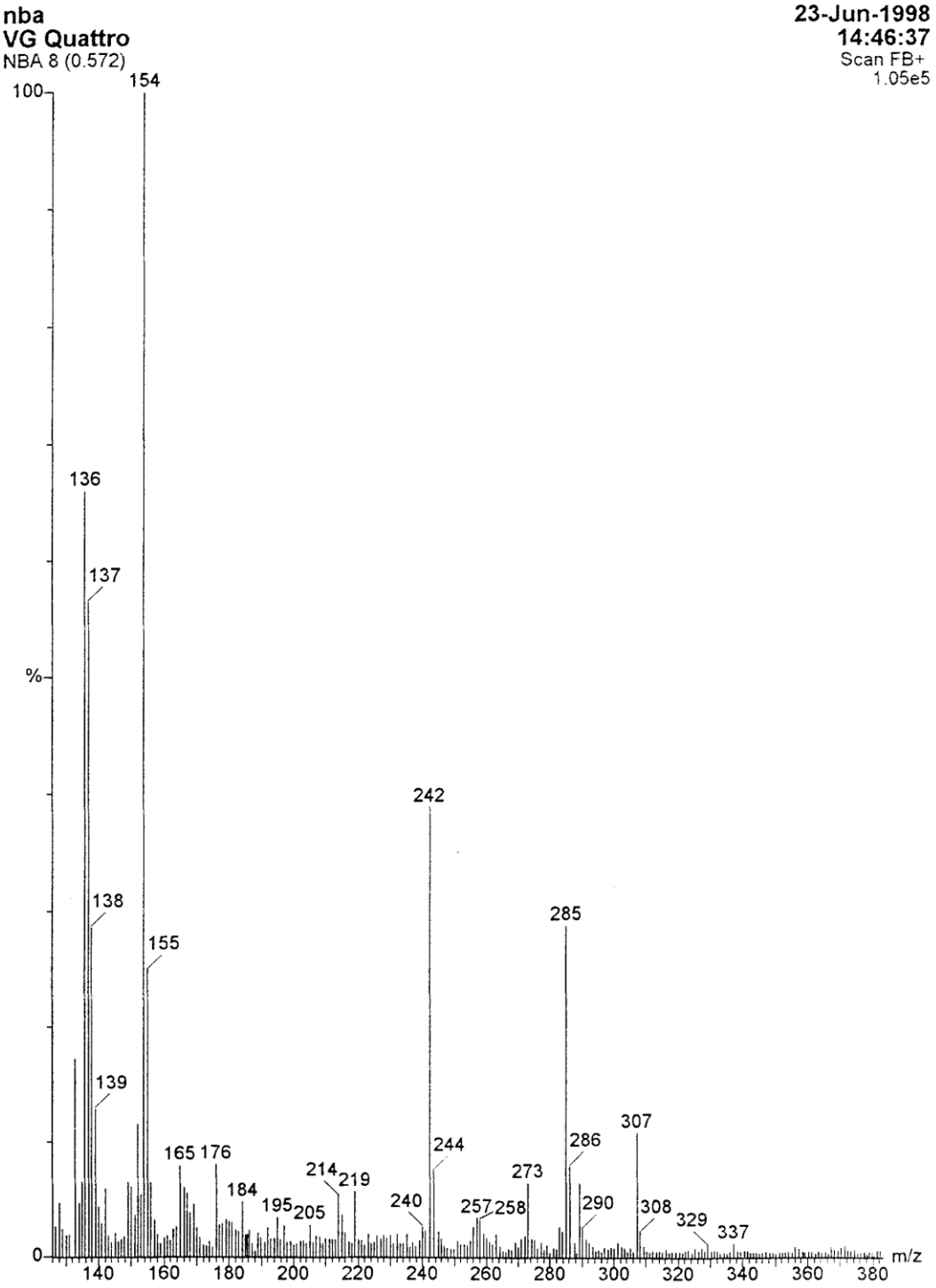

Appendix Figure 3.3. LSIMS^{+} of free ligand bpy in glycerol. MW 156+1.

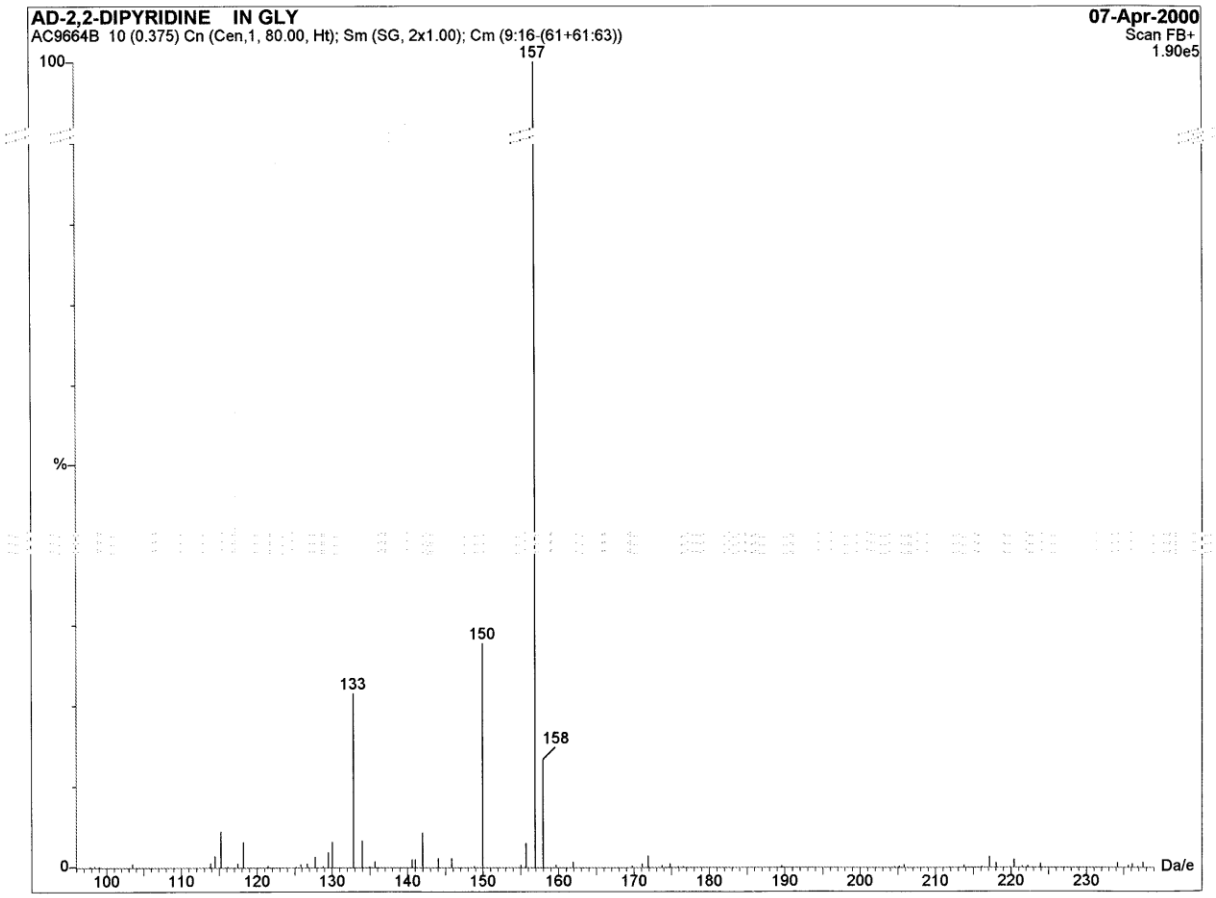

Appendix Figure 3.4. LSIMS^{+} of free ligand dpq in glycerol. MW 284+1.

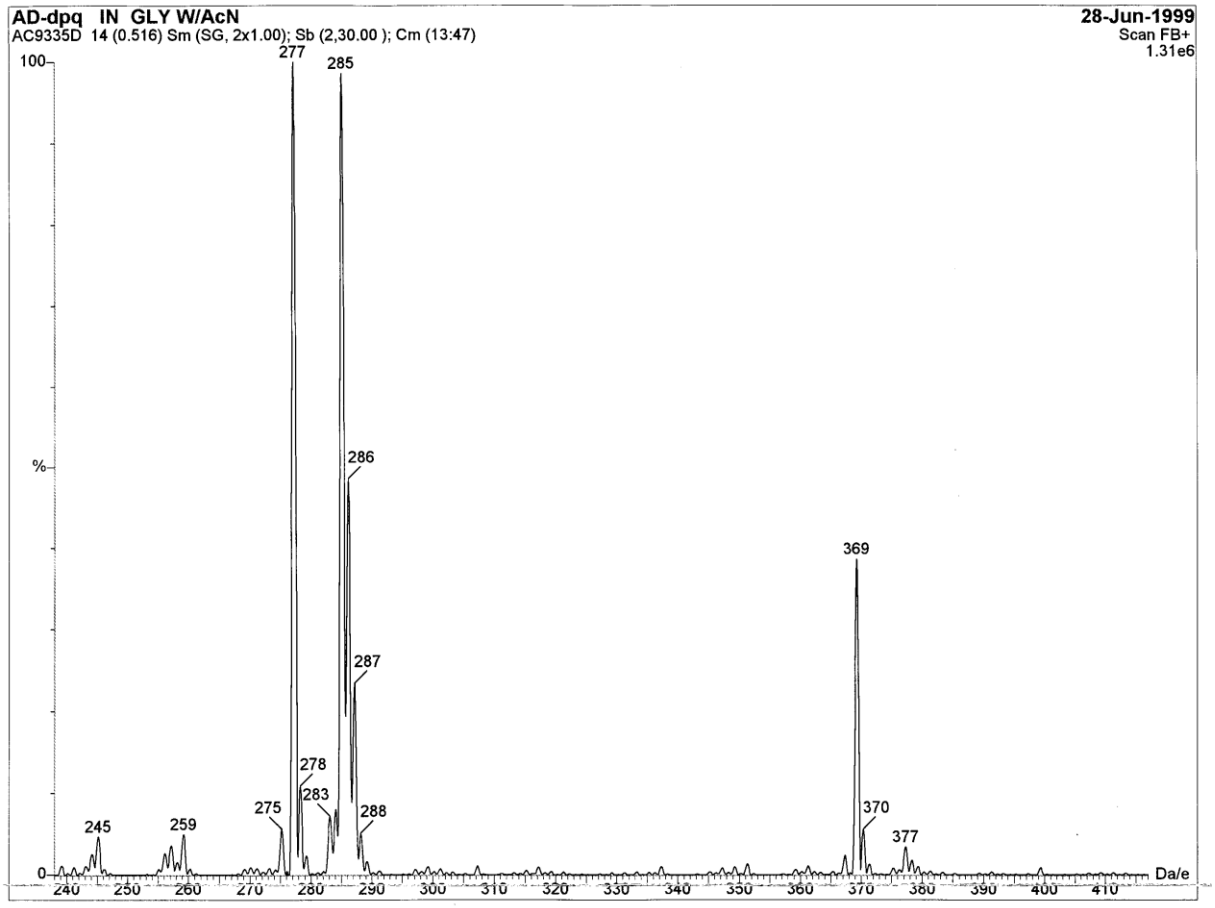

Appendix Figure 3.5. LSIMS^{+} of free ligand dpb in glycerol. MW 334+1.

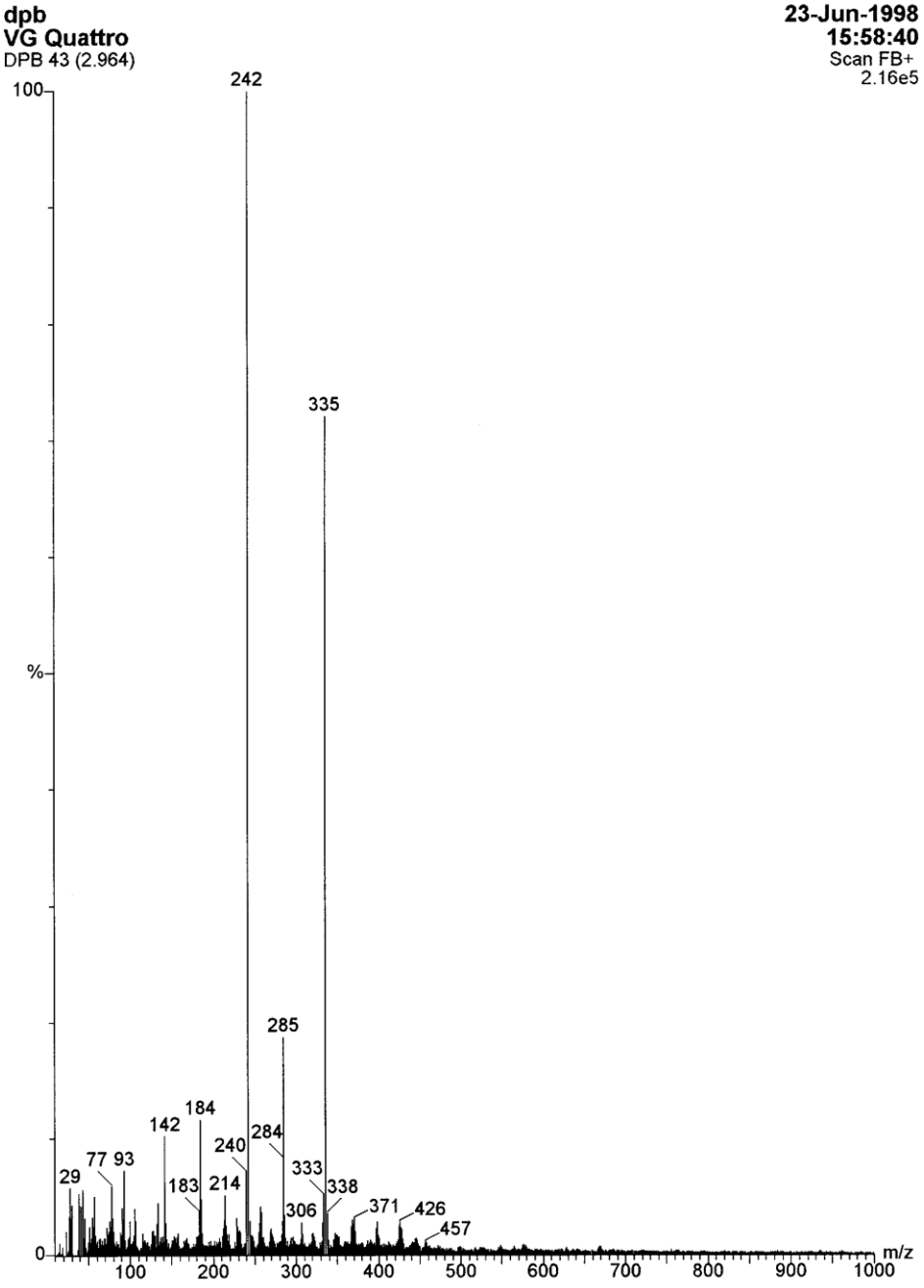

Appendix Figure 3.6. Electrospray (+) MS of $Ru(bpy)Cl_4$ in acetonitrile/water. MW= 399.

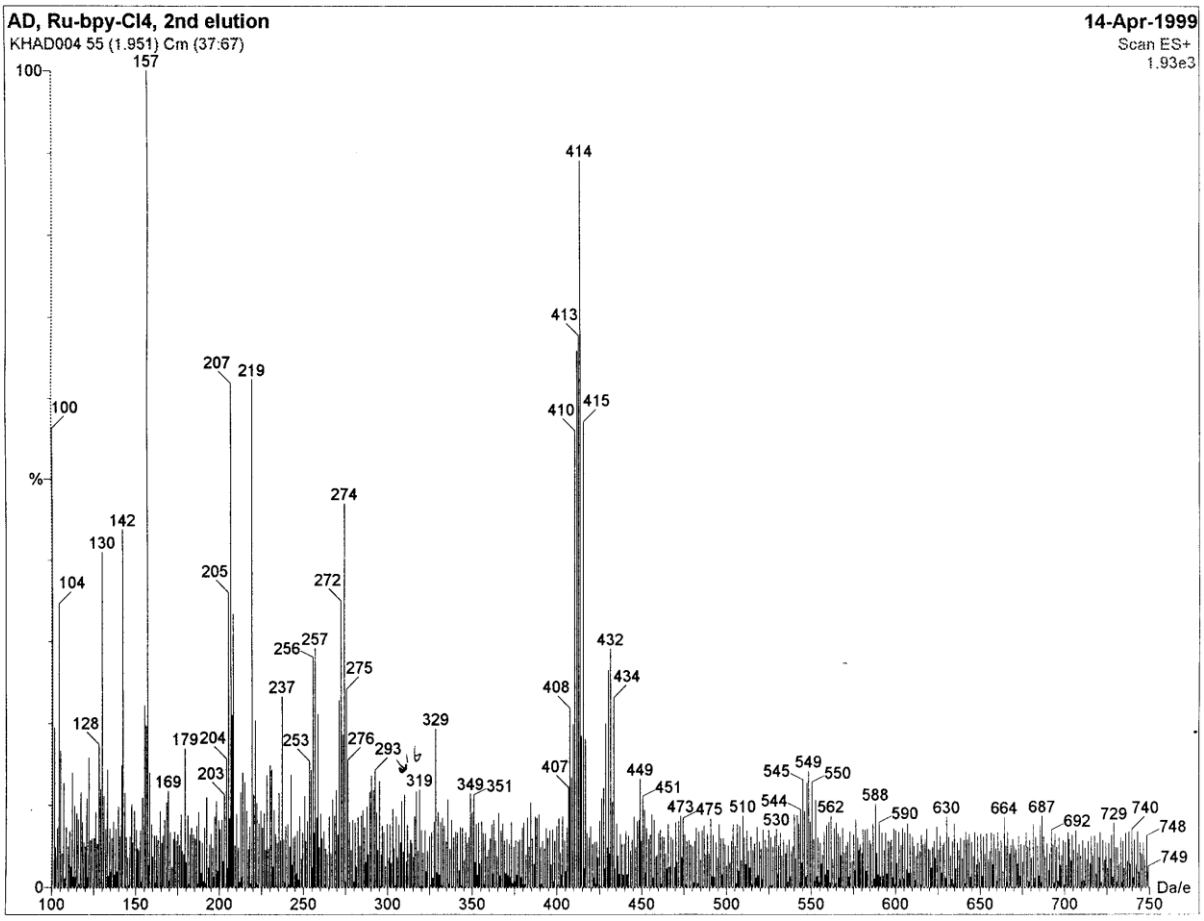

Appendix Figure 3.7.. UV-Vis spectroelectrochemistry of ferrocene. (__= 0 V, ….. = 1.7 V).

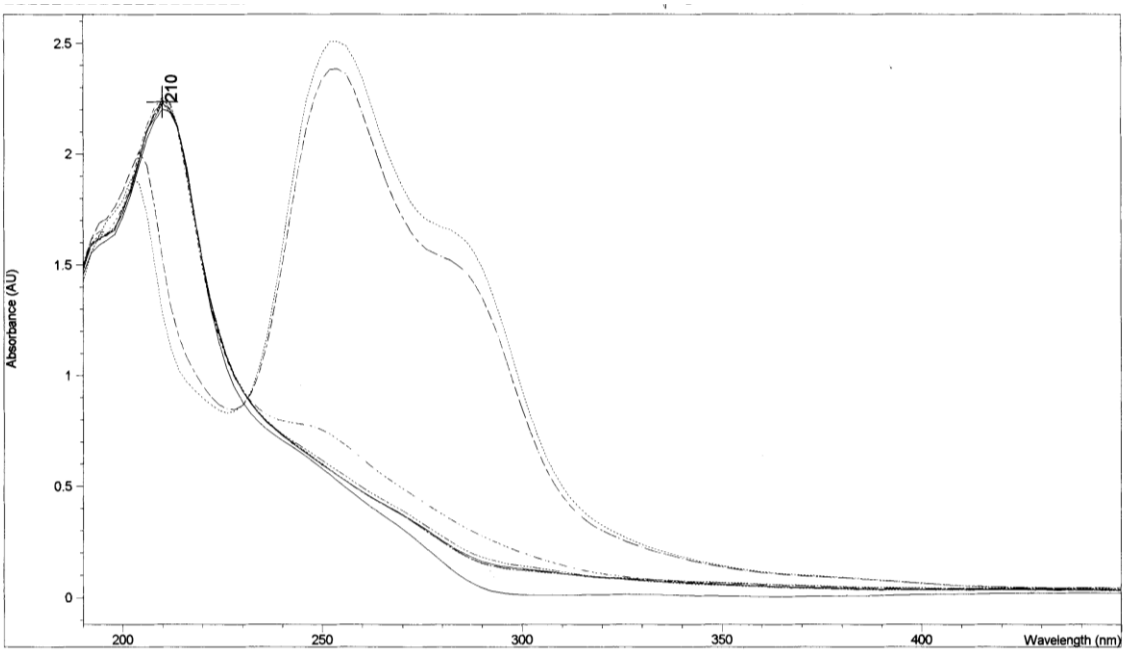

Appendix Figure 3.8. LSIMS$^-$ of $RuCl_3 \bullet 3H_2O$ in NBA. MW= 255+1.

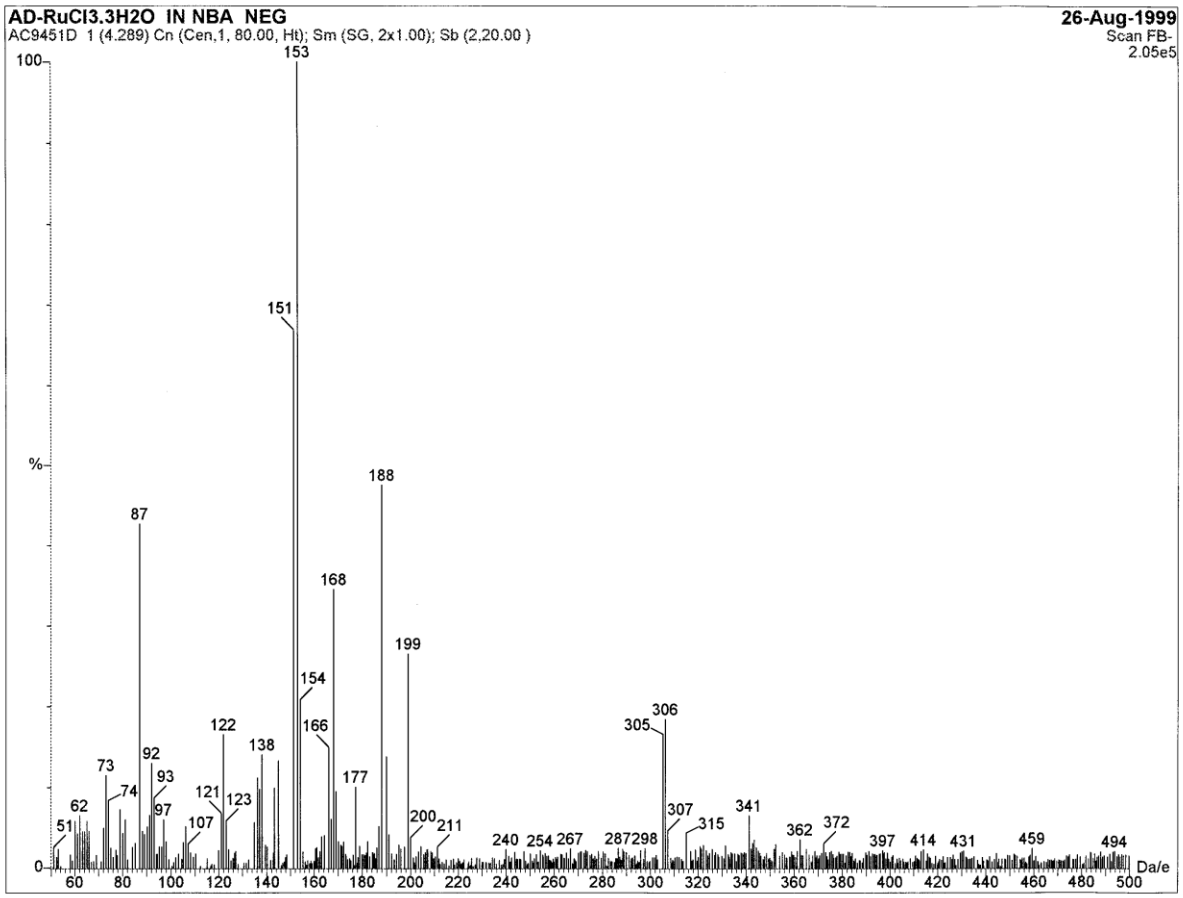

Appendix Figure 3.9. The electronic absorption spectra of the two fractions of $Ru(bpy)Cl_4$ in water. (Where bpy= 2,2' bipyridine).